71-25,271

HAN, Chang Sun, 1935-
ANALYSIS OF CYCLOTRON-TYPE ELECTRIC LENSES
AND THE EFFECTS OF POSTS.

University of Maryland, Ph.D., 1970
Engineering, electrical

University Microfilms, A XEROX Company, Ann Arbor, Michigan

THIS DISSERTATION HAS BEEN MICROFILMED EXACTLY AS RECEIVED

Reproduced with permission of the copyright owner. Further reproduction prohibited without permission.

ANALYSIS OF CYCLOTRON-TYPE ELECTRIC LENSES AND THE EFFECTS OF POSTS

by

Chang Sun Han

Thesis submitted to the Faculty of the Graduate School
of the University of Maryland in partial fulfillment
of the requirements for the degree of
Doctor of Philosophy
1970

Copy

Reproduced with permission of the copyright owner. Further reproduction prohibited without permission.

APPROVAL SHEET

Title of Thesis: Analysis of Cyclotron-Type Electric Lenses and the Effects of Posts

Name of Candidate: Chang Sun Han

Thesis and Abstract Approved: Martin P. Reiser

Martin P. Reiser
Professor
Department of Electrical Engineering
and
Department of Physics and Astronomy

Date Approved Oct. 23, 1970

Reproduced with permission of the copyright owner. Further reproduction prohibited without permission.

ABSTRACT

Title of Thesis: Analysis of Cyclotron-Type Electric Lenses and the Effects of Posts

Chang Sun Han, Doctor of Philosophy, 1971

Thesis directed by: Dr. Martin P. Reiser, Professor

The focusing properties of cyclotron-type electric lenses with time-varying potentials were numerically investigated. The main emphasis of the study was on the aspects of lens effects which had not been previously investigated: (a) The behavior of the lenses at large transit times or rf frequencies for which the approximations of analytical theory are not valid. (b) The effects of posts (or grids) placed at one or both sides of the gap. A simple expression for electric focusing in a two-dimensional lens was derived and compared with theoretical results by other investigators. An analytical expression was also derived for the case where the downstream side of the lens is covered with a grid. The lens parameters, i.e. focal lengths and location of principal planes, were computed numerically for several geometries using electric field data obtained by computer with relaxation method. Computations were carried out for several two-dimensional and three-dimensional gap geometries at three different frequencies of the gap voltage as a function of kinetic energy and rf phase of the particles at the center of the gap. A criterion for the validity

Reproduced with permission of the copyright owner. Further reproduction prohibited without permission.

of first-order theory was established. At very low frequency the gap fields were found to be focusing over the entire half period of the rf during which acceleration occurs. As the frequency (or transit angle of the particles) increases the lenses become defocusing at large negative phases of the rf voltage. The phase angle, at which the transition from focusing to defocusing takes place, shifts with increasing frequency in positive direction, i.e. the defocusing phase interval increases. Use of posts at the exit side of the gap improves the vertical focusing substantially at the expense of introducing some defocusing in horizontal direction. In cyclotrons this horizontal defocusing poses no problem as sufficient horizontal focusing is available from magnetic force to counteract this effect.

Reproduced with permission of the copyright owner. Further reproduction prohibited without permission.

ACKNOWLEDGEMENT

I wish to express my heartfelt gratitude to Professor Martin P. Reiser. His thoughtful guidance throughout my graduate career and also his devotion to this work will always be deeply appreciated.

I would like to extend my sincere appreciation to Drs. H. Kim, M. Craddock, and D. Nelson and Mr. R. Louis for many useful discussions and contributions and much helpful advice.

I am greatly indebted to Professor H. Holmgren for his encouragement and support throughout the years of my graduate study.

Finally I wish to thank the TRIUMF project (Vancouver, Canada) for financial assistance and the National Aeronautics and Space Administration for providing computer time under Grant NsG-398 to the University of Maryland. I am also indebted to the University of Maryland Cyclotron project use of the computer facilities.

Reproduced with permission of the copyright owner. Further reproduction prohibited without permission.

TABLE OF CONTENTS

Chapter		Page
I.	INTRODUCTION	1
II.	ANALYTICAL THEORY OF ELECTRICAL FOCUSING AND ITS LIMITATION	
	2.1 Two-Dimensional Electric Lenses	8
	2.2 The Effects of Grids on the Focusing Action of the Lens	22
	2.3 The Three-Dimensional Lens with Posts	27
	2.4 Definition of Cardinal Points of an Electric Lens	31
	2.5 Limitation of the Analytic Theory of Two-Dimensional Electric Lenses	35
III.	DESCRIPTION OF COMPUTATIONAL METHODS	
	3.1 Lens Geometries and Potential Maps	40
	3.2 Numerical Integration of Equation of Motion and Determination of the Cardinal Points	45
	3.3 The Linear Region and Error Involved in the Numerical Computation	50
IV.	NUMERICAL RESULTS FOR THE FOCAL PROPERTIES OF THE TWO- AND THREE-DIMENSIONAL ELECTRIC LENSES	
	4.1 Choice of Parameters for Computer Runs	53
	4.2 Results for the Two-Dimensional Lens Geometries	58
	4.3 Results for the Three-Dimensional Lenses with Posts	
	4.3.1 Vertical Focusing	64
	4.3.2 Horizontal Focusing	70
V.	DISCUSSION OF RESULTS	
	5.1 Trajectories	76
	5.2 Focal Length and Convergence	81
	5.3 Transition Phase and Peak-focusing Phase	86
	5.4 Principal Planes and Width of the Electric Lenses	91

Reproduced with permission of the copyright owner. Further reproduction prohibited without permission.

TABLE OF CONTENTS (cont.)

Chapter		Page
	5.5 Energy Gain	93
	5.6 Horizontal Motion in the Three-Dimensional Lens	96
VI.	APPLICATION TO CYCLOTRONS	98
VII.	CONCLUSION	102
APPENDIX A		106
APPENDIX B		108
REFERENCES		112

Reproduced with permission of the copyright owner. Further reproduction prohibited without permission.

LIST OF TABLES

Table		Page
1	Vertical displacement of protons at x = 10" from the gap center line	37
2	Parameters of lens geometries	41
3	Transit time across a distance b of particles having an average velocity v for f = [illegible], 22.9 MHz	56
4	Lens parameters for G1, f = 2.29 MHz	58
5	Lens parameters for G1, f = 4.58 MHz	60
6	Lens parameters for G1, f = 22.9 MHz	62
7	Lens parameters for G5V, f = 2.29 MHz	64
8	Lens parameters for G5V, f = [illegible]	66
9	Lens parameters for G5V, f = 22.9 MHz	68
10	Lens parameters for G5H, f = 2.29 MHz	70
11	Lens parameters for G5H, f = [illegible]	72
12	Lens parameters for G5H, f = 22.9 MHz	74
13	Typical b/f_2 values of the low and high frequency case for several values of θ_c and [illegible]	80
14	Transition phases in degree obtained by analytical and numerical methods for Geometry 1 and 5V	87
15	Peak-focusing phases (in degree) obtained by analytical and numerical methods for Geometry 1 and Geometry 5V	90
16	Comparison of Geometry 1 and Geometry 5V	95
17	Electric axial betatron oscillation frequency for geometries 1 and 5V, E_c/E_g = 3.0, f = 22.9 MHz, θ_c = 75°, 45°, 0°, -15°	101

Reproduced with permission of the copyright owner. Further reproduction prohibited without permission.

LIST OF FIGURES

1.(A) A typical cyclotron-type electric lens geometry

(B) Potential function V(x), $\partial V/\partial x$, $\partial^2 V/\partial x^2$ on the median plane for $a \to 0$, $c \to \infty$, $b = 1.5"$

2. Qualitative representation of V(x,0,0) and the first and second derivatives in arbitrary units

3. Potential distribution along z axis for no posts (Geometry 1), posts on one side (Geometry 5) and posts on two sides (Geometry 4)

4. Focal points and principal planes of a thick lens

5. Normalized convergence, b/f_2 in Geometry 1, for phase angle $\theta_c = 45^\circ$, frequency f = 22,9 MHz

6. Comparison of normalized convergence for f = 2.29, 4.58, and 22.9 MHz in Geometry 1 for energy ratio $E_c/E_g = 1.0$

7. Lens Geometry 1 and potential distribution (a/b = .6, c/b = 3.0)

8. Lens Geometry 4 and Geometry 5

9. Potential distribution in x-z plane of Geometry 5

10. Difference in computed focal length, f_2, due to different initial z displacement (Geometry 1, static conditions) for two energies

11 Ion trajectories for different phases θ_c in Geometry 1 and Geometry 5V for f = 22.9 MHz, E_c = .2 MeV

Reproduced with permission of the copyright owner. Further reproduction prohibited without permission.

12. Time-variation factor of electric field seen by a particle on its path through the gap along x axis for different phase angles θ_c, f = 22.9 MHz E_c/E_g = 1.0 (a) $\theta_c = 75^\circ$, (b) $\theta_c = 45^\circ$, (c) $\theta_c = 0^\circ$ (d) $\theta_c = -75^\circ$

13 Comparison of normalized convergence, b/f_2, at $\theta_c = 45^\circ$ (a) for different lens geometries, f = 22.9 MHz (b) for different rf frequencies, Geometry 1

14. Normalized convergence, b/f_2 of Geometry 1 for f = 22.9 MHz at E_c/E_g= .75, 1.0, 2.0

15 Normalized convergence, b/f_2 in Geometry 1, f = 4.58 MHz

16. Normalized convergence, b/f_2 in Geometry 1, f = 22.9 MHz

17. Normalized convergence, b/f_2 in Geometry 1, f = 2.29 MHz

18. Normalized convergence, b/f_2 in Geometry 1, f = 4.58 MHz

N9. Normalized convergence, b/f_2 in Geometry 1, f = 22.9 MHz

20. Normalized convergence, b/f_2 in Geometry 5V, f= 2.29 MHz

21. Normalized convergence, b/f_2 in Geometry 5V, f= 4.58 MHz

22. Normalized convergence, b/f_2 in Geometry 5V, f= 22.9 MHz

23. Normalized thickness of the lens, Geometry 1, f=2.29 MHz

24. The normalized thickness of the lenses at rf phase $\theta_c = 45^\circ$ for different rf frequencies and geometries

25. Location of object-side principal plane, d_2/b, at rf phase $\theta_c = 45^\circ$ for different geometries and frequencies

26. Relative energy gain $\Delta E/E_g$ for f= 22.9 MHz at E_c/E_g=.75 and 6. Solid curve: Geometry 1. Dashed curve: Geometry 5V. Dotted curve: cos θ_c

Reproduced with permission of the copyright owner. Further reproduction prohibited without permission.

27. Normalized convergence, b/f_2, in Geometry 5H, f=2.29 MHz

28. Normalized convergence, b/f_2, in Geometry 5H, f=22.9 MHz

Reproduced with permission of the copyright owner. Further reproduction prohibited without permission.

CHAPTER I

INTRODUCTION

Historically the field of electron and ion optics was born in 1924 when Busch[1] discovered that an axially symmetric magnetic field could focus electron beams like a glass lens focuses light rays. Several years later, in 1932, Davisson and Calbick[2], and independently, Bruche and Johanson[3] showed that axially symmetric electric fields could also be used to focus electron beams. Since its birth, electron and ion optics experienced a substantial development and made indispensable contributions to science and technology, such as cathode ray tubes, electron microscopes, image converters, mass spectrometers, and many other devices. During World War II, the field of electron optics received new impulses from war requirements and played an important role in the development of klystron and magnetron tubes. The advancement of nuclear physics and the emergence of various types of particle accelerators added a new dimension to ion optics and led to the invention of new types of focusing methods, such as magnetic gradient focusing, quadrupole lenses, etc.

Of particular interest is the role which was played by the cyclotron in this development. Ever since Lawrence invented the concept of the cyclotron, the stabilization of the ion beam in this accelerator was one of the most crucial questions to be answered. It was soon discovered that magnetic gradient focusing alone was not sufficient to get all particles captured into stable orbits. There was still

Reproduced with permission of the copyright owner. Further reproduction prohibited without permission.

substantial loss of beam in the central region. It was not until 1938 when Rose[4], and independently, Wilson[5] recognized that the nonuniform electric field in the cyclotron acceleration gap provides a force perpendicular to the median plane. This force can be focusing as well as defocusing in nature depending on the rf phase when the ions traverse the gap. Later, in 1953, Cohen[6], and most recently Reiser[7] improved Rose's analysis on electric focusing in the time-varying field of a cyclotron. The most important conclusion from these various theoretical studies was that the focusing action depends strongly on the phase of the applied rf voltage. If an ion passes the center line of the acceleration gap while the electric field is rising in time, it gets a net defocusing effect; on the other hand, if it reaches the gap center line when the field is decreasing in time, a net focusing effect results. Unfortunately, a large fraction of particles from the ion source enter the acceleration process at negative phases with respect to the rf voltage, and, as a result, there is a relatively high loss of beam in most cyclotrons due to electrical defocusing. A method of avoiding these losses was independently proposed by Smith[8] and Reiser[9]. In this method the path length of the ion orbits between first and second gap crossing is increased, which shifts the useful group of ions to positive phases where they are electrically focused.

In the central region of cyclotrons the magnetic vertical focusing is relatively ineffective compared to the

Reproduced with permission of the copyright owner. Further reproduction prohibited without permission.

focusing effect of the electric field. Electric focusing or defocusing effects decrease with the ion energy, i.e. they are strongest near the ion source. At a distance not too close to the ion source the potential distribution can be approximated by a two-dimensional geometry. This approximation permits a theoretical analysis of the focusing problem by utilizing the concepts of ion optics as they were first applied to electrostatic lenses. In ion optics the effects of the electric field are represented by a lens with four cardinal points. The cardinal points vary with the geometry of the electrodes (defining the electric field), the applied potentials, and the kinetic energy of the ions. All these principles of static ion optics can be applied to the dynamic case[10] where the applied voltage varies with time. In the latter case one has the rf phase as an additional parameter. The cardinal points in a time-varying electric lens are defined in the same way as in the electrostatic case. The basic restriction in either case is that first-order approximation can be assumed, i.e. the ion trajectories stay close to the optical axis or, in the two-dimensional case, close to the plane of symmetry ("median plane" in cyclotrons). Under such circumstances one can expand the potential function in the region close to the axis or median plane. Retaining only terms up to first order, one obtains an equation of motion in which the vertical component of the force on the ions is proportional to the distance z from the median plane. In this first-order approximation the cardinal

Reproduced with permission of the copyright owner. Further reproduction prohibited without permission.

points are independent of the displacement z of the trajectory for given particle energy and operating conditions.

The problem of defocusing in a time-varying electric field does also exist in linear accelerators. In these machines the requirement of negative rf phase for phase stability is not compatible with the transverse electric focusing which occurs, as in the cyclotron, at positive rf phase (i.e. decreasing voltage)[11]. Several schemes to overcome this difficulty were proposed[12,13]. The simplest solution is that of grid focusing, where the defocusing action in the downstream side of the gap is depressed by covering the gap opening with a dense grid or thin foil. Since a grid or thin foil would intercept a large fraction of the beam one was forced to accept a compromise by replacing the dense grid with a few ribbons of metal.

The method of grid focusing is also applicable to cyclotrons and was first investigated experimentally by H. Blosser[14]. Instead of using a grid two metal bars or posts are placed at the exit side of the cyclotron acceleration gap. This reduces the defocusing effect vertically while increasing it horizontally. However, this is acceptable as magnetic focusing is rather strong in horizontal (radial) direction, but weak vertically. Hence, improving electric focusing vertically at the expense of weakening the overall focusing in radial direction gives better beam transmission. The effects of such posts in cyclotron-type lenses has, to our knowledge, never been investigated theoretically.

Reproduced with permission of the copyright owner. Further reproduction prohibited without permission.

The main reason for this lack of theory is the difficulty of mathematical analysis in such a three-dimensional system. The improvements in computer analysis of complex field geometries during recent years made it possible for us to undertake an investigation of this problem.

The potential distribution of axially symmetric or two-dimensional lens geometries were studied by a number of people using analytical and experimental as well as numerical methods. Bertram[15] obtained analytical expressions for the potential distribution between two cylinders separated by a finite distance. Murry and Ratner[16] derived expressions for the potential configuration in cyclotron-type two-dimensional electric lenses using the Schwarz-Christoffel transformation, and recently Reiser[7] extended this method to include a grounded outer electrode (called the "liner" in cyclotrons). An automated electrolytic tank system[17] was used to measure the potential distribution and study the vertical motion of the ions in the central region near the ion source of the Maryland cyclotron[18]. Since digital computers became standard research tools, the well known relaxation method was developed into perhaps the most powerful technique of solving Laplace's equation by iteration processes. This method is relatively inexpensive as well as readily available to many people. The potential maps for our investigation were obtained by the relaxation method, using a computer program developed at the University of Maryland by D. Nelson[19], and the computations were carried

Reproduced with permission of the copyright owner. Further reproduction prohibited without permission.

out on an IBM 360/44.

Once the potential maps are generated, the next problem is the calculation of the particle trajectory. From the various trajectory tracing methods, we chose the numerical integration of the equations of motion by the Runge-Kutta technique. A computer program was available which had been used earlier in central-region design studies for the Michigan State and Maryland cyclotrons. In this program, called PINWHEEL,[20] relativistic effects are fully accounted for to ensure the correctness of the results even in the case of high energy particles. Analytical formulas for the electric focusing effects in time-varying fields were derived by a simplified approach. Results obtained agree well with those derived by previous authors except for a geometry factor. The analytical theory was extended to include the effects of grids. This permitted a discussion and qualitative understanding of the action of posts in the three-dimensional case.

From the trajectory information obtained by numerical integration, the cardinal points of each lens were computed with a specially developed program. The results are compared with the analytically predicted values, and some limitations of the first-order theory of electric lenses for time-varying fields are discussed.

In the numerical analysis the vertical motion of ions was studied using five different lens geometries, three having different gap width-to-height ratio, one with

Reproduced with permission of the copyright owner. Further reproduction prohibited without permission.

posts at both sides of the gap, and one with posts on one side only. Lens geometries as well as operating conditions were chosen to represent situations that are typical for cyclotrons. The computations were done for protons as particles using three different values of rf frequency, 2.29, 4.58, and 22.9 MHz. The gap voltage was assumed to be 200 kV and the lens properties were determined for seven injection energies and different rf phases. By using the pertinent scaling laws, the results obtained can readily be applied to other particles or operating conditions.

Only the most important results are presented in tabular or graphic form. A more comprehensive and detailed set of computer results can be found in a separate technical report.[21]

The main emphasis of this study is on electric focusing properties at high rf frequency, (or, rather, at large transit times where the analytical theory does not hold) and on the effects of posts. The application to cyclotrons and the implications for cyclotron beam dynamics, particularly the case where the rf operates on a high harmonic of the cyclotron ion frequency, is briefly discussed.

No effort was made to include space charge effects which, as is well known, may significantly alter the results of single-particle optics.

Reproduced with permission of the copyright owner. Further reproduction prohibited without permission.

CHAPTER II

ANALYTICAL THEORY OF ELECTRICAL FOCUSING AND ITS LIMITATIONS

2.1 Two-Dimensional Electric Lenses

At sufficient distance from the ion source the acceleration gap in most cyclotrons can be approximated by a two-dimensional electric lens for a theoretical analysis of focusing action. Let us choose a cartesian coordinate system with the y axis representing the gap center line, the x axis across the gap in direction of particle motion, and the z axis in vertical direction (perpendicular to cyclotron median plane). The potential is only a function of x, z, i.e. $V=V(x,z)$, and the median plane is a plane of symmetry such that the potential value at each point in the negative z-plane is the same as at the corresponding position in the positive z-plane. A typical cyclotron-type electric lens geometry with the static equipotential lines in the upper half of the x-z plane is schematically shown in Fig. 1(A). In an actual cyclotron the acceleration voltage changes in time. However, since the wavelength of the rf field is usually very large compared to gap dimensions, it is quite possible to separate space and time variation such that $V(x,z,t)=V(x,z)\cos\omega_e t$.

Consider first an ion trajectory in such an electric lens under a static applied voltage, i.e. no time variation. Let us assume a positive ion is injected from a point in

Reproduced with permission of the copyright owner. Further reproduction prohibited without permission.

the field-free region at the left side of the lens and the ion has no momentum component in the z-direction. The ion will acquire a small downward momentum component after entering the field region since the electric field vector points towards the median plane, as shown in Fig. 1(A). As soon as the ion crosses the gap center line the z-directional electric force changes its sign and the ion acquires an upward momentum component. If the potential distribution is antisymmetric about the z-axis, as is the case in the lens shown here, the ion gains as much downward momentum component in entering the lens as it does upward momentum component after crossing the gap center line of the lens provided the energy gain during the passage can be neglected. Consequently, there will be no net change in the slope of the ion trajectory, but a slight net shift of the trajectory closer to the median plane. We may expect this to be the case for very high incident energy and low acceleration voltage. If, however, the energy gain is appreciable so that traveling times in the left and right sides of the lens are significantly different, then the ion spends a longer time in the focusing region and in turn the resulting total downward momentum is bigger than the upward momentum. This will give a net focusing effect. Alternately, if the ion travels from right to left, it is decelerated by the lens field shown in Fig. 1(A), and it spends, as in the previous case, longer time in the focusing region than in the defocusing region which will give again a net focusing

Reproduced with permission of the copyright owner. Further reproduction prohibited without permission.

effect.

In this discussion we neglected the variation of the electric field z-component, $E_z = -\frac{\partial V}{\partial z}$, as the particle's z position changes. As will be shown, in the gap region ($z<b$) E_z is a monotonically increasing function of z starting from zero at the median plane. From the above arguments it is clear that the focusing action always takes place at larger z values than that of the defocusing force. This effect thus further increases the net focusing effect. From these arguments we conclude that a static electric lens is always focusing.

Now let us include the sinusoidal time-varying factor of the acceleration voltage. We assume a slow time-variation such that the particle's travel time across the gap is small compared to the rf period, say less than 90^{o}. Then, if the ion approaches the gap center line while the electric field is rising in time, the focusing force in the negative x region is weaker than the defocusing force in the positive x region which results in an overall net defocusing action. On the other hand, if the ion crosses the gap center line while the electric field is decreasing, a net focusing will result by the reverse argument.

Let us now turn to the theoretical derivation of first-order electric focusing action in a two-dimensional lens. At any point inside the lens the potential function satisfies the Laplace equation in two dimensions:

$$\nabla^2 V(x,z) = 0 \qquad (2.1)$$

Reproduced with permission of the copyright owner. Further reproduction prohibited without permission.

From this we have

$$\frac{\partial^2 V}{\partial Z^2} = -\frac{\partial^2 V}{\partial x^2} \tag{2.2}$$

The potential distribution is a smooth function of x and z, and, by reasons of symmetry, it is an even function in z which can be expanded in a Taylor series as follows:

$$V(x,z) = V(x,o) + \frac{1}{2}\left(\frac{\partial^2 V}{\partial Z^2}\right)_{Z=0} Z^2 + \frac{1}{24}\left(\frac{\partial^4 V}{\partial Z^4}\right)_{Z=0} Z^4 + \cdots\cdots \tag{2.3}$$

The electric field z-component can be obtained by differentiating Eq. (2.3) with respect to z. If the ion stays very close to the median plane throughout the entire travel across the lens, we obtain to first order:

$$E_z = -\frac{\partial V}{\partial Z} = -\left(\frac{\partial^2 V}{\partial Z^2}\right)_{Z=0} \cdot Z \tag{2.4}$$

which, from Eq. (2.2) may be written as

$$E_z = \left(\frac{\partial^2 V}{\partial X^2}\right)_{Z=0} Z = -\left(\frac{\partial E_x}{\partial X}\right)_{Z=0} \cdot Z \tag{2.5}$$

Eq. (2.5) indicates that, in the region close to the median plane, the z-component of the electric field can be readily computed if the electric potential function on the median plane is known. As an example, consider the gap geometry with potential $+V_o$ on one side and $-V_o$ on the other, as shown in Fig. 1(A). The potential distribution for this case has been obtained by Schwarz-Christoffel transformation[7]. The analytical form of the potential distribution along the

Reproduced with permission of the copyright owner. Further reproduction prohibited without permission.

x axis is relatively simple only for the case $c \to \infty, a \to 0$ where one obtains

$$V(x) = V_o\left[\frac{2}{\pi}\tan^{-1}\left(\frac{1}{\sinh\frac{\pi}{2b}x}\right) - 1\right] \tag{2.6}$$

The derivative dV/dx at x=0 is found to be

$$\frac{\partial V}{\partial x} = -\frac{V_o}{b} \tag{2.7}$$

If $a \neq 0$, but still $c \to \infty$ one finds[7,16] for the field strength at the gap center $\frac{\partial V}{\partial x} = (1-m^2)\frac{V_o}{b}$ where the parameter m depends on the ratio a/b. Fig. 1(B) shows V(x), dV(x)/dx, and $\frac{d^2V}{dx^2}$ for the case where a=0 as an illustration.

The electric-force z-component acting on an ion with charge q is given by

$$F_z = qE_z = -q\left(\frac{\partial E_x}{\partial x}\right)_{z=0} \cdot z \tag{2.8}$$

The change of the momentum z-component is thus

$$\frac{dp_z}{dt} = -q\left(\frac{\partial E_x}{\partial x}\right)_{z=0} \cdot z = q\left(\frac{\partial^2 V}{\partial x^2}\right)_{z=0} z \,. \tag{2.9}$$

Integration of Eq. (2.9) with respect to time from $-\infty$ to $+\infty$ gives the total change in the momentum z-component, Δp_z. Since the electric field is assumed to be confined in a finite region we can replace the upper and the lower limits by t_1 and t_2, respectively. The change in the z-component of the momentum, Δp_z, is then

$$\Delta p_z = -q\int_{t_1}^{t_2}\left(\frac{\partial E_x}{\partial x}\right)_{z=0} z\, dt \,. \tag{2.10}$$

Reproduced with permission of the copyright owner. Further reproduction prohibited without permission.

We assume that the ion stays very close to the x-axis and that the momentum z-component is much smaller than the x-component. Then,

$$V_z \ll V_x = V \tag{2.11}$$

where v is the total velocity of the ion. Now, dt=dx/v(x), and we can replace the upper and the lower limits by the x coordinates of the points where the electric field vanishes. Denoting these points by $+x_1$ and $-x_1$, we can write Eq. (2.10) as follows:

$$\Delta p_z = -q\int_{-x_1}^{x_1} \frac{\partial E_x}{\partial x}\,\frac{Z(x)}{V(x)}\,dx \tag{2.12}$$

This equation for the momentum change cannot be solved exactly even in the static case because for finite gap width the potential distribution cannot be expressed analytically in a closed form as a function of x. Besides, v(x) and z(x) are functions of x whose form can only be determined by solving numerically the equations of motion. However, with a few simplifying assumptions, a solution can be found. Such a first-order analysis of electric focusing under static conditions was carried out by several authors[7,22,23]. The focusing effect under time-varying conditions was treated by Rose[4], Wilson[5], Cohen[6], and Reiser[7].

The present investigation was only concerned with electric focusing in this latter case of a time-varying potential. In the following we will derive an expression

Reproduced with permission of the copyright owner. Further reproduction prohibited without permission.

for the momentum change Δp_z in a slightly different way than is found in the literature. As first discussed by Rose, we can separate the effect due to time variation of the field (keeping the energy constant) and that due to increase in energy at fixed rf phase. We will also assume that z remains constant while the ion crosses the field region. For the purpose of the following mathematical derivation we will assume a lens geometry of the type shown in Fig. 1(A). First we consider the time-variation effect. Let t_c be the time at which the ion reaches the center line of the gap. The velocity of the ion is considered constant. Then the time t can be expressed by

$$t = t_c + \frac{x}{v} \tag{2.13}$$

The electric potential and the field in the median plane can be expressed as a function of x and the time t as follows:

$$V(x,t) = V(x) \cos \omega_e \left(t_c + \frac{x}{v} \right) \tag{2.14}$$

$$E_x(x,t) = \mathcal{E}_x(x) \cos \omega_e \left(t_c + \frac{x}{v} \right) , \tag{2.15}$$

where ω_e is the rf radian frequency and $\theta_c = \omega_e t_c$ represents the rf phase angle when the ion arrives at the gap center line. The partial derivative encountered in Eq. (2.12) can be evaluated in terms of the total derivative and the partial derivative with respect to time t:

$$\frac{dE_x}{dx} = \frac{\partial E_x}{\partial x} + \frac{\partial E_x}{\partial t} \frac{\partial t}{\partial x}$$

Reproduced with permission of the copyright owner. Further reproduction prohibited without permission.

and, hence,

$$\frac{\partial E_x}{\partial x} = \frac{d E_x}{d x} - \frac{1}{V}\frac{\partial E_x}{\partial t} \quad .$$

Substituting Eq.(2.16) into Eq.(2.12), Δp_z can be expressed by an integral with respect to x:

$$\Delta P_z = -\frac{qz}{V}\int_{-x_1}^{x_1}\left(\frac{dE_x}{dx} - \frac{1}{V}\frac{\partial E_x}{\partial t}\right)dx \qquad (2.17)$$

Note that the second term of the integrand originates from the electric field variation in time, not in space. For a static field we can therefore write Eq.(2.17) as

$$\Delta P_z = -\frac{qz}{V}\int_{-x_1}^{x_1}\frac{dE_x}{dx}dx = -\frac{qz}{V}E_x\Big|_{-x_1}^{x_1} \quad . \qquad (2.18)$$

Since by assumption $E_x(x)$ vanishes at both limits, $\pm x_1$, Eq.(2.19) gives zero for the momentum change. This, of course, is not surprising as we have assumed that both z and velocity v do not change when the ion passes through the lens.

In the case of a time-varying field, we can express Δp_z as:

$$\Delta P_z = -\frac{qz}{V}\int_{-x_1}^{x_1} d\left[\mathcal{E}_x(x)\cos\omega_e t\right] + \frac{qz}{V^2}\int_{-x_1}^{x_1}\frac{\partial}{\partial t}\left[\mathcal{E}_x(x)\cos\omega_e t\right]dx \qquad (2.19)$$

The first term is zero since x is chosen such that $\mathcal{E}_x(x = \pm x_1,\ t) = 0$ for all times. The integrand of the second term may be evaluated as follows:

$$\frac{\partial}{\partial t}\left[\mathcal{E}_x(x)\cos\omega_e t\right] = -\omega_e\,\mathcal{E}_x(x)\sin\omega_e\left(t_c + \frac{x}{V}\right)$$

$$\Delta P_z = -\frac{qz\omega_e}{V^2}\int_{-x_1}^{x_1}\mathcal{E}_x(x)\sin\omega_e\left(t_c + \frac{x}{V}\right)dx \qquad (2.20)$$

Reproduced with permission of the copyright owner. Further reproduction prohibited without permission.

In order to integrate Eq. (2.20) we approximate the actual field by a constant average field $\mathcal{E}_m = \frac{V_o}{2x_1}$. Substituting into Eq. (2.20) we have:

$$\Delta p_z = -\frac{qz}{v^2}\,\mathcal{E}_m\,\omega_e \int_{-x_1}^{x_1} \sin\omega_e\left(t_c + \frac{x}{v}\right) dx$$

$$= -\frac{2qz}{v}\,\frac{V_o}{x_1}\,\sin\theta_c\,\sin\frac{\omega_e x_1}{v} \qquad (2.21)$$

For small $\frac{\omega_e x_1}{v} \ll 1$ we find

$$\Delta p_z = -\frac{2qV_o}{v}\,\frac{\omega_e}{v}\,\sin\theta_c \qquad (2.22)$$

The change in slope, $\Delta(dz/dx)$, is

$$\Delta\left(\frac{dz}{dx}\right)_e = \frac{\Delta p_z}{mv} = -\left(\frac{qV_o}{E_K}\right)\frac{\omega_e}{v}\,z\,\sin\theta_c \qquad (2.23)$$

where the subscript e stand for constant energy.

Now we will consider the other extreme case, namely that the field stays constant in time but the energy of the ion changes. This assumption implies that the transit time, Δt, of the ion is very small compared to the rf period i.e. $\omega_e \Delta t \ll 1$. In this case we can write Eq. (2.15) in the following form,

$$E_x = \mathcal{E}_x(x)\cos\theta_c \qquad (2.24)$$

which corresponds to a static lens with reduced applied voltage by the factor $\cos\theta_c$.

Now let us consider the simplest case. If the x-component of electric field along the x axis is represented by a

Reproduced with permission of the copyright owner. Further reproduction prohibited without permission.

rectangular shape with very short width then there is no z-component of electric field and an ion will gain the energy $2qV_o \cos\theta_c$ without change of the momentum z-component in passing through the gap at rf phase θ_c. However, even in the absence of a vertical field component, vertical focusing takes place due to the energy gain. This can be demonstrated as follows. The energy of the outgoing ion is related with that of the incoming ion by

$$E_+ = E_- + 2qV_o \cos\theta_c \quad . \tag{2.25}$$

Introducing the energy E_c when the ion reaches the gap center line at rf phase θ_c, we can write:

$$E_+ = E_c + qV_o \cos\theta_c \tag{2.26}$$

$$E_- = E_c - qV_o \cos\theta_c \tag{2.27}$$

and the velocity of the outgoing and incoming ion are respectively:

$$V_+ = \sqrt{\frac{2}{m} E_c \left(1 + \frac{qV_o}{E_c} \cos\theta_c\right)} \tag{2.28}$$

$$V_- = \sqrt{\frac{2}{m} E_c \left(1 - \frac{qV_o}{E_c} \cos\theta_c\right)} \tag{2.29}$$

The slope change of the ion trajectory is:

$$\Delta\left(\frac{dZ}{dx}\right)_f = \left(\frac{dZ}{dx}\right)_+ - \left(\frac{dZ}{dx}\right)_- = \frac{\left(\frac{dZ}{dt}\right)_+}{\left(\frac{dx}{dt}\right)_+} - \frac{\left(\frac{dZ}{dt}\right)_-}{\left(\frac{dx}{dt}\right)_-} \quad . \tag{2.30}$$

Reproduced with permission of the copyright owner. Further reproduction prohibited without permission.

Since there is no momentum z-component change,

$$\Delta\left(\frac{dz}{dx}\right)_f = \frac{dz}{dt}\left(\frac{1}{v_+} - \frac{1}{v_-}\right) \tag{2.31}$$

Expanding Eqs.(2.28) and (2.29) in power series of $qV_o/E_c\cos\theta_c$ we get the first order expression:

$$\frac{1}{v_+} - \frac{1}{v_-} = \frac{1}{v_c}\frac{qV_o}{E_c}\cos\theta_c \tag{2.32}$$

Substituting Eq.(2.32) into Eq.(2.31) we get

$$\Delta\left(\frac{dz}{dx}\right)_f = -\frac{qV_o}{E_c}\cos\theta_c\left(\frac{dz}{dx}\right)_- . \tag{2.33}$$

This is the intrinsic focusing effect which an ion experiences in crossing the gap due to the energy gain, $2qV_o\cos\theta_c$.

Let us return to the real field. Substituting Eq.(2.24) into Eq.(2.12) we get:

$$\Delta p_z = -qz\cos\int_{-x_1}^{x_1}\frac{d\mathcal{E}_x}{dx}\frac{1}{v}\,dx. \tag{2.34}$$

To integrate Eq.(2.34) the velocities in the positive and the negative x regions are assumed to be constant, namely v_+ and v_- as defined in Eqs.(2.28) and (2.29). Now Eq.(2.34) may be separated for the negative and the positive region:

$$\begin{aligned}\Delta p_z &= -qz\cos\theta_c\left[\frac{1}{v_-}\int_{-x_1}^{0}\frac{d\mathcal{E}_x}{dx}dx + \frac{1}{v_+}\int_{0}^{x_1}\frac{d\mathcal{E}_x}{dx}dx\right]\\ &= -qz\cos\theta_c\,\mathcal{E}_x(0)\left[\frac{1}{v_-} - \frac{1}{v_+}\right]\\ &= -qz\cos\theta_c\,\mathcal{E}_x(0)\frac{qV_o}{v_c E_c}\cos\theta_c\end{aligned} \tag{2.35}$$

Reproduced with permission of the copyright owner. Further reproduction prohibited without permission.

Then the slope change is:

$$\Delta\left(\frac{dz}{dx}\right)_f = \frac{p_{z+}}{mv_+} - \frac{p_{z-}}{mv_-} = \frac{1}{mv_c}\left(\frac{p_{z+}}{\sqrt{1+\frac{qV_o}{E_c}\cos\theta_c}} - \frac{p_{z-}}{\sqrt{1-\frac{qV_o}{E_c}\cos\theta_c}}\right)$$

$$= \frac{1}{mv_c}\left[p_{z+}\left(1-\frac{1}{2}\frac{qV_o}{E_c}\cos\theta_c\right) - p_{z-}\left(1-\frac{1}{2}\frac{qV_o}{E_c}\cos\theta_c\right)\right]$$

$$= \frac{\Delta p_z}{mv_c}\left(1-\frac{1}{2}\frac{qV_o}{E_c}\cos\theta_c\right) - \left(\frac{dz}{dt}\right)_-\left(\frac{qV_o}{E_c}\right)\frac{\cos\theta_c}{v_c} \qquad (2.36)$$

Substituting Δp_z of Eq.(2.35) into Eq.(2.36) and using $\mathcal{E}_x(0) = V_o/b$ (Eq. 2.7)

$$\Delta\left(\frac{dz}{dx}\right)_f = -\left(\frac{qV_o}{E_c}\right)^2 \frac{z}{2b}\cos^2\theta_c\left(1-\frac{1}{2}\frac{qV_o}{E_c}\cos\theta_c\right)$$

$$-\left(\frac{dz}{dt}\right)_-\left(\frac{qV_o}{E_c}\right)\frac{\cos\theta_c}{v_c} \qquad (2.37)$$

If $qV_o/E_c \ll 1$, Eq.(2.37) becomes

$$\Delta\left(\frac{dz}{dx}\right)_f = -\left(\frac{qV_o}{E_c}\right)^2 \frac{z}{2b}\cos^2\theta_c - \frac{qV_o}{E_c}\left(\frac{dz}{dx}\right)_-\cos\theta_c \qquad (2.38)$$

If the ion is injected parallel to the x axis then the last term drops out and we may write

$$\Delta\left(\frac{dz}{dx}\right)_f = -\left(\frac{qV_o}{E_c}\right)^2 \frac{z}{2b}\cos^2\theta_c \qquad (2.39)$$

In a more rigorous analysis where the potential function V(x) given in Eq.(2.6) is taken, integration yields the refined result:

Reproduced with permission of the copyright owner. Further reproduction prohibited without permission.

$$\Delta\left(\frac{dz}{dx}\right)_f = -\frac{2}{\pi}\left(\frac{qV_o}{E_c}\right)^2 \frac{z}{b}\cos^2\theta_c - \left(\frac{qV_o}{E_c}\right)\left(\frac{dz}{dx}\right)_- \cos\theta_c \qquad (2.40)$$

For other geometries, where a ≠ 0, c finite, one expects to get a geometry factor G(a,b,c) and the equation for the change of slope should be of the form,

$$\Delta\left(\frac{dz}{dx}\right)_f = -\left(\frac{qV_o}{E_c}\right)^2 \frac{Gz}{2b}\cos^2\theta_c - \left(\frac{qV_o}{E_c}\right)\left(\frac{dz}{dx}\right)_- \cos\theta_c \qquad (2.41)$$

The general analysis was carried out by Reiser[7] whose geometry factor F is related to G by $G = 4F/\pi$. For a = 0, F = 1, one gets $G = 2/\pi$, in agreement with Eq. (2.40). If we let $\theta_c = 0^\circ$ in Eq.(2.38) we get the corresponding slope change in the static case.

The combined action of the time-variation and energy-variation effects gives

$$\Delta\left(\frac{dz}{dx}\right) = -\left(\frac{qV_o}{E_c}\right)\frac{\omega_e z}{v_c}\sin\theta_c - \left(\frac{qV_o}{E_c}\right)^2 \frac{Gz}{2b}\cos^2\theta_c$$

$$-\left(\frac{qV_o}{E_c}\right)\left(\frac{dz}{dx}\right)_- \cos\theta_c \qquad (2.42)$$

Now, following Reiser[7] we introduce a factor $\Delta\theta_g$ defined by:

$$\Delta\theta_g = \frac{\omega_e b}{v_c}\left(\frac{E_c}{2qV_o}\right)^{1/2} = \frac{2\pi f b}{c}\sqrt{\frac{qV_o}{E_o}} \qquad (2.43)$$

This has a constant value for a given V_o , E_o (rest energy of particle), and rf frequency. Then Eq.(2.42) can be written in the following form:

$$\Delta\left(\frac{dz}{dx}\right) = -\frac{\sqrt{2}\,\Delta\theta_g z}{b}\left(\frac{qV_o}{E_c}\right)^{3/2}\sin\theta_c - \frac{Gz}{2b}\left(\frac{qV_o}{E_c}\right)^2\cos^2\theta_c - \left(\frac{qV_o}{E_c}\right)\left(\frac{dz}{dx}\right)_-\cos\theta_c \qquad (2.44)$$

Reproduced with permission of the copyright owner. Further reproduction prohibited without permission.

Eq.(2.44) reveals the fundamental features of the two-dimensional electric lenses with time-varying potential. The first term represents the time-varying nature of the electric field and is negative (focusing) for positive phases and positive (defocusing) for negative phases. The coefficient of the sine term is directly proportional to the factor $\Delta\theta_g$ or the rf frequency. The second term, derived from the static approximation, is always focusing and the coefficient is independent of rf frequency, Thus, for large rf frequency the sine term dominates and negative phases give defocusing. The overall effects of the combined two first terms may be either focusing or defocusing depending on the phase as well as the magnitudes of the coefficients. The slope change decreases rapidly as the energy increases. By setting both $\Delta(dz/dx)$ and $(dz/dx)_-$ to zero, we can find the particular phase which yields zero change of slope for given V_o , E_c , rf frequency, and geometry. This particular phase is called the "transition phase" and denoted by θ_t in subsequent discussion.

Reproduced with permission of the copyright owner. Further reproduction prohibited without permission.

2.2 The Effects of Grids on the Focusing Action on the Lens

As we have seen at the end of the last section, the focusing strength may be improved either by adjusting operating conditions or, to some extent, by optimizing the geometry. However, in practice the possibilities for adjusting such parameters are usually quite limited. In a cyclotron, for instance, the rf frequency is a fixed parameter and quite often gap size as well as the dee voltage are also determined by other requirements. The only possibility to improve the situation in such a case is to place grids or posts at the exit side of the lens gap, thereby reducing the defocusing force in this part of the gap. A similar technique was adopted in linear accelerators to improve transverse focusing.[12,13,24]

Consider an idealized case. Let the lens opening at $x= a$ be completely covered with a thin foil or rather a fine wire mesh which is so dense that all the lines of force terminate on the grid. The potential distribution in this case is also two-dimensional with no variation in y direction. As before, at far left, say $x=-x_2$, the electric field vanishes. But at the surface of the grid, $x= a$, $\mathcal{E}_x(a)=\mathcal{E}_g$. In this case we will consider, as in the previous case, the field variation and the energy variation effects separately.

Let us first discuss the field variation effect. In this case Eq.(2.19) becomes,

$$\Delta P_z = -\frac{qz}{V}\int_{-x_2}^{a} d\left(E_x(x,t)\right) - \frac{qz\omega_e}{V^2}\int_{-x_2}^{a} \mathcal{E}_x \sin\omega_e\left(t_c+\frac{x}{V}\right) dx \qquad (2.45)$$

Reproduced with permission of the copyright owner. Further reproduction prohibited without permission.

In order to obtain a simple expression which we can easily compare with the no-grid results, let us choose the geometry in such a way that we can approximate as follows: $\mathcal{E}_x = \mathcal{E}_g = V_o/b$ for $-x_2 < x < a$, and $\mathcal{E}_x = 0$ out side this region. This implies that $a + x_2 = 2b$ and we may choose our upper and lower limits for the integrals in Eq.(2.45) as +b and -b, respectively, i.e.

$$\Delta p_z = -\frac{qz}{v}\int_{-b}^{b} d(E_x \cos\omega_e t) - \frac{qz\omega_e}{v^2}\int_{-b}^{b} \mathcal{E}_g \sin\omega_e(t_c+\frac{x}{v})\,dx \qquad (2.45a)$$

The first term, which was zero in the previous no-grid case, no longer vanishes, but has the value $-\frac{qz}{v}\mathcal{E}_g \cos\omega_e(t_c+\frac{b}{v})$. The second term is readily integrated, as before, and the total momentum change becomes

$$\Delta p_z = -\frac{qz}{v}\mathcal{E}_g \cos\omega_e(t_c+\frac{b}{v}) + \frac{qz}{v}\mathcal{E}_g\left[\cos\omega_e(t_c+\frac{b}{v}) - \cos\omega_e(t_c-\frac{b}{v})\right] \qquad (2.46)$$

and therefore,

$$\Delta p_z = -\frac{qz}{v}\mathcal{E}_g\left(\cos\theta_c \cos\frac{\omega_e b}{v} + \sin\theta_c \sin\frac{\omega_e b}{v}\right) \qquad (2.47)$$

With the assumption $\frac{\omega_e b}{v} \ll 1$ and $\mathcal{E}_g = \frac{V_o}{b}$ one finally obtains

$$\Delta p_z = -\frac{qz}{v}\frac{V_o}{b}\cos\theta_c - \frac{qzV_o}{v}\frac{\omega_e}{v}\sin\theta_c \qquad (2.48)$$

The corresponding change in slope is

Reproduced with permission of the copyright owner. Further reproduction prohibited without permission.

$$\Delta\left(\frac{dz}{dx}\right)_e = -\left(\frac{qV_o}{E_c}\right)\frac{z}{2b}\cos\theta_c - \left(\frac{qV_o}{E_c}\right)\frac{\omega_e z}{2V_c}\sin\theta_c \qquad (2.49)$$

Now we will consider the energy variation effect. Following the same procedure that led to Eq.(2.35) and using again the assumption $\mathcal{E}_x = \mathcal{E}_g = \frac{V_o}{b}$ in a region of width $\Delta x = 2b$, we can write

$$\Delta p_z = -qz\cos\theta_c\left(\frac{1}{V_-}\int_{-b}^{o} d\mathcal{E}_x + \frac{1}{V_+}\int_{o}^{b} d\mathcal{E}_x\right) \qquad (2.50)$$

With $\mathcal{E}_x(-b) = 0$, $\mathcal{E}_x(0) = \mathcal{E}_x(b) = \mathcal{E}_g = \frac{V_o}{b}$ one obtains

$$\Delta p_z = -\frac{qz}{V_-}\mathcal{E}_g\cos\theta_c$$

which may also be written in the form;

$$\Delta p_z = -qz\mathcal{E}_g\cos\theta_c\left(\frac{1}{V_-} - \frac{1}{V_+}\right) - \frac{1}{V_+}qz\mathcal{E}_g\cos\theta_c \qquad (2.51)$$

The first term of Eq.(2.51) is identical to the momentum change in the absence of a grid. The second term represents the cancellation of defocusing action in the positive x region due to the grid. By similar arguments used in the previous case we can express the slope change in the following way.

$$\Delta\left(\frac{dz}{dx}\right)_f = \frac{\Delta p_z}{mV_c}\left(1 - \frac{1}{2}\frac{qV_o}{E_c}\cos\theta_c\right) - \frac{qV_o}{E_c}\left(\frac{dz}{dx}\right)_- \cos\theta_c$$

$$= \frac{(\Delta p_z)_{\text{no-grid}}}{mV_c}\left(1 - \frac{1}{2}\frac{qV_o}{E_c}\cos\theta_c\right) - \frac{qV_o}{E_c}\left(\frac{dz}{dx}\right)_- \cos\theta_c$$

$$- \frac{1}{V_+}qz\mathcal{E}_g\cos\theta_c\frac{1}{mV_c}\left(1 - \frac{1}{2}\frac{qV_o}{E_c}\cos\theta_c\right)$$

Reproduced with permission of the copyright owner. Further reproduction prohibited without permission.

Together the first and second terms become exactly the same as the slope change in the no-grid case with static approximation given by Eq.(2.37). Retaining up to the first order terms of power series expansion of $\frac{1}{V_+}$, we get;

$$\frac{1}{V_+} = \frac{1}{V_c}\left(1 - \frac{1}{2}\left(\frac{qV_o}{E}\right)\cos\theta_c\right) .$$

Substituting this expression into $\frac{1}{V_+}$ of the third term of the above expression, we get:

$$3\text{rd term} = -\frac{qz\mathcal{E}_g}{mV_c^2}\cos\left(1 - \frac{1}{2}\frac{qV_o}{E_c}\cos\theta_c\right)^2$$

$$= -\frac{qV_o}{E_c}\frac{z}{2b}\cos\theta_c - \left(\frac{qV_o}{E_c}\right)^2\frac{z}{2b}\cos^2\theta_c$$

$$-\left(\frac{qV_o}{E_c}\right)^3\frac{z}{8b}\cos^3\theta_c$$

Therefore, the slope change $\Delta(dz/dx)$ is:

$$\Delta\left(\frac{dz}{dx}\right)_f = -\left(\frac{qV_o}{E_c}\right)\frac{z}{2b}\cos^2\theta_c - \left(\frac{qV_o}{E_c}\right)^3\frac{z}{4b}\cos^3\theta_c$$

$$-\left(\frac{qV_o}{E_c}\right)\frac{z}{2b}\cos\theta_c - \left(\frac{qV_o}{E_c}\right)^2\frac{z}{2b}\cos^2\theta_c - \left(\frac{qV_o}{E_c}\right)^3\frac{z}{8b}\cos^3\theta_c$$

$$-\left(\frac{qV_o}{E_c}\right)\left(\frac{dz}{dx}\right)_-\cos\theta_c$$

$$= -\left(\frac{qV_o}{E_c}\right)\frac{z}{2b}\cos\theta_c + \left(\frac{qV_o}{E_c}\right)^3\frac{z}{8b}\cos^3\theta_c - \frac{qV_o}{E_c}\left(\frac{dz}{dx}\right)_-\cos\theta_c \quad (2.52)$$

The total slope change is the sum of the time-variation and energy-variation effects. Combining Eqs.(2.47) and (2.52) we have:

Reproduced with permission of the copyright owner. Further reproduction prohibited without permission.

$$\Delta\left(\frac{dz}{dx}\right)=-\frac{qV_o}{E_c}\frac{z}{b}\cos\theta_c-\left(\frac{qV_o}{E_c}\right)\frac{\omega_e z}{2v}\sin\theta_c$$

$$+\left(\frac{qV_o}{E_c}\right)^3\frac{z}{8b}\cos^3\theta_c-\frac{qV_o}{E_c}\cos\theta_c\left(\frac{dz}{dx}\right)- \qquad (2.53)$$

If (qV_o/E_c) is small we neglect the third term and $\Delta(dz/dx)$ is:

$$\Delta\left(\frac{dz}{dx}\right)=-\left(\frac{qV_o}{E_c}\right)\frac{z}{b}\cos\theta_c-\left(\frac{qV_o}{E_c}\right)\frac{\omega_e z}{2v}\sin\theta_c-\left(\frac{qV_o}{E_c}\right)\cos\theta_c\left(\frac{dz}{dx}\right)-$$

This can also be written in the following form by adding $\frac{qV_o}{E_c}\frac{z}{2b}\cos^2\theta_c$ and substracting the same term.

$$\Delta\left(\frac{dz}{dx}\right)=\Delta\left(\frac{dz}{dx}\right)_{no\text{-}grid}-\frac{qV_o}{E_c}\frac{z}{b}\cos\theta_c\left(1-\frac{qV_o}{2E_c}\cos\theta_c\right) \qquad (2.54)$$

We can see from Eq.(2.54) that by using a grid the focusing action increases by the amount $\frac{qV_o}{E_c}\frac{z}{b}\cos\theta_c\left(1-\frac{qV_o}{2E_c}\cos\theta_c\right)$.

The effectiveness of the grid decreases with increase in energy as well as phase angle. If the grid is not an ideal dense wire mesh like one we considered here, we expect no longer a total cancellation of defocusing action in the positive x region. Thus, the magnitude of the last term of Eq. (2.54) should depend on the geometry of the grid.

Reproduced with permission of the copyright owner. Further reproduction prohibited without permission.

2.3 The Three-Dimensional Lens with Posts

In practice a dense grid would stop a large fraction of the ions and thereby diminish its usefulness. This disadvantage can be avoided by using two posts placed at the exit side of the lens opening. In this case one obtains a three-dimensional lens with focusing or defocusing action in both z and y direction. Two posts defining a slit (through which the beam passes) of height $\Delta Z = 2b$ and width $\Delta y = W$, would reduce the z-force component in the exit region at the expense of introducing a y-force component. The result would be a weakening of the defocusing effect in the z direction while getting a defocusing force in the y direction. In cyclotrons such a "redistribution" of the transverse forces would be acceptable as there is usually sufficient focusing in the radial (or y) direction from the magnetic field. Another function of posts is to reduce the effective gap width, and hence the transit time of the particle, which also influences the focusing effect of the lens. In some cases it could even be desirable to have posts on both exit and entrance side of the gap. For this investigation we have considered both cases, i.e. posts on the exit side only as well as posts on either side of the gap. In a three-dimensional lens configuration such as this the following equation holds:

$$-\frac{\partial E_z}{\partial z} = \frac{\partial E_x}{\partial x} + \frac{\partial E_y}{\partial y} \qquad (2.55)$$

Reproduced with permission of the copyright owner. Further reproduction prohibited without permission.

If posts are present on either side the potential function satisfies the symmetry properties

$$V(x,y,z) = V(x,y,-z) = V(x,-y,z) = V(x,-y,-z)$$

$$V(x,y,z) = -V(-x,y,z)$$

$$V(\pm\infty,y,z) = \mp V_o$$

With posts on one side only the potential function is not symmetric with respect to x. Expanding the potential function along the x axis by Taylor series, one has;

$$V(x,y,z) = V(x,0,0) + \frac{1}{2}\left(\frac{\partial^2 V}{\partial z^2}\right)_{\substack{z=0\\y=0}} z^2 - \frac{1}{2}\left(\frac{\partial^2 V}{\partial y^2}\right)_{\substack{z=0\\y=0}} y^2 - \frac{1}{2}\left(\frac{\partial^2 V}{\partial z \partial y}\right)_{\substack{z=0\\y=0}} yz \quad (2.56)$$

The force in z and y direction are

$$F_z = -q\frac{\partial V}{\partial z} = -q\left[\left(\frac{\partial^2 V}{\partial z^2}\right)_{\substack{z=0\\y=0}} z - \left(\frac{\partial^2 V}{\partial z \partial y}\right)_{\substack{z=0\\y=0}} y\right] \quad (2.57)$$

$$F_y = -q\frac{\partial V}{\partial y} = -q\left[\left(\frac{\partial^2 V}{\partial y^2}\right)_{\substack{z=0\\y=0}} y - \left(\frac{\partial^2 V}{\partial z \partial y}\right)_{\substack{z=0\\y=0}}\right] \quad (2.58)$$

From Eqs.(2.55) and (2.57), and (2.58) we get

$$F_z = -q\left[\left(\frac{\partial E_x}{\partial x}\right)_{\substack{z=0\\y=0}} z + \left(\frac{\partial E_y}{\partial y}\right)_{\substack{z=0\\y=0}} z + \left(\frac{\partial E_y}{\partial z}\right)_{\substack{z=0\\y=0}} y\right] \quad (2.59)$$

$$F_y = -q\left[\left(\frac{\partial E_x}{\partial x}\right)_{\substack{z=0\\y=0}} y + \left(\frac{\partial E_z}{\partial z}\right)_{\substack{z=0\\y=0}} y + \left(\frac{\partial E_z}{\partial y}\right)_{\substack{z=0\\y=0}} z\right] \quad (2.60)$$

If we restrict the ion trajectory to either the x-y plane or x-z plane we can treat each case as a quasi-two-dimensional lens and determine the focusing properties in each plane separately. In this case the last "coupling" terms in Eqs.(2.59) and (2.60) are zero. The major difference to the strictly two-dimensional lens is the fact that the z force

Reproduced with permission of the copyright owner. Further reproduction prohibited without permission.

depends on the derivative of the field in x as well as y direction. Knowledge of the potential V(x) along the x axis and dV(x)/dx alone is no longer sufficient. Following the vertical focusing treatment in the two-dimensional case, we may obtain the vertical and the horizontal focusing action separately in the two planes for this three-dimensional lens.

$$(\Delta P_z)_V = -q \int_{-x_1}^{x_2} \left(\frac{\partial E_x}{\partial x} + \frac{\partial E_y}{\partial y}\right) \frac{z(x)}{v(x)}\, dx \qquad (2.61)$$

$$(\Delta P_y)_H = -q \int_{-x_1}^{x_2} \left(\frac{\partial E_x}{\partial x} + \frac{\partial E_z}{\partial z}\right) \frac{y(x)}{v(x)}\, dx \qquad (2.62)$$

The general behavior of the potential distribution and the corresponding first and second derivatives in x and y direction are schematically shown in Fig.2. From the figure we can see that E_x and $\partial E_x/\partial x$ are positive for negative x and are negative for positive x. By contrast, in the region close to x axis (y = 0, z = 0), $\partial E_y/\partial y$ (and also $\partial E_z/\partial z$) are negative for negative x and are positive for positive x. Of course, the numerical values of these quantities depend on the actual lens geometry, and $\partial E_y/\partial y$ and $\partial E_z/\partial z$ both change along the x axis. Qualitatively we know that the narrower the width of the slit, W, the larger the magnitude of $\partial E_y/\partial y$ will be, and consequently $(\Delta p_z)_V$ will decrease while $(\Delta p_y)_H$ will increase. In other words, by putting

Reproduced with permission of the copyright owner. Further reproduction prohibited without permission.

posts on either side, we transfer part of the vertical focusing force in to a horizontal defocusing force.

For qualitative understanding of the effect of the posts on the exit side of the gap, consider the potential distribution V(x) in Fig.3 which were obtained by computer for three particular lens geometries as will be discussed later. One curve represents the two-dimensional gap with no posts, Geometry 1 ($a/b = .6$, $c/b = 3$) while the two other curves show the behavior for posts on the exit side only Geometry 5 and for posts on either side of the gap, Geometry 4. The "one-side posts" case is seen to reduce the field region and increase the gradient on the exit side ($x > 0$) while approaching to the "no-posts" situation on the left side ($x < 0$). Also the point where $V = 0$ is shifted towards negative x to a point x_o . At x_o the force z-component changes its sign.

Reproduced with permission of the copyright owner. Further reproduction prohibited without permission.

2.4 Definition of Cardinal Points of an Electric lens

All two-dimensionalelectrostatic fields confined in a finite region focus the ion trajectory close to the symmetry plane like an optical lens focuses light rays. The cardinal points of an electrostatic lens are determined by solving the paraxial ray equation. Expressed in the cartesian coordinate system used before, with prime indicating the derivative with respect to x, the two-dimensional nonrelativistic paraxial ray equation is

$$Z'' + \frac{V'}{V} Z' + \frac{V''}{2V} Z = 0 \qquad (2.63)$$

For a derivation of this equation see Appendix A. The most general solution of a second order differential equation contains two constants which should be determined by two initial conditions of each problem. Now let us assume that we have obtained two linearly independent particular solutions of Eq.(2.63), $z_1(x)$ and $z_2(x)$. Then any linear combination of the two independent solutions is a general solution of the equation, i.e.

$$z(x) = A\, z_1(x) + B\, z_2(x) \qquad (2.64)$$

Given the initial conditions

$$z = z_o,\ z' = z'_o \text{ at } x = x_o \qquad (2.65)$$

we get

$$z_o(x_o) = Az_1(x_o) + Bz_2(x_o)$$

Reproduced with permission of the copyright owner. Further reproduction prohibited without permission.

$$z_o'(x_o) = Az_1'(x_o) + Bz_2'(x_o)$$

The constants A and B are then determined by the following equations

$$A = \frac{\begin{vmatrix} z_o(x_o) & z_1(x_o) \\ z_o'(x_o) & z_2'(x_o) \end{vmatrix}}{\Delta} \tag{2.66}$$

$$B = \frac{\begin{vmatrix} z_1(x_o) & z_o(x_o) \\ z_1'(x_o) & z_o'(x_o) \end{vmatrix}}{\Delta} \tag{2.67}$$

where

$$\Delta = \begin{vmatrix} z_1(x_o) & z_2(x_o) \\ z_1'(x_o) & z_2'(x_o) \end{vmatrix}$$

In other words, an ion specified by the initial conditions of Eq.(2.65) follows the trajectory defined by Eq.(2.64) with the constants A and B given by Eqs.(2.66) and (2.67). $z_1(x)$ and $z_2(x)$ are any two linearly independent particular solutions of Eq.(2.63). For simplicity we choose as the two particular solutions the two ion trajectories denoted by $z_f(x)$ and $z_b(x)$ in Fig.4. The trajectory $z_f(x)$ is parallel to the x axis and unity distance above the median plane in the field-free region to the left of the lens and $z_b(x)$ is parallel to the x axis and unity distance below the median plane in the field-free region to the right of the gap. Both trajectories cross the x axis due to the focusing properties of electrostatic lenses. The crossing

Reproduced with permission of the copyright owner. Further reproduction prohibited without permission.

points are denoted by F_2 and F_1 . The exact locations of those points and the slopes of the trajectories after passing through the lens are, of course, not determined until we solve the paraxial ray equation. But let us assume the equation has been solved. The straight line-extraplolation of the incoming and outgoing ion trajectories intersect at points P_2 for $z_f(x)$ and P_1 for $z_b(x)$, respectively. The image- and object-side focal lengths and locations of the two corresponding principal planes, f_2 , f_1, d_2, d_1, are defined as shown in Fig.4. Since we are interested only in the ion trajectory outside of the field region, we can replace the electric field by a lens determined by these four quantities. Such an electric lens can be represented by a model in which an ion travels without experiencing a force until it reaches the gap center line. At this point the lens action is represented by a z displacement of the trajectory and a change of slope. Mathematically this effect can be described by a matrix relating the position and slope of the outgoing ion (z_+ , z'_+) to the incoming vector (z_-, z'_-) as follows:

$$\begin{pmatrix} z_+ \\ z'_+ \end{pmatrix} = \begin{pmatrix} a_{11} & a_{12} \\ a_{21} & a_{22} \end{pmatrix} \begin{pmatrix} z_- \\ z'_- \end{pmatrix} \qquad (2.68)$$

The matrix elements can be expressed in terms of the cardinal-point parameters by the relations:

Reproduced with permission of the copyright owner. Further reproduction prohibited without permission.

$$a_{11} = 1 - \frac{d_2}{f_2} \tag{2.69}$$

$$a_{12} = f_1\left(\frac{d_1}{f_1} + \frac{d_2}{f_2} - \frac{d_1\, d_2}{f_1\, f_2}\right) \tag{2.70}$$

$$a_{21} = -\frac{1}{f_2} \tag{2.71}$$

$$a_{22} = \frac{f_1}{f_2}\left(1 - \frac{d_1}{f_1}\right) \tag{2.72}$$

For a derivation of these equations see Appendix B.

This mathematical representation of the action of an electric lens is also applicable to a time-varying field. From position and slope of the incoming and outgoing trajectory the cardinal points and focal parameters may be determined as in the static case. The only difference is that time is added as an independent parameter. Also, as was pointed out, in the time-varying case the lens can be both focusing as well as defocusing depending on the rf phase at which the ion traverses the gap.

Reproduced with permission of the copyright owner. Further reproduction prohibited without permission.

2.5 Limitation of the Analytic Theory of Two-Dimensional Electric Lenses

All the previously published papers, as well as the derivation presented here, on two-dimensional electric lenses with time-varying fields, were restricted by the assumption that the relative velocity change, $\Delta v/v$, in passing the lens is small compared to unity and that the ion transit time is very short compared to the rf period. The limitation which is imposed by these assumptions can best be demonstrated by a comparison between first-order theory and results obtained by exact integration of the equation of motion by computer. The latest theoretical result for the image-side focal length is the formula by Reiser[7], referred to earlier, who obtained

$$\frac{b}{f_2} = \left(\frac{qV_o}{E_c}\right) \frac{\omega_c b}{v_c} \sin\theta_c + \frac{2F}{\pi} \left(\frac{qV_o}{E_c}\right)^2 \cos^2\theta_c \qquad (2.73)$$

F is a geometry factor which depends on the parameters a, b, c (Fig.1). The first and the second term have the same form as the ones we obtained in Eqs.(2.23) and (2.39) except for the different geometry factor F which has a maximum value of 1.0 for a = 0.

Let us examine the validity of Eq.(2.73) by comparing this equation with the results obtained from exact numerical solutions of the equation of motion which will be

Reproduced with permission of the copyright owner. Further reproduction prohibited without permission.

described in a later chapter. For the convenience of application to lenses with different size or different applied voltage the results will be presented in dimensionless form. Lengths are measured in units of b, energies are expressed in units of E_g ($E_g = 2qV_o$), and time is measured by the corresponding rf phase angle in degrees or radians given by $\theta_c = \omega_e t$. For the purpose of numerical comparison we chose a lens geometry of a/b = .6, c/b = 3.0, and b = 1.5"; the calculations were done for protons, a voltage V_o= 100 kV and three values of rf frequencies, 2.29, 4.58, and 22.9 MHz. The F factor for this case was calculated by Reiser to be .885. Fig.5 shows the normalized convergence b/f_2 plotted against energy E_c/E_g for the three different rf frequencies for a phase of $\theta_c = 45^o$. The dashed lines indicate the analytical results from Eq.(2.73) and points represent the results obtained by exact numerical integration. Fig.6 shows again the difference between the numerical results and the analytical predictions for a given energy factor $E_c/E_g = 1.0$ as a function of phase angle θ_c . From these figures we notice that the analytical theory agrees with the numerical results quite well for all energy ranges if the rf frequency is low, say, less than 4.58 MHz. As the rf frequency increases, however, the discrepancy between analytical theory and numerical results is substantial even at an energy as high as $E_c/E_g = 4.0$. And, according

Reproduced with permission of the copyright owner. Further reproduction prohibited without permission.

to Fig.6, we see, furthermore, that a particular phase angle θ_c at which the convergence changes its sign (we call it the "transition phase") was predicted to occur at $\theta_c = -17^o$ while numerical result gave $+2^o$ for an rf frequency of 22.9 MHz and $E_c/E_g = 1.0$.

Now let us calculate differences in beam spread between the actual beam and the analytically computed beam. For this purpose we use the above results obtained for b/f_2. Let a proton be injected with z = .15" and with such an energy so that it will reach .? MeV at the gap center line at a rf phase $\theta_c = 30^o$. Its z value at x = 10" from the gap center line was computed using the analytically and numerically obtained convergences b/f_2, and the results are listed in Table 1.

Table 1

Vertical displacement of protons
at x = 10" from the gap center line

f(MHz)	E_c/E_g	θ_c (deg)	$z_{num}-z_{an}$	z_{num}
2.29	1	30	.015	-.124
4.58	1	30	.024	-.150
22.9	1	30	.2	-.327

From this table we can see that, for the highest frequency

Reproduced with permission of the copyright owner. Further reproduction prohibited without permission.

22.9 MHz, the analytical theory underestimates the beam spread as much as 60 % while for the two other cases it predicts the actual value to better than 16 %.

Finally, Fig.5 and 6 indicate that the analytic results always tend to overestimate the focusing effect.

From this comparison we conclude that the focal properties of this type of lens can be computed with reasonable accuracy by the analytical method only for low frequencies or short transit times. However, for a high frequency, such as 22.9 MHz in our case, we cannot rely on the analytical method.

The numerical example discussed in this paper was done for protons at conditions that are typical for cyclotrons. We can, however, apply the above arguments to other ions, such as deuterons, alpha particles, etc. as well as to electrons using the scaling rules for different types of charged particles. According to Eq.(2.73) the relative convergence b/f_2 remains the same if the following scaling rules are observed:

$$\frac{qV_o}{E_c} = \frac{V_o}{V_c} = \text{constant} \ , \tag{2.74}$$

where V_c is the voltage equivalent of the particle's kinetic energy. Furthermore,

$$\frac{\omega_e b}{v_c} = \frac{2\pi f b}{\sqrt{\frac{2qV_c}{m}}} = \text{constant} \ . \tag{2.75}$$

Reproduced with permission of the copyright owner. Further reproduction prohibited without permission.

The last relation implies that for given gap height, 2b, the ratio of rf frequency, f, and velocity, v_c, must remain constant. The velocity in turn depends on the charge-to-mass ratio, q/m, and the voltage "equivalent" V_c (nonrelativistically). As an example, the above proton-case value of f=22.9 MHz would scale to $22.9/\sqrt{2}$ = 16.2 MHz for alpha particles ($q/m = \frac{1}{2}(q/m)_{proton}$) if V_o and V_c are kept the same. Considering lenses of different geometric size, the focal length f_2 is proportional to b provided the ratio a/b and c/b remains constant and the scaling rules, Eqs.(2.74) and (2.75) are observed.

The obvious limitation of the analytical theory and the interest in the effects of posts motivated the more detailed numerical investigation by computer methods that will be described in subsequent chapters. It should be mentioned that most of this work was sponsored by the TRIUMF cyclotron project at Vancouver, Canada, where electrical focusing effects play an important role in central-region beam dynamics. The frequency of 22.9 MHz, the elctrode voltage of V_o = 100 kV, and most of the geometric parameters correspond closely to design values for the TRIUMF project. But in view of the scaling laws our results can be easily applied to other cyclotrons or other lenses of the type studied herein.

Reproduced with permission of the copyright owner. Further reproduction prohibited without permission.

CHAPTER III

DESCRIPTION OF COMPUTATIONAL METHODS

3.1 Lens Geometries and Potential Maps

Several cyclotron-type gap geometries were chosen for our study of the focal properties of electric lenses. In practice all such electric lenses are, in a strict sense, three-dimensional as they have boundaries in all three directions. But if gap dimensions (a,b,c) are small compared to the size of the electodes in x and y direction then we can treat the lens as two-dimensional. The upper half of such a two-dimensional electric lens with equipotentials is shown in Fig.7. The bottom half of the lens is exactly symmetric about the x axis. Note that in this study the upper boundary at zero potential (in cyclotrons called "liner") was included. The geometries of three-dimensional lenses with posts are shown in Fig. 8 and the equipotentials in the x-z plane for the case $W' \rightarrow \infty$ are shown in Fig. 9. Whereas in the two-dimensional cases the electrodes were assumed to be infinitesimally thin, perfect conductors, a finite electrode thickness was assumed for the three-dimensional lenses with posts. The values of the geometry parameters for the two- and three-dimensional lenses that were investigated are listed in Table 2. Geometry 4V and Geometry 4H have the same dimensions, but the former is the potential map in the x-z plane and the latter is the

Reproduced with permission of the copyright owner. Further reproduction prohibited without permission.

potential map in the x-y plane. The same is true for Geometry 5V and Geometry 5H.

Table 2

Parameters of lens geometries
(for the definition of each parameter see Figs. 7 and 8)

a. Two-dimensional lens geometries

Geometry	Notation	a/b	c/b
1	G1	.6	3.0
2	G2	1.0	3.0
3	G3	1.6	3.0

b. Three-dimensional lens geometries

Geometry	Notation	a/b	c/b	W/b	W'/b	d/b	Trajectory plane
		$\frac{1}{1.5}$	$\frac{2.6}{1.5}$	$\frac{1}{3}$	$\frac{1}{3}$	$\frac{6}{15}$	
4V	G4V						x-z
4H	G4H	"	"	"	"	"	x-y
5V	G5V	"	"	"		"	x-z
5H	G5H	"	"	"		"	

Theoretically the potential function, V, is uniquely determined by the boundary conditions and the fact that it must satisfy Laplace's equation, $\nabla^2 V = 0$, in the charge free region within the given boundaries. Whether or not V is difficult to calculate depends entirely upon the complexity of the boundary conditions of the given problem.

Reproduced with permission of the copyright owner. Further reproduction prohibited without permission.

Unfortunately, it is impossible to solve Laplace's equation in simple form for the majority of electric lens problems. For the two-dimensional geometries considered herein it is possible to calculate the potential function if the gap width approaches zero (i.e. $a \rightarrow 0$) and, at the same time, c goes to infinity. Under this condition the potential is expressed by Eq.(2.6) presented earlier. The more general case of finite a and c was solved by Reiser[7] by means of a Schwarz-Christoffel transformation. No analytical method has been developed to solve the potential problem of the three-dimensional geometries 4 and 5. In determining the potential distribution of such a complex system, the electrolytic tank analog has in the past been one of the most powerful methods. In recent years, this technique was extensively used in studing ion beam trajectories in the central region of cyclotrons[17,20,25-29]. A fully automatic electrolytic-tank system[17] was built at the University of Maryland. Three-dimensional potential maps were obtained[18] using this facility for the study of vertical ion motion near the ion source of the University of Maryland Cyclotron.

With the increasing use of sophisticated digital computers the relaxation method[19] has become a very powerful technique of field mapping. In this method the partial derivatives in the Laplace equation are replaced by finite differences. The region of interest is divided up into a

Reproduced with permission of the copyright owner. Further reproduction prohibited without permission.

two- or three-dimensional lattice of equidistant mesh points. It can be shown that the potential V(x,y,z) at any given mesh point is the arithmetic mean of the values of V at the six neighboring points plus some error.

$$V(x,y,z) = \frac{1}{6}V(x+h,y,z)+V(x-h,y,z)+V(x,y+h,z) +V(x,y-h,z)+V(x,y,z+h)+V(x,y,z-h) - \frac{h^4}{3\times 4!}\left(\frac{\partial^4 V}{\partial x^4} - \frac{\partial^4 V}{\partial y^4} - \frac{\partial^4 V}{\partial z^4}\right) \qquad (3.1)$$

where h is the spacing between neighboring mesh points. A series of successive approximations produces an ever closer estimate of the true potential at each lattice point. This method is particularly suited to a digital computer due to the very simple arithmetic manipulations involved. The major problem with this method is the limited capacity of computers. For example, typical problems may involve more than half a million points which greatly exceeds the amount of fast storage available in most computers. Nelson[19] at the University of Maryland solved this problem by writing a computer program which uses additional mass storage devices such as magnetic tapes, etc. All of the potential maps in our present study were obtained using Nelson's "Relaxation Code". Potential maps obtained by the digital computer (IBM 360/44) for geometries 1 and 5V are shown in Figs. 7 and 9. The computer program requires

Reproduced with permission of the copyright owner. Further reproduction prohibited without permission.

either potential values on the entire boundary or on part of it when the remaining portions of the boundary are lines or planes of symmetry. In our calculations the electrodes were extended to sufficiently large distance from the gap center line ($x_{max} = 6b$ for two-dimensional cases and $x_{max} = 4.3b$ for the three-dimensional problems) so that the assumption can be made that $V(x_{max}, z) = -V_o$.

Reproduced with permission of the copyright owner. Further reproduction prohibited without permission.

3.2 Numerical Integration of Equations of Motion and Determination of the Cardinal Points

As has been mentioned in the previous chapter, the determination of the cardinal points of an electricl lens requires a complete knowledge of trajectories from the field-free region on the left to the field-free region on the far right of the lens. Since the analytical theory, discussed previously, is limited to short transit times or low frequencies, a more accurate determination of lens parameters was carried out with the computer. The relativistic equations of motion for each of the different lens geometries listed in Table 2 was solved by numerical integration with program PINWHEEL[20] using the University of Maryland's digital computer IBM 7094. Program PINWHEEL integrates numerically by the Runge-Kutta method the relativistic equations of motion in a plane of symmetry of a time-varying electric and static magnetic field. For our purpose of studying electric focusing a magnetic field was not included. At each point of a R-K step the electric field components are calculated by four-point Lagrange interpolation method using the two-dimensional array of potential values supplied as input to the computer. Particle motion and lens properties were calculated in terms of the particle's energy and the rf phase when the particle arrives at the gap center line. With these two independent parameters the initial conditions, i.e. the rf phase angle

Reproduced with permission of the copyright owner. Further reproduction prohibited without permission.

θ_{in} , the injection energy E_{in}, and the ratio of x- and z-components of momentum at the injection point (x_{in}, z_{in}), have to be chosen for each case in such a way that the particle will reach the gap center line, x = 0, with energy E_c and rf phase $\theta = \theta_c$. Such a set of initial conditions was obtained by making time-reversed runs with initial conditions, $\theta = \theta_c$, $E = E_c$, z = 0, t = 0 at x = 0. Letting the particle travel along the x axis far into the field-free region, we obtain the desired initial conditions θ_{in} , E_{in}, x_{in} . Injecting a particle having these initial conditions, plus additional conditions such as $p_{zin} = 0$, $z_{in} = b/10$ we get a particle trajectory corresponding to the particular solution of the paraxial ray equation, $z_f(x)$. The final conditions of the trajectory, after passing through the gap field, are denoted by $E_{out}^{(P)}$(energy), $p_{xout}^{(P)}$, $p_{zout}^{(P)}$(momentum x- and z-components), $\theta_{out}^{(P)}$ (rf phase), $x_{out}^{(P)}$,$z_{out}^{(P)}$ (coordinates). These informations are sufficient to determine the image-side cardinal-point parameters, f_2 and d_2, which, by simple geometry considerations, are given by the relations

$$d_2 = (z_{in} - z_{out}^{(P)}) \frac{p_{xout}^{(P)}}{p_{zout}^{(P)}} + x_{out}^{(P)} \qquad (3.2)$$

Reproduced with permission of the copyright owner. Further reproduction prohibited without permission.

$$f_2 = x_{out} - \frac{p^{(p)}_{xout}}{p^{(p)}_{zout}} z^{(p)}_{out} - d_2 \qquad (3.3)$$

Another linearly independent particular solution is required to determine the remaining lens parameters, f_1 and d_1 . Using Eqs.(2.70) amd (2.72), f_1 and d_1 can be expressed in terms of f_2, d_2 , a_{12} , and a_{22} as follow:

$$f_1 = (f_2 - d_2) a_{22} + a_{12} \qquad (3.4)$$

$$d_1 = a_{12} - d_2 a_{22} \qquad (3.5)$$

f_1 and d_1 could be determined by a backward trajectory, $z_b(x)$ in the same way as f_2 and d_2 were found by a forward trajectory $z_f(x)$. In principle, making backward runs should involve the same amount of effort as one needs for forward runs, and this statement is always true for static conditions. However, if the applied voltage is time-varying, the initial and final conditions for backward runs are a little more difficult to determine. Therefore, we chose a different particular solution which is linearly independent to the incident parallel trajectory. For convenience of computation, we selected a trajectory in such a way that it would pass through the origin (x = 0, z = 0), if there were no electric field. Then from Eq.(2.68) we have following relation:

Reproduced with permission of the copyright owner. Further reproduction prohibited without permission.

$$\begin{pmatrix} z_+ \\ z'_+ \end{pmatrix} = \begin{pmatrix} a_{11} & a_{12} \\ a_{21} & a_{22} \end{pmatrix} \begin{pmatrix} 0 \\ z'_- \end{pmatrix}$$

hence,

$$a_{12} = \frac{z_+}{z'_-} \tag{3.6}$$

$$a_{22} = \frac{z'_+}{z'_-} \tag{3.7}$$

But now

$$z_+ = \left[z_{out}^{(n)} - \frac{p_{zout}^{(n)}}{p_{xout}^{(n)}} x_{out}^{(n)} \right] \frac{p_{xin}}{p_{zin}} \tag{3.8}$$

$$a_{12} = \left(z_{out}^{(n)} - \frac{p_{zout}^{(n)}}{p_{xout}^{(n)}} x_{out}^{(n)} \right) \frac{p_{xin}}{p_{zin}} \tag{3.9}$$

$$a_{22} = \frac{p_{zout}^{(n)}}{p_{xout}^{(n)}} \frac{p_{xin}}{p_{zin}} \tag{3.10}$$

Therefore,

$$f_1 = (f_2 - d_2) \frac{p_{zout}^{(n)}}{p_{xout}^{(n)}} \frac{p_{xin}}{p_{zin}} + \left(z_{out}^{(n)} - \frac{p_{zout}^{(n)}}{p_{xout}^{(n)}} x_{out}^{(n)} \right) \frac{p_{xin}}{p_{zin}} \tag{3.11}$$

and

$$d_1 = \left(z_{out}^{(n)} - \frac{p_{zout}^{(n)}}{p_{xout}^{(n)}} x_{out}^{(n)} \right) \frac{p_{xin}}{p_{zin}} - d_2 \frac{p_{zout}^{(n)}}{p_{xout}^{(n)}} \frac{p_{xin}}{p_{zin}} \tag{3.12}$$

Reproduced with permission of the copyright owner. Further reproduction prohibited without permission.

For the non-parallel trajectory, the initial conditions were the same as in the case of the parallel trajectory except p_{zin} was not zero. The different path resulted in slightly different arrival times at the gap center line, and hence the energy E_c and the phase angle θ_c were not exactly identical to those of the parallel trajectory. But the differences were generally small enough that they could be neglected.

Reproduced with permission of the copyright owner. Further reproduction prohibited without permission.

3.3 The Linear Region and Error Involved in the Numerical Computation

If the effects of electric fields on the particle trajectory are approximated by the action of a lens with cardinal points and parameters f_1 , f_2 , d_1 , d_2 , then the electric force z-component must be linear in z. A linear force gives the same image-side focal length f_2 independent of the displacement z from the axis. The actual field is, of course, nonlinear and can be represented by the potential on the axis through the power series given in Eq.(2.56). Therefore, there is no linear region in a strict sense. But we can define a "linear" region within a tolerable error limit by comparing the f_2 values obtained by exact integration for particles with different displacements z . We have done this for our lens geometries by calculating f_2 for different incident z under static field condition. In fact, this permitted the choice of $z_- = b/10$ for all the computer runs. In Fig. 10 is plotted the percentage error

$$\frac{\Delta f_2}{f_2} = \frac{f_2(b/10) - f_2(z_-)}{f_2(b/10)} \times 100 \qquad (3.13)$$

which was found in this way for the case of geometry 1. We may conclude that, within 30 % of the lens height, the linear approximation is good to within 2 % if $E_c/E_g = 1$, and better than 3 % for $E_c/E_g = 6$. But in the latter case,

Reproduced with permission of the copyright owner. Further reproduction prohibited without permission.

the convergence $1/f_2$ is much smaller than in the former case, and the 3 % error would have much smaller effect on the particle trajectory. No effort was made to evaluate $\Delta f_2/ f_2$ under time-varying conditions, and it was assumed that the linear region obtained for the static case would be typical also for the other geometries and time-varying conditions. In the actual calculation all trajectories stayed within the vertical region of $-.15 < z/b < +.15$. One would, in view of Fig. 10, therefore conclude that the error in f_2 due to non-linear force terms would be less than $\frac{1}{2}$ to 1 %.

In computing the potential distributions by the relaxation method, one has a systematic intrinsic error which is proportional to the fourth power of the mesh size of the spatial lattice[19] . With the mesh size chosen for our calculation, namely h = b/15, this error should be less than 1 %, as was estimated by calculations with the analytically known geometry of Eq.(2.6). The error originating from the slight differences in the parallel and the non-parallel trajectories turned out to be negligible. The energy difference at the gap center line was no more than .03 % of E_c , and the phase angle differed no more than .2 degree. Therefore, the combined error in the values of the focal parameters is estimated to be about 2 % or better. This, of course, is true only if we can neglect space charge effects which, as is well known, can drastically alter the results for

Reproduced with permission of the copyright owner. Further reproduction prohibited without permission.

beams with high intensity. The results presented herein are based on the validity of single-particle dynamics. No attempt was made to include the space charge effects due to the mutual interaction of the particles.

Reproduced with permission of the copyright owner. Further reproduction prohibited without permission.

CHAPTER IV

NUMERICAL RESULTS FOR THE FOCAL PROPERTIES OF THE TWO- AND THREE-DIMENSIONAL ELECTRIC LENSES

4.1 Choice of Parameters for Computer Runs

As mentioned previously, the gap geometries and operating parameters used for the numerical computations were chosen to simulate conditions in the central region of the TRIUMF cyclotron. The particles to be accelerated in this machine are negative hydrogen ions (H^-). In our studies we have used protons instead, but the results are, of course, directly applicable to electric focusing in the case of H^- acceleration. The geometries 1, 4, and 5 have a/b ratios roughly corresponding to the dimensions of the TRIUMF cyclotron acceleration gaps at the first and second gap crossing points of the first orbit. Furthermore, c/b value of geometry 1 also represents the TRIUMF situation. But the c/b ratios of the geometries 4 and 5 were reduced as shown in Table 2 to save computing time. The error is negligible since we know from previously mentioned studies[7] that the field near the median plane is affected significantly only if c/b is small.

To broaden the scope of our investigation we also chose other geometries with different a/b ratios which may represent the acceleration gaps of other cyclotrons or at other gap crossing points of the TRIUMF cyclotron.

In the TRIUMF cyclotron the accelerating system will

Reproduced with permission of the copyright owner. Further reproduction prohibited without permission.

operate at a frequency of 22.9 MHz which is the 5^{th} harmonic of the ions' cyclotron frequency. The dee voltage V_o is 100 kV, i.e. the maximum potential drop across the acceleration gap is 200 kV. We have done all of our computer studies with a value of V_o = 100 kV and for three values of rf frequencies: 22.9, 4.58, and 2.29 MHz. The highest energy value considered in the numerical computation was 1.2 MeV (E_c/E_g= 6) because at that point the analytical theory can be applied, as seen in Fig. 5, and the lowest energy value was .15 MeV (E_c/E_g= .75). In addition five more energy values in between the highest and the lowest values were included in the computation. The numerical computations were made at each phase angle with 15° steps from -75° to +75° for each given geometry, frequency, and energy. In short, the numerical computation were carried out for seven potential maps and three frequencies for each potential map, seven energy values for each frequency and eleven phase angles for each energy value, which amounts to a total of 1617 different cases.

To permit easy application to other operating conditions, the various parameters are presented as dimensionless quantities as follows:

$$1/f_2 \longrightarrow b/f_2$$

$$1/f_1 \longrightarrow b/f_1$$

$$d_2 \longrightarrow d_2/b$$

Reproduced with permission of the copyright owner. Further reproduction prohibited without permission.

$$d_1 \longrightarrow d_1 / b$$

$$E_c \longrightarrow E_c / E_g$$

Beside these quantities, the following parameters are also presented in the Tables which summarize the computer results:

$$\text{THETA-} = \theta_{in}^{(P)} - 2\pi f \frac{x_{in}^{(P)}}{v_{xin}}$$

$$\text{THETA+} = \theta_{out}^{(P)} - 2\pi f \frac{x_{out}^{(P)}}{v_{xout}^{(P)}}$$

$$DE/V(T) = \frac{E_{out} - E_{in}}{E_g \cos \theta_c}$$

The fixed parameters in the computation were:

E_o = 938.254 MeV

V_o = 100 kV

q = 1.602×10^{-19} coulombs

$\Delta x = \Delta y = \Delta z = h = b/15 = .1"$ (unit mesh size)

Now we will consider in detail the criterion for the validity of analytical theory under the present geometric and operational parameters. In deriving the analytical expression for a slope change, we assumed the transit time of an ion was small so that we could approximate; $\cos \omega_c b/v_c = 1$

Reproduced with permission of the copyright owner. Further reproduction prohibited without permission.

and $\sin\omega_e b/v_c = \omega_e b/v_c$. One can see that $\omega_e b/v_c$ is a rf phase angle advanced during the time an ion with an average velocity v_c travels a distance b. The numerical values of $\omega_e b/v_c$ for f = 2.29, 4.58, 22.9 MHz and E_c/E_g = .75, 1, 2, 3, 4, 5, 6 are shown in Table 3.

Table 3

Transit time across a distance b of particles having an average velocity v for f = 2.29, 4.58, 22.9 MHz

	2.29 MHz	4.58 MHz	22.9 MHz
E_c/E_g	$\omega_e b/v_c$(deg)	$\omega_e b/v_c$(deg)	$\omega_e b/v_c$(deg)
.75	5.9	11.9	58.5
1.0	4.1	10.2	50.8
2.0	3.6	7.2	36.0
3.0	2.9	5.9	29.3
4.0	2.6	5.1	25.5
5.0	2.3	4.6	22.8
6.0	2.1	4.2	20.8

From Table 3 one can see that it is indeed possible to replace $\cos\omega_e b/v_c$ by 1 and $\sin\omega_e b/v_c$ by $\omega_e b/v_c$ with maximum error less than 2 % for f =2.29 and 4.58 MHz cases over the entire energy range considered. But when the

Reproduced with permission of the copyright owner. Further reproduction prohibited without permission.

rf frequency is 22.9 MHz the approximations give a maximum error of 48 % and minimum error of 7 % corresponding to the lowest and the highest energies considered. Furthermore in deriving the energy variation term of the first-order theory of electric focusing the electric field was assumed constant in time, $E_x = \mathcal{E}_x(x) \cos \theta_c$ during the ion's travel from -b to +b. But the rf phase angle difference between the two points x = -b and x = +b are 42° at $E_c/E_g = 6$ and 117° at $E_c/E_g = .75$ for f= 22.9 MHz. Therefore, replacing the field by a constant in time cannot be justified.

Based on these arguments and the numbers shown in Fig. 5 we can conclude that the first-order theory can be applied for the case of $\omega_e b/v_c < .35$ radians or 20°. This condition can be, of course, met at either low frequency or high energy or both.

We will call the different rf frequencies 2.29, 4.58, and 22.9 MHz as low, intermediate, and high frequency, respectively.

The computer results for the fields G1, 5V, and 5H are presented in this paper. A more comprehensive and detailed set of computer results can be found in a separate technical report[21].

Reproduced with permission of the copyright owner. Further reproduction prohibited without permission.

4.2 Result for the Two-Dimensional Lens Geometry 1

a. Low Frequency, f = 2.29 MHz, $\Delta\theta_g$= .0885

Table 4

Lens parameters for G1, f = 2.29 MHz

E_c/E_g = .75

THETA DEG	B/F2	B/F1	D2/B	D1/B	THETA- DEG	THETA+ DEG	DE/V(T)
75.0	0.076	0.092	2.459	-2.322	75.9	75.2	1.0057
60.0	0.109	0.159	3.107	-2.981	61.7	60.5	1.0043
45.0	0.151	0.263	3.063	-2.915	47.8	45.2	1.0023
30.5	0.189	0.379	2.936	-2.756	34.4	31.3	0.9995
15.5	0.209	0.461	2.877	-2.675	20.2	15.9	0.9961
0.0	0.205	0.458	2.933	-2.738	4.7	0.4	0.9922
-14.5	0.174	0.368	3.176	-3.013	-10.6	-13.6	0.9890
-29.5	0.122	0.230	3.856	-3.730	-26.8	-28.1	0.9864
-44.5	0.060	0.098	6.185	-6.061	-42.9	-43.2	0.9845
-59.5	-0.000	-0.000	-923.715	904.861	-58.7	-58.3	0.9835
-75.0	-0.048	-0.057	-2.964	2.828	-74.8	-74.0	0.9823

E_c/E_g = 1.0

75.0	0.049	0.057	2.746	-2.666	75.5	74.6	1.0026
60.0	0.067	0.088	3.659	-3.579	60.9	59.8	1.0022
45.0	0.091	0.134	3.695	-3.609	46.4	45.0	1.0007
30.0	0.112	0.181	3.584	-3.486	31.8	30.1	0.9988
15.5	0.123	0.210	3.550	-3.445	17.6	15.6	0.9969
0.5	0.120	0.208	3.681	-3.579	2.6	0.7	0.9947
-14.5	0.101	0.171	4.091	-4.000	-12.6	-14.3	0.9926
-30.0	0.070	0.110	5.208	-5.129	-28.6	-28.9	0.9907
-45.0	0.032	0.046	9.155	-9.057	-44.1	-44.4	0.9891
-60.0	-0.005	-0.006	-43.945	43.414	-59.5	-59.5	0.9885
-75.0	-0.033	-0.037	-3.475	3.385	-74.8	-74.7	0.9875

E_c/E_g = 2.0

74.5	0.017	0.018	3.926	-3.897	74.6	74.6	1.0000
60.0	0.021	0.024	5.713	-5.683	60.2	60.1	0.9998
44.5	0.027	0.033	6.262	-6.230	44.9	44.7	0.9993
30.0	0.032	0.040	6.350	-6.316	30.4	29.7	0.9987
15.5	0.034	0.044	6.506	-6.471	16.0	15.3	0.9981
0.5	0.032	0.042	7.012	-6.978	1.0	0.3	0.9973
-14.5	0.027	0.034	8.239	-8.204	-14.0	-14.7	0.9966
-30.0	0.017	0.021	11.535	-11.493	-29.6	-29.2	0.9959
-44.5	0.006	0.008	25.802	-25.726	-44.2	-44.3	0.9954
-60.0	-0.005	-0.005	-24.755	24.664	-59.8	-59.8	0.9950
-74.5	-0.012	-0.013	-5.113	5.080	-74.4	-74.4	0.9952

Reproduced with permission of the copyright owner. Further reproduction prohibited without permission.

Table 4 (cont.)

$E_c/E_g = 3.0$

THETA DEG	B/F2	B/F1	D2/B	D1/B	THETA- DEG	THETA+ DEG	DE/V(T)
74.5	0.009	0.010	4.855	-4.838	74.6	74.0	0.9995
59.5	0.011	0.012	7.511	-7.492	59.6	59.6	0.9995
45.0	0.013	0.015	8.541	-8.520	45.2	44.6	0.9992
30.0	0.015	0.018	9.009	-8.987	30.2	30.1	0.9988
15.5	0.016	0.019	9.497	-9.474	15.7	15.2	0.9986
0.5	0.015	0.018	10.504	-10.480	0.7	0.2	0.9981
-14.5	0.012	0.014	12.719	-12.692	-14.3	-14.8	0.9977
-30.0	0.007	0.008	19.026	-18.992	-29.8	-29.8	0.9973
-45.0	0.002	0.002	64.882	-64.774	-44.9	-44.4	0.9970
-59.5	-0.003	-0.004	-24.946	24.897	-59.4	-59.4	0.9968
-75.0	-0.007	-0.007	-5.883	5.864	-75.0	-74.9	0.9966

$E_c/E_g = 4.0$

75.0	0.006	0.006	5.503	-5.492	75.0	74.5	0.9993
60.0	0.007	0.007	8.977	-8.963	60.1	59.6	0.9992
44.5	0.008	0.009	10.657	-10.642	44.6	44.6	0.9992
29.5	0.009	0.010	11.526	-11.510	29.6	29.1	0.9989
15.5	0.009	0.011	12.380	-12.362	15.6	15.1	0.9987
0.5	0.009	0.010	13.979	-13.960	0.7	0.1	0.9985
-14.5	0.007	0.007	17.405	-17.383	-14.4	-13.9	0.9982
-29.5	0.004	0.004	27.122	-27.093	-29.4	-28.9	0.9980
-45.0	0.001	0.001	168.369	-168.190	-44.9	-44.9	0.9978
-60.0	-0.003	-0.003	-23.875	23.845	-59.9	-59.4	0.9977
-75.0	-0.005	-0.005	-6.709	6.697	-75.0	-74.5	0.9975

$E_c/E_g = 5.0$

75.0	0.004	0.004	6.197	-6.189	75.0	75.0	0.9993
59.5	0.005	0.005	10.459	-10.448	59.6	59.0	0.9994
44.5	0.006	0.006	12.646	-12.632	44.6	44.1	0.9992
29.5	0.006	0.007	13.948	-13.931	29.6	29.6	0.9991
14.5	0.006	0.007	15.298	-15.280	14.6	14.6	0.9989
0.5	0.006	0.006	17.425	-17.404	0.6	0.6	0.9986
-14.5	0.004	0.005	22.242	-22.217	-14.4	-14.4	0.9985
-29.5	0.002	0.002	37.071	-37.034	-29.4	-29.4	0.9983
-44.5	0.000	0.000	761.786	-761.096	-44.4	-43.9	0.9982
-59.5	-0.002	-0.002	-25.735	25.711	-59.5	-59.0	0.9982
-75.0	-0.003	-0.004	-7.433	7.424	-75.0	-75.0	0.9980

$E_c/E_g = 6.0$

75.0	0.003	0.003	6.828	-6.822	75.0	75.0	0.9991
60.0	0.004	0.004	11.622	-11.614	60.0	60.0	0.9994
45.0	0.004	0.004	14.452	-14.440	45.1	45.0	0.9992
29.5	0.004	0.005	16.302	-16.288	29.6	29.6	0.9990
14.5	0.004	0.005	18.164	-18.149	14.6	14.6	0.9990
0.5	0.004	0.004	20.995	-20.979	0.6	0.6	0.9988
-14.5	0.003	0.003	27.452	-27.431	-14.4	-14.4	0.9987
-29.5	0.001	0.002	48.763	-48.727	-29.4	-29.4	0.9986
-45.0	-0.000	-0.000	-317.714	317.487	-44.9	-44.5	0.9984
-75.0	-0.003	-0.003	-8.082	8.074	-75.0	-75.0	0.9983
-60.0	-0.002	-0.002	-25.475	25.463	-60.0	-60.0	0.9984

Reproduced with permission of the copyright owner. Further reproduction prohibited without permission.

b. Intermediate Frequency, f = 4.58 MHz, $\Delta\theta_g$ = .177

Table 5

Lens parameters for G1, f = 4.58 MHz

E_c/E_g = .75

THETA DEG	B/F2	B/F1	D2/B	D1/B	THETA- DEG	THETA+ DEG	DE/V(T)
75.0	0.130	0.160	1.670	-1.394	77.4	75.0	0.9977
60.0	0.154	0.228	2.427	-2.170	64.2	60.7	0.9953
45.0	0.183	0.324	2.675	-2.419	51.4	46.1	0.9906
30.1	0.205	0.415	2.742	-2.481	38.3	31.5	0.9844
15.1	0.208	0.450	2.806	-2.550	24.1	16.7	0.9774
0.1	0.186	0.399	3.001	-2.770	8.2	1.8	0.9708
-15.0	0.138	0.277	3.576	-3.365	-8.8	-13.2	0.9653
-30.0	0.074	0.132	5.555	-5.288	-25.9	-28.2	0.9614
-45.0	0.003	0.005	110.568	-104.644	-42.8	-43.3	0.9586
-60.0	-0.063	-0.085	-3.647	3.328	-59.2	-58.5	0.9569
-75.0	-0.113	-0.132	-1.148	0.930	-75.1	-73.8	0.9559

E_c/E_g = 1.0

75.0	0.087	0.100	1.713	-1.543	76.3	75.0	0.9959
60.0	0.099	0.130	2.651	-2.493	62.2	60.5	0.9945
45.0	0.114	0.170	3.044	-2.893	48.1	45.8	0.9918
30.0	0.126	0.204	3.223	-3.074	33.8	31.1	0.9881
15.0	0.126	0.214	3.410	-3.265	19.1	16.2	0.9839
0.0	0.111	0.191	3.783	-3.644	3.9	1.3	0.9798
-15.0	0.082	0.136	4.695	-4.556	-11.7	-13.7	0.9761
-30.0	0.043	0.066	7.816	-7.616	-27.7	-28.7	0.9730
-45.0	-0.002	-0.003	-142.240	138.036	-43.6	-43.8	0.9706
-60.0	-0.043	-0.055	-4.418	4.206	-59.4	-58.9	0.9690
-75.0	-0.075	-0.084	-1.406	1.258	-75.0	-74.2	0.9677

E_c/E_g = 2.0

75.0	0.031	0.034	2.125	-2.068	75.3	75.1	0.9956
60.0	0.034	0.038	3.664	-3.609	60.6	60.2	0.9955
45.0	0.037	0.044	4.621	-4.567	45.8	45.4	0.9944
30.0	0.038	0.048	5.272	-5.219	30.9	30.5	0.9932
15.0	0.037	0.047	5.975	-5.923	16.0	15.5	0.9918
0.0	0.031	0.040	7.147	-7.093	1.0	0.6	0.9903
-15.0	0.022	0.027	9.896	-9.830	-14.1	-14.4	0.9890
-30.0	0.009	0.011	21.450	-21.308	-29.3	-29.4	0.9877
-45.0	-0.005	-0.006	-30.315	30.080	-44.5	-44.5	0.9867
-60.0	-0.018	-0.020	-6.167	6.091	-59.7	-59.6	0.9859
-75.0	-0.027	-0.029	-2.151	2.094	-74.9	-74.7	0.9856

Reproduced with permission of the copyright owner. Further reproduction prohibited without permission.

Table 5 (cont.)

$E_c/E_g = 3.0$

THETA DEG	B/F2	B/F1	D2/B	D1/B	THETA- DEG	THETA+ DEG	DE/V(T)
75.0	0.017	0.018	2.549	-2.517	75.2	75.0	0.9961
60.0	0.018	0.020	4.574	-4.543	60.3	60.1	0.9961
45.0	0.019	0.021	6.032	-6.000	45.4	45.2	0.9956
30.0	0.019	0.022	7.195	-7.164	30.4	30.3	0.9950
15.0	0.018	0.021	8.501	-8.468	15.5	15.3	0.9944
0.0	0.014	0.017	10.655	-10.618	0.5	0.3	0.9935
-15.0	0.009	0.011	15.852	-15.801	-14.6	-14.7	0.9927
-30.0	0.003	0.003	47.355	-47.204	-29.6	-29.7	0.9921
-45.0	-0.004	-0.005	-25.552	25.455	-44.7	-44.7	0.9915
-60.0	-0.011	-0.012	-7.278	7.235	-59.8	-59.8	0.9911
-75.0	-0.015	-0.016	-2.675	2.642	-75.0	-74.9	0.9907

$E_c/E_g = 4.0$

75.0	0.011	0.012	2.926	-2.906	75.1	75.0	0.9969
60.0	0.011	0.012	5.377	-5.356	60.2	60.1	0.9967
45.0	0.012	0.013	7.287	-7.265	45.2	45.1	0.9964
30.0	0.012	0.013	8.944	-8.922	30.3	30.2	0.9961
15.0	0.011	0.012	10.889	-10.865	15.3	15.2	0.9956
0.0	0.008	0.009	14.153	-14.124	0.3	0.2	0.9951
-15.0	0.005	0.006	22.548	-22.506	-14.7	-14.8	0.9945
-30.0	0.001	0.001	107.077	-106.875	-29.8	-29.8	0.9941
-45.0	-0.003	-0.004	-24.769	24.712	-44.8	-44.8	0.9937
-60.0	-0.007	-0.008	-8.179	8.151	-59.9	-59.9	0.9934
-75.0	-0.010	-0.010	-3.106	3.084	-75.0	-74.9	0.9931

$E_c/E_g = 5.0$

75.0	0.008	0.008	3.266	-3.252	75.1	75.0	0.9972
60.0	0.008	0.009	6.099	-6.083	60.1	60.1	0.9971
45.0	0.008	0.009	8.447	-8.429	45.2	45.1	0.9969
30.0	0.008	0.009	10.600	-10.580	30.2	30.1	0.9966
15.0	0.007	0.008	13.177	-13.154	15.2	15.2	0.9963
0.0	0.005	0.006	17.631	-17.602	0.2	0.2	0.9959
-15.0	0.003	0.003	29.954	-29.908	-14.8	-14.8	0.9956
-30.0	0.000	0.000	380.480	-379.909	-29.8	-29.8	0.9953
-45.0	-0.003	-0.003	-24.597	24.555	-44.9	-44.9	0.9950
-60.0	-0.005	-0.006	-8.947	8.926	-59.9	-59.9	0.9949
-75.0	-0.007	-0.007	-3.478	3.462	-75.0	-74.9	0.9947

$E_c/E_g = 6.0$

75.0	0.006	0.006	3.577	-3.566	75.1	75.0	0.9975
60.0	0.006	0.006	6.764	-6.752	60.1	60.1	0.9973
45.0	0.006	0.006	9.526	-9.512	45.1	45.1	0.9972
30.0	0.006	0.006	12.172	-12.155	30.1	30.1	0.9971
15.0	0.005	0.005	15.444	-15.426	15.2	15.1	0.9968
0.0	0.004	0.004	21.235	-21.212	0.2	0.1	0.9966
-15.0	0.002	0.002	38.512	-38.472	-14.9	-14.9	0.9963
-30.0	-0.000	-0.000	-644.808	644.094	-29.9	-29.9	0.9961
-45.0	-0.002	-0.002	-24.826	24.794	-44.9	-44.9	0.9957
-60.0	-0.004	-0.004	-9.639	9.623	-59.9	-59.9	0.9956
-75.0	-0.006	-0.006	-3.812	3.800	-75.0	-75.0	0.9958

Reproduced with permission of the copyright owner. Further reproduction prohibited without permission.

c. High Frequency, f = 22.9 MHz, $\Delta\theta_g$ = .885

Table 6

Lens parameters for G1, f = 22.9 MHz

THETA DEG	B/F2	B/F1	D2/B	D1/B	THETA- DEG	THETA+ DEG	DE/V(T)
E_c/E_g =.75							
75.0	0.347	0.397	0.234	0.075	90.7	63.5	0.5327
60.0	0.296	0.385	0.238	-0.066	74.9	52.0	0.5374
44.9	0.230	0.327	0.169	-0.157	57.2	40.4	0.5451
29.9	0.149	0.223	0.019	-0.163	38.2	28.5	0.5545
14.9	0.058	0.088	-0.426	0.058	19.0	16.0	0.5645
-0.1	-0.035	-0.052	1.136	-0.992	0.3	3.1	0.5742
-15.1	-0.126	-0.177	0.328	-0.487	-17.8	-10.2	0.5831
-30.1	-0.209	-0.278	0.155	-0.381	-35.0	-23.9	0.5908
-45.1	-0.282	-0.351	0.059	-0.317	-51.6	-37.9	0.5968
-60.1	-0.341	-0.394	-0.010	-0.265	-67.6	-52.2	0.6013
-75.1	-0.385	-0.412	-0.068	-0.217	-83.2	-66.8	0.6038
E_c/E_g = 1.0							
75.0	0.117	0.124	0.463	-0.245	78.4	73.2	0.8091
60.0	0.105	0.117	0.820	-0.613	63.8	59.1	0.8078
45.0	0.088	0.102	1.227	-1.033	48.9	44.9	0.8066
30.0	0.065	0.078	1.816	-1.623	33.7	30.7	0.8050
15.0	0.038	0.047	3.098	-2.850	18.1	16.3	0.8036
0.0	0.008	0.010	13.628	-12.618	2.4	1.8	0.8023
-15.0	-0.023	-0.028	-4.337	3.945	-13.6	-12.8	0.8013
-30.0	-0.055	-0.064	-1.600	1.387	-29.5	-27.5	0.8006
-45.0	-0.083	-0.094	-0.852	0.673	-45.4	-42.4	0.8000
-60.0	-0.106	-0.116	-0.493	0.324	-61.1	-57.4	0.7997
-75.0	-0.123	-0.129	-0.266	0.099	-76.7	-72.6	0.7994
E_c/E_g = 2.0							
75.1	0.258	0.286	0.361	0.038	85.5	68.1	0.6382
60.0	0.225	0.275	0.491	-0.169	70.8	55.4	0.6392
45.0	0.180	0.237	0.597	-0.366	54.7	42.7	0.6414
30.0	0.124	0.172	0.739	-0.577	37.7	29.7	0.6447
15.0	0.060	0.085	1.187	-0.997	20.1	16.5	0.6487
-0.1	-0.009	-0.012	-6.170	4.547	2.4	2.9	0.6528
-15.1	-0.078	-0.105	-0.516	0.206	-15.0	-11.0	0.6568
-30.1	-0.144	-0.185	-0.232	-0.034	-32.0	-25.1	0.6606
-45.1	-0.202	-0.246	-0.154	-0.109	-48.6	-39.5	0.6637
-60.1	-0.250	-0.285	-0.129	-0.137	-64.7	-54.1	0.6661
-75.1	-0.285	-0.304	-0.122	-0.146	-80.5	-69.0	0.6670

Reproduced with permission of the copyright owner. Further reproduction prohibited without permission.

Table 6 (cont.)

E_c/E_g = 3.0

THETA DEG	B/F2	B/F1	D2/B	D1/B	THETA- DEG	THETA+ DEG	DE/V(T)
75.0	0.070	0.073	0.525	-0.395	76.7	74.2	0.8687
60.0	0.063	0.068	1.003	-0.876	62.0	59.7	0.8678
45.0	0.053	0.059	1.573	-1.450	47.1	45.2	0.8667
30.0	0.040	0.046	2.399	-2.272	32.1	30.6	0.8652
15.0	0.024	0.028	4.182	-4.014	16.9	16.0	0.8637
0.0	0.007	0.008	15.366	-14.811	1.6	1.2	0.8621
-15.0	-0.012	-0.014	-7.588	7.277	-13.9	-13.6	0.8608
-30.0	-0.031	-0.035	-2.636	2.487	-29.4	-28.5	0.8595
-45.0	-0.048	-0.053	-1.378	1.257	-44.9	-43.4	0.8587
-60.0	-0.062	-0.066	-0.771	0.659	-60.4	-58.5	0.8579
-75.0	-0.072	-0.074	-0.377	0.267	-75.8	-73.7	0.8570
E_c/E_g = 4.0							
75.0	0.048	0.049	0.586	-0.498	76.0	74.6	0.8998
60.0	0.043	0.046	1.161	-1.075	61.2	59.9	0.8990
45.0	0.036	0.039	1.857	-1.772	46.3	45.2	0.8980
30.0	0.027	0.030	2.898	-2.807	31.4	30.5	0.8967
15.0	0.017	0.019	5.107	-4.986	16.3	15.7	0.8955
0.0	0.005	0.005	18.267	-17.881	1.1	0.9	0.8941
-15.0	-0.008	-0.009	-10.013	9.777	-14.2	-14.0	0.8928
-30.0	-0.021	-0.023	-3.443	3.335	-29.5	-28.9	0.8918
-45.0	-0.032	-0.035	-1.795	1.709	-44.8	-43.9	0.8908
-60.0	-0.042	-0.044	-0.995	0.914	-60.1	-59.0	0.8903
-75.0	-0.048	-0.049	-0.471	0.393	-75.4	-74.1	0.8900
E_c/E_g = 5.0							
75.0	0.035	0.036	0.647	-0.582	75.7	74.8	0.9184
60.0	0.032	0.033	1.308	-1.244	60.8	60.0	0.9179
45.0	0.027	0.029	2.118	-2.055	45.9	45.2	0.9171
30.0	0.020	0.022	3.336	-3.267	31.0	30.4	0.9162
15.0	0.012	0.014	5.941	-5.847	15.9	15.6	0.9150
0.0	0.003	0.004	21.556	-21.252	0.8	0.7	0.9140
-15.0	-0.006	-0.006	-11.849	11.666	-14.4	-14.2	0.9130
-30.0	-0.015	-0.016	-4.105	4.021	-29.6	-29.2	0.9120
-45.0	-0.024	-0.025	-2.144	2.079	-44.8	-44.2	0.9111
-60.0	-0.031	-0.032	-1.188	1.128	-60.0	-59.3	0.9106
-75.0	-0.035	-0.036	-0.554	0.495	-75.3	-74.4	0.9105
E_c/E_g = 6.0							
75.0	0.027	0.028	0.707	-0.657	75.5	74.8	0.9314
60.0	0.025	0.026	1.441	-1.391	60.6	60.0	0.9307
45.0	0.021	0.022	2.360	-2.310	45.7	45.2	0.9301
30.0	0.016	0.017	3.739	-3.685	30.7	30.3	0.9293
15.0	0.010	0.010	6.720	-6.645	15.7	15.5	0.9285
0.0	0.003	0.003	24.990	-24.741	0.6	0.5	0.9276
-15.0	-0.005	-0.005	-13.252	13.108	-14.5	-14.4	0.9266
-30.0	-0.012	-0.013	-4.664	4.598	-29.6	-29.4	0.9259
-45.0	-0.018	-0.019	-2.449	2.397	-44.8	-44.4	0.9252
-60.0	-0.024	-0.025	-1.356	1.308	-60.0	-59.5	0.9247
-75.0	-0.027	-0.028	-0.627	0.580	-75.2	-74.6	0.9249

Reproduced with permission of the copyright owner. Further reproduction prohibited without permission.

4.3 Results for the three-Dimensional Lens with Posts

4.3.1 Vertical Focusing

a. Low Frequency, f = 2.29 MHz, $\Delta\theta_g$ = .0885

Table 7

Lens parameters for G5V, f = 2.29 MHz

E_c/E_g = .75

THETA DEG	B/F2	B/F1	D2/B	D1/B	THETA- DEG	THETA+ DEG	DE/V(T)
75.0	0.116	0.138	1.488	-1.156	75.9	74.6	1.0889
60.0	0.185	0.263	1.667	-1.007	61.9	59.8	1.0443
44.5	0.253	0.414	1.791	-0.771	47.9	44.9	1.0221
30.0	0.290	0.531	1.992	-0.603	35.1	30.5	1.0138
15.1	0.307	0.604	2.140	-0.500	21.5	15.0	1.0038
0.5	0.307	0.613	2.120	-0.489	7.0	1.1	0.9915
-14.9	0.289	0.566	1.950	-0.563	-9.8	-14.9	0.9841
-29.5	0.252	0.459	1.723	-0.674	-26.1	-28.5	0.9705
-45.0	0.181	0.297	1.612	-0.881	-43.0	-44.0	0.9601
-60.0	0.111	0.156	1.493	-1.057	-59.1	-59.6	0.9448
-74.5	0.040	0.044	1.396	-1.296	-74.3	-73.8	0.8970

E_c/E_g = 1.0

74.5	0.084	0.096	1.423	-1.188	75.0	74.1	1.0729
60.0	0.135	0.176	1.531	-1.083	61.0	60.2	1.0391
45.0	0.179	0.261	1.646	-0.978	46.6	44.8	1.0310
29.5	0.216	0.342	1.694	-0.853	31.7	29.3	1.0218
15.5	0.237	0.394	1.721	-0.775	18.1	15.9	1.0141
0.0	0.237	0.403	1.721	-0.763	2.6	-0.1	1.0064
-15.0	0.219	0.364	1.683	-0.810	-12.7	-15.1	0.9981
-29.5	0.182	0.288	1.640	-0.915	-27.8	-28.6	0.9864
-45.0	0.140	0.203	1.527	-0.992	-43.9	-44.2	0.9828
-59.5	0.089	0.115	1.464	-1.129	-58.9	-58.8	0.9575
-74.5	0.034	0.037	1.409	-1.329	-74.3	-74.3	0.9180

E_c/E_g = 2.0

75.0	0.038	0.040	1.332	-1.230	75.1	74.5	1.0401
59.5	0.064	0.073	1.397	-1.204	59.8	59.1	1.0061
45.0	0.085	0.102	1.445	-1.170	45.4	44.6	1.0009
29.5	0.102	0.128	1.478	-1.133	30.0	29.6	1.0015
15.5	0.110	0.142	1.493	-1.105	16.1	15.7	0.9972
0.5	0.112	0.146	1.495	-1.094	1.1	0.7	0.9924
-14.5	0.106	0.136	1.485	-1.108	-14.0	-14.3	0.9882
-30.0	0.092	0.115	1.461	-1.137	-29.6	-29.4	0.9825
-45.0	0.072	0.086	1.431	-1.187	-44.7	-44.4	0.9721
-59.5	0.048	0.055	1.396	-1.229	-59.3	-58.9	0.9546
-75.0	0.020	0.021	1.387	-1.349	-74.9	-74.9	0.9386

Reproduced with permission of the copyright owner. Further reproduction prohibited without permission.

Table 7 (cont.)

E_c/E_g= 3.0

THETA DEG	B/F2	B/F1	D2/B	D1/B	THETA- DEG	THETA+ DEG	DE/V(T)
75.0	0.024	0.025	1.309	-1.272	75.1	74.5	1.0347
59.5	0.042	0.044	1.356	-1.283	59.6	59.5	1.0000
44.5	0.057	0.064	1.382	-1.198	44.7	44.6	0.9931
29.5	0.067	0.079	1.400	-1.173	29.7	29.1	0.9898
15.0	0.073	0.088	1.417	-1.162	15.3	15.1	0.9968
0.0	0.074	0.090	1.420	-1.158	0.3	0.1	0.9935
-15.0	0.070	0.085	1.414	-1.163	-14.7	-14.9	0.9902
-29.5	0.062	0.073	1.395	-1.175	-29.3	-28.9	0.9750
-44.5	0.050	0.053	1.382	-1.286	-44.3	-44.4	0.9682
-59.5	0.033	0.035	1.366	-1.305	-59.4	-59.4	0.9585
-75.0	0.014	0.015	1.369	-1.343	-75.0	-74.5	0.9445

E_c/E_g = 4.0

74.5	0.018	0.018	1.311	-1.282	74.5	74.0	1.0115
59.5	0.031	0.032	1.345	-1.291	59.6	59.0	0.9946
44.5	0.042	0.044	1.367	-1.293	44.6	44.0	0.9852
30.0	0.050	0.053	1.387	-1.297	30.1	30.1	0.9870
15.0	0.054	0.058	1.395	-1.297	15.2	15.1	0.9827
0.0	0.055	0.059	1.398	-1.298	0.2	0.1	0.9797
-15.0	0.053	0.056	1.396	-1.300	-14.8	-14.9	0.9772
-30.0	0.046	0.049	1.389	-1.304	-29.9	-29.9	0.9750
-44.5	0.037	0.039	1.374	-1.306	-44.4	-44.0	0.9586
-59.5	0.025	0.026	1.364	-1.317	-59.4	-59.0	0.9595
-74.5	0.012	0.012	1.369	-1.348	-74.5	-74.0	0.9367

E_c/E_g = 5.0

75.0	0.014	0.014	1.293	-1.265	75.0	75.0	1.0110
59.5	0.025	0.026	1.331	-1.278	59.6	59.0	0.9859
44.5	0.033	0.035	1.350	-1.276	44.6	44.0	0.9847
29.5	0.040	0.042	1.362	-1.271	29.6	29.0	0.9813
14.5	0.044	0.046	1.369	-1.267	14.6	14.0	0.9777
0.5	0.044	0.047	1.371	-1.267	0.6	0.0	0.9758
-14.5	0.042	0.045	1.370	-1.270	-14.4	-14.0	0.9734
-29.5	0.038	0.040	1.365	-1.276	-29.4	-29.0	0.9719
-44.5	0.030	0.032	1.359	-1.287	-44.4	-44.0	0.9685
-59.5	0.021	0.021	1.348	-1.298	-59.5	-59.0	0.9501
-75.0	0.009	0.010	1.344	-1.320	-75.0	-75.0	0.9429

E_c/E_g = 6.0

74.5	0.012	0.012	1.315	-1.294	74.5	74.0	1.0071
59.5	0.020	0.021	1.340	-1.302	59.5	59.0	0.9812
44.5	0.027	0.028	1.356	-1.301	44.6	44.0	0.9795
29.5	0.033	0.034	1.368	-1.300	29.6	29.0	0.9828
14.5	0.036	0.038	1.375	-1.299	14.6	14.0	0.9797
0.5	0.037	0.039	1.378	-1.299	0.6	0.0	0.9774
-14.5	0.035	0.037	1.377	-1.302	-14.4	-14.0	0.9752
-29.5	0.031	0.033	1.373	-1.307	-29.4	-29.0	0.9731
-44.5	0.025	0.026	1.366	-1.315	-44.4	-44.0	0.9628
-59.5	0.017	0.018	1.361	-1.327	-59.5	-59.0	0.9520
-74.5	0.008	0.008	1.371	-1.354	-74.5	-74.0	0.9427

Reproduced with permission of the copyright owner. Further reproduction prohibited without permission.

b. Intermediate Frequency, f = 4.58 MHz, $\Delta\theta_g$ = .177

Table 8

Lens parameter for G5V, f = 4.58 MHz

E_c/E_g = .75

THETA DEG	B/F2	B/F1	D2/B	D1/B	THETA- DEG	THETA+ DEG	DE/V(T)
75.0	0.153	0.181	1.516	-1.108	77.7	75.2	1.1721
60.0	0.222	0.314	1.674	-0.930	64.9	60.5	1.0770
45.1	0.273	0.447	1.853	-0.750	53.0	45.8	1.0392
30.1	0.301	0.550	1.997	-0.588	40.9	30.9	1.0112
15.1	0.308	0.601	2.039	-0.522	27.3	16.0	0.9928
0.1	0.299	0.595	1.928	-0.539	11.0	1.1	0.9723
-15.0	0.269	0.524	1.731	-0.609	-6.9	-13.9	0.9583
-30.0	0.207	0.380	1.607	-0.757	-24.9	-29.0	0.9422
-45.0	0.145	0.235	1.424	-0.866	-42.3	-44.1	0.9161
-60.0	0.072	0.088	1.312	-1.149	-59.0	-59.2	0.8878
-75.0	-0.001	-0.001	1.521	-1.454	-75.1	-74.4	0.7938

E_c/E_g = 1.0

75.0	0.107	0.122	1.427	-1.152	76.4	75.1	1.1529
60.0	0.156	0.202	1.555	-1.062	62.5	60.4	1.0684
45.0	0.194	0.283	1.666	-0.955	48.6	45.5	1.0448
30.0	0.228	0.359	1.675	-0.817	34.7	30.7	1.0255
15.0	0.238	0.396	1.693	-0.767	20.2	15.7	1.0090
0.0	0.230	0.390	1.663	-0.766	4.9	0.8	0.9945
-15.0	0.198	0.330	1.654	-0.853	-11.0	-14.2	0.9793
-30.0	0.163	0.256	1.542	-0.904	-27.2	-29.3	0.9640
-45.0	0.115	0.167	1.461	-0.996	-43.3	-44.3	0.9461
-60.0	0.063	0.073	1.359	-1.208	-59.2	-59.5	0.9121
-75.0	0.007	0.007	1.584	-1.522	-75.0	-74.6	0.8305

E_c/E_g = 2.0

74.4	0.047	0.050	1.324	-1.214	74.8	74.3	1.0916
59.2	0.072	0.082	1.395	-1.185	59.8	59.1	1.0494
45.0	0.091	0.110	1.442	-1.148	45.8	45.0	1.0321
30.8	0.105	0.132	1.472	-1.116	31.8	31.1	1.0220
15.6	0.111	0.145	1.490	-1.096	16.7	15.1	1.0068
0.6	0.110	0.145	1.490	-1.088	1.7	0.9	1.0033
-14.2	0.102	0.133	1.471	-1.100	-13.2	-13.9	0.9886
-29.2	0.087	0.109	1.444	-1.127	-28.4	-28.9	0.9752
-45.0	0.065	0.077	1.404	-1.181	-44.4	-43.9	0.9696
-59.8	0.040	0.042	1.381	-1.296	-59.5	-58.8	0.9378
-74.4	0.012	0.013	1.469	-1.432	-74.3	-73.9	0.8880

Reproduced with permission of the copyright owner. Further reproduction prohibited without permission.

Table 8 (cont.)

$E_c/E_g = 3.0$

THETA DEG	B/F2	B/F1	D2/B	D1/B	THETA- DEG	THETA+ DEG	DE/V(T)
74.8	0.029	0.030	1.298	-1.251	75.0	74.8	1.0700
59.8	0.046	0.050	1.347	-1.216	60.1	59.9	1.0313
44.6	0.060	0.067	1.383	-1.205	45.0	43.9	1.0139
29.6	0.069	0.080	1.406	-1.191	30.1	29.8	1.0109
15.6	0.074	0.087	1.418	-1.182	16.1	15.8	1.0044
0.6	0.074	0.087	1.421	-1.181	1.1	0.8	0.9976
-14.4	0.069	0.081	1.412	-1.186	-13.9	-14.2	0.9823
-29.4	0.059	0.069	1.396	-1.198	-29.0	-29.2	0.9747
-44.2	0.046	0.052	1.378	-1.220	-43.9	-43.3	0.9654
-59.2	0.029	0.031	1.371	-1.316	-59.0	-59.1	0.9434
-75.0	0.010	0.010	1.439	-1.414	-74.9	-74.1	0.9056

$E_c/E_g = 4.0$

75.0	0.021	0.021	1.288	-1.253	75.1	74.6	1.0885
59.6	0.034	0.036	1.334	-1.242	59.8	59.7	1.0391
44.6	0.044	0.048	1.360	-1.232	44.9	44.3	1.0246
29.6	0.051	0.057	1.377	-1.223	29.9	29.3	1.0194
15.2	0.055	0.062	1.391	-1.220	15.5	15.3	1.0187
0.2	0.056	0.063	1.393	-1.219	0.5	0.3	1.0090
-14.8	0.052	0.059	1.390	-1.225	-14.5	-14.7	1.0056
-29.4	0.045	0.050	1.379	-1.234	-29.1	-28.7	0.9922
-44.4	0.035	0.037	1.369	-1.300	-44.2	-43.7	0.9834
-60.0	0.022	0.023	1.365	-1.320	-59.9	-59.3	0.9732
-75.0	0.008	0.008	1.419	-1.398	-75.0	-74.4	0.9291

$E_c/E_g = 5.0$

74.6	0.016	0.017	1.281	-1.255	74.7	74.0	1.0698
59.2	0.027	0.028	1.322	-1.274	59.3	59.0	1.0384
44.2	0.035	0.037	1.342	-1.277	44.4	44.1	1.0228
29.2	0.041	0.045	1.356	-1.226	29.4	29.1	1.0150
15.2	0.044	0.049	1.365	-1.221	15.4	15.1	1.0181
0.2	0.045	0.050	1.368	-1.221	0.4	0.1	1.0130
-14.8	0.042	0.046	1.366	-1.226	-14.6	-14.9	1.0037
-29.8	0.036	0.038	1.361	-1.290	-29.6	-28.9	0.9981
-44.8	0.028	0.030	1.354	-1.297	-44.7	-43.9	0.9862
-59.4	0.019	0.019	1.351	-1.312	-59.3	-58.9	0.9768
-74.4	0.008	0.008	1.389	-1.371	-74.4	-74.0	0.9379

$E_c/E_g = 6.0$

74.2	0.013	0.014	1.290	-1.267	74.3	74.2	1.0557
59.2	0.022	0.023	1.322	-1.283	59.3	59.2	1.0260
44.6	0.029	0.030	1.344	-1.268	44.7	44.6	1.0208
29.6	0.034	0.036	1.357	-1.266	29.8	29.7	1.0142
15.6	0.037	0.039	1.364	-1.265	15.8	15.7	1.0110
0.6	0.037	0.040	1.368	-1.266	0.8	0.7	1.0052
-14.4	0.035	0.037	1.368	-1.270	-14.2	-14.3	0.9985
-29.4	0.030	0.032	1.364	-1.278	-29.3	-29.3	0.9922
-44.8	0.024	0.025	1.358	-1.311	-44.7	-44.3	0.9873
-59.8	0.016	0.016	1.361	-1.330	-59.7	-59.8	0.9704
-74.8	0.006	0.006	1.405	-1.390	-74.8	-74.8	0.9414

Reproduced with permission of the copyright owner. Further reproduction prohibited without permission.

c. High frequency, f = 22.9 MHz, $\Delta\theta_g$ = .885

Table 9

Lens parameters for G5V, f = 22.9 MHz

E_c/E_g = .75

THETA DEG	B/F2	B/F1	D2/B	D1/B	THETA- DEG	THETA+ DEG	DE/V(T)
75.1	0.266	0.294	0.849	-0.820	94.5	71.2	1.0581
60.0	0.253	0.280	0.716	-0.716	78.2	58.4	0.8292
45.0	0.224	0.262	0.505	-0.530	59.2	45.3	0.7428
29.9	0.181	0.220	0.203	-0.320	39.2	31.7	0.6989
14.9	0.132	0.164	-0.263	-0.012	19.0	17.8	0.6694
-0.1	0.079	0.099	-1.187	0.607	-0.3	3.6	0.6450
-15.1	0.027	0.033	-5.270	3.427	-18.6	-10.8	0.6211
-30.1	-0.025	-0.031	7.018	-5.108	-36.0	-25.4	0.5918
-45.1	-0.074	-0.091	2.649	-2.073	-52.6	-40.2	0.5492
-60.0	-0.122	-0.145	1.715	-1.442	-68.6	-55.3	0.4530
-75.1	-0.167	-0.193	1.262	-1.142	-84.0	-70.4	0.2232

E_c/E_g = 1.0

75.1	0.201	0.220	1.032	-0.874	87.7	73.0	1.1901
60.1	0.204	0.250	0.960	-0.727	73.4	59.3	0.9475
45.0	0.191	0.246	0.838	-0.635	57.1	45.5	0.8521
30.0	0.166	0.199	0.664	-0.578	39.5	31.5	0.7936
15.0	0.132	0.162	0.415	-0.409	21.3	17.3	0.7601
-0.0	0.091	0.113	0.001	-0.119	3.0	2.8	0.7256
-15.1	0.048	0.059	-0.996	0.613	-14.9	-11.8	0.6965
-30.1	0.004	0.005	-23.355	17.599	-32.3	-26.6	0.6625
-45.1	-0.040	-0.048	2.961	-2.435	-49.0	-41.5	0.6153
-60.1	-0.083	-0.096	1.692	-1.492	-65.2	-56.6	0.5342
-75.1	-0.123	-0.139	1.232	-1.170	-80.9	-72.0	0.2853

E_c/E_g = 2.0

75.1	0.095	0.100	1.126	-0.977	78.8	74.6	1.2628
60.0	0.106	0.118	1.128	-0.917	64.4	60.1	1.0474
45.0	0.109	0.129	1.114	-0.862	49.6	45.5	0.9703
30.0	0.105	0.129	1.074	-0.813	34.4	30.8	0.9193
15.0	0.094	0.119	1.011	-0.765	18.8	16.1	0.8811
-0.0	0.078	0.087	0.918	-0.801	2.9	1.3	0.8392
-15.0	0.056	0.062	0.764	-0.689	-13.2	-13.6	0.8072
-30.0	0.031	0.034	0.447	-0.431	-29.3	-28.5	0.7722
-45.0	0.005	0.005	-3.017	2.657	-45.3	-43.6	0.7239
-60.0	-0.023	-0.024	1.688	-1.621	-61.1	-58.7	0.6488
-75.0	-0.049	-0.051	1.205	-1.211	-76.8	-73.9	0.4425

Reproduced with permission of the copyright owner. Further reproduction prohibited without permission.

Table 9 (cont.)

E_c/E_g = 3.0

THETA DEG	B/F2	B/F1	D2/B	D1/B	THETA- DEG	THETA+ DEG	DE/V(T)
75.0	0.058	0.061	1.147	-1.044	76.8	74.9	1.2846
60.0	0.068	0.074	1.158	-1.008	62.2	60.1	1.0768
45.0	0.073	0.083	1.156	-0.974	47.4	45.3	1.0039
30.0	0.073	0.086	1.143	-0.944	32.4	30.5	0.9573
15.0	0.069	0.075	1.116	-0.997	17.2	15.7	0.9173
-0.0	0.059	0.065	1.072	-0.964	1.8	0.8	0.8881
-15.0	0.046	0.051	1.010	-0.921	-13.7	-14.1	0.8542
-30.0	0.030	0.033	0.898	-0.839	-29.2	-29.1	0.8222
-45.0	0.012	0.013	0.596	-0.579	-44.8	-44.2	0.7791
-60.0	-0.007	-0.007	1.828	-1.765	-60.3	-59.3	0.7035
-75.0	-0.026	-0.026	1.186	-1.191	-75.8	-74.4	0.4919

E_c/E_g = 4.0

75.0	0.041	0.041	1.153	-1.097	76.1	74.9	1.2592
60.0	0.049	0.051	1.170	-1.095	61.3	60.1	1.0629
45.0	0.054	0.057	1.181	-1.094	46.5	45.3	0.9983
30.0	0.056	0.059	1.179	-1.086	31.5	30.4	0.9586
15.0	0.053	0.057	1.168	-1.077	16.4	15.5	0.9302
0.0	0.047	0.050	1.147	-1.063	1.2	0.6	0.9057
-15.0	0.038	0.041	1.119	-1.048	-14.0	-14.4	0.8820
-30.0	0.026	0.028	1.072	-1.021	-29.4	-29.4	0.8548
45.0	0.054	0.057	1.181	-1.094	46.5	45.3	0.9983
-60.0	-0.001	-0.001	2.375	-2.311	-60.1	-59.5	0.7475
-75.0	-0.015	-0.016	1.131	-1.135	-75.4	-74.6	0.5603

E_c/E_g = 5.0

75.0	0.031	0.031	1.167	-1.127	75.7	75.0	1.2316
60.0	0.038	0.039	1.181	-1.118	60.9	60.1	1.0463
45.0	0.043	0.045	1.189	-1.109	46.0	45.2	0.9936
30.0	0.045	0.047	1.192	-1.102	31.0	30.3	0.9606
15.0	0.043	0.046	1.189	-1.095	16.0	15.4	0.9377
0.0	0.039	0.042	1.177	-1.087	0.9	0.4	0.9179
-15.0	0.032	0.035	1.159	-1.078	-14.3	-14.5	0.8986
-30.0	0.023	0.025	1.134	-1.067	-29.5	-29.5	0.8756
-45.0	0.013	0.014	1.096	-1.047	-44.8	-44.6	0.8441
-60.0	0.001	0.002	0.942	-0.918	-60.0	-59.6	0.7829
-75.0	-0.010	-0.010	1.128	-1.120	-75.2	-74.7	0.6111

E_c/E_g = 6.0

75.0	0.025	0.025	1.163	-1.129	75.5	75.0	1.2332
60.0	0.031	0.032	1.194	-1.145	60.7	60.1	1.0679
45.0	0.035	0.036	1.210	-1.148	45.8	45.2	1.0090
30.0	0.037	0.039	1.219	-1.148	30.8	30.2	0.9747
15.0	0.036	0.038	1.221	-1.148	15.8	15.3	0.9498
0.0	0.033	0.035	1.218	-1.148	0.7	0.3	0.9284
-15.0	0.028	0.029	1.212	-1.150	-14.4	-14.7	0.9076
-30.0	0.020	0.021	1.204	-1.154	-29.6	-29.7	0.8840
-45.0	0.012	0.012	1.201	-1.167	-44.8	-44.7	0.8442
-60.0	0.002	0.003	1.314	-1.293	-60.0	-59.7	0.7862
-75.0	-0.007	-0.007	1.075	-1.077	-75.2	-74.8	0.6296

Reproduced with permission of the copyright owner. Further reproduction prohibited without permission.

4.3.2 Horizontal Focusing

a. Low frequency, f = 2.29 MHz, $\Delta\theta_g$ = .0885

Table 10

Lens parameters for G5H, f = 2.29 MHz

E_c/E_g = .75

THETA DEG	B/F2	B/F1	D2/B	D1/B	THETA- DEG	THETA+ DEG	DE/V(T)
75.0	-0.056	-0.183	-0.728	-0.297	75.9	74.6	1.0921
60.0	-0.118	0.353	-0.716	-1.165	61.9	59.8	1.0445
44.5	-0.163	0.165	-0.707	-2.130	47.9	44.9	1.0250
30.0	-0.194	0.128	-0.701	-3.022	35.1	30.4	1.0126
15.0	-0.214	0.118	-0.693	-3.606	21.5	15.0	1.0017
0.5	-0.221	0.119	-0.691	-3.645	7.0	1.0	0.9923
-15.0	-0.220	0.135	-0.686	-3.055	-9.8	-15.0	0.9822
-29.5	-0.207	0.173	-0.686	-2.171	-26.1	-28.5	0.9733
-45.0	-0.182	0.298	-0.690	-1.237	-43.0	-44.1	0.9620
-60.0	-0.146	-24.103	-0.697	-0.399	-59.1	-59.7	0.9443
-74.5	-0.095	-0.139	-0.706	0.258	-74.3	-73.8	0.9018

E_c/E_g = 1.0

74.5	-0.047	-0.087	-0.724	-0.004	75.0	74.1	1.0738
60.0	-0.094	-1.593	-0.717	-0.549	61.0	60.2	1.0357
45.0	-0.132	0.363	-0.707	-1.098	46.6	44.8	1.0191
29.5	-0.159	0.222	-0.703	-1.603	31.7	29.3	1.0083
15.5	-0.175	0.193	-0.699	-1.881	18.1	15.4	1.0005
-0.0	-0.182	0.194	-0.696	-1.906	2.6	-0.1	0.9927
-15.0	-0.180	0.220	-0.694	-1.667	-12.7	-15.1	0.9853
-29.5	-0.168	0.301	-0.696	-1.240	-27.8	-28.7	0.9777
-45.0	-0.146	0.806	-0.698	-0.686	-43.9	-44.2	0.9672
-59.5	-0.115	-0.454	-0.703	-0.157	-58.9	-58.8	0.9538
-74.5	-0.072	-0.097	-0.712	0.350	-74.3	-74.4	0.9159

E_c/E_g = 2.0

74.2	-0.027	-0.034	-0.733	0.397	74.3	73.6	1.0489
59.6	-0.053	-0.087	-0.730	0.121	59.9	59.1	1.0220
45.0	-0.074	-0.159	-0.721	-0.091	45.4	44.5	1.0116
29.4	-0.090	-0.378	-0.715	-0.246	29.9	29.5	1.0044
15.8	-0.100	-0.651	-0.710	-0.314	16.4	15.5	1.0008
0.8	-0.104	-0.840	-0.710	-0.342	1.4	1.0	0.9957
-14.2	-0.102	-0.598	-0.708	-0.278	-13.7	-13.4	0.9912
-29.6	-0.094	-0.343	-0.714	-0.176	-29.2	-29.5	0.9860
-45.0	-0.080	-0.153	-0.718	0.005	-44.7	-44.5	0.9789
-59.4	-0.061	-0.091	-0.724	0.233	-59.2	-58.9	0.9701
-74.8	-0.036	-0.042	-0.725	0.518	-74.7	-74.3	0.9412

Reproduced with permission of the copyright owner. Further reproduction prohibited without permission.

Table 10 (cont.)

$E_c/E_g = 3.0$

THETA DEG	B/F2	B/F1	D2/B	D1/B	THETA- DEG	THETA+ DEG	DE/V(T)
75.0	-0.017	-0.020	-0.749	0.523	75.1	74.4	1.0434
59.4	-0.036	-0.050	-0.746	0.324	59.5	59.4	1.0187
44.8	-0.051	-0.082	-0.737	0.177	45.0	44.9	1.0091
29.8	-0.062	-0.115	-0.732	0.070	30.0	29.9	1.0047
14.8	-0.069	-0.142	-0.730	-0.004	15.1	14.9	1.0008
0.8	-0.072	-0.152	-0.730	-0.022	1.1	0.9	0.9974
-14.2	-0.071	-0.142	-0.729	0.014	-13.9	-14.1	0.9940
-29.2	-0.065	-0.116	-0.730	0.100	-29.0	-29.1	0.9901
-44.6	-0.055	-0.085	-0.735	0.223	-44.4	-44.1	0.9847
-59.6	-0.041	-0.054	-0.739	0.385	-59.5	-59.5	0.9767
-75.0	-0.023	-0.026	-0.737	0.581	-75.0	-74.6	0.9532
$E_c/E_g = 4.0$							
74.6	-0.014	-0.016	-0.730	0.579	74.6	73.8	1.0356
59.8	-0.028	-0.034	-0.725	0.457	59.9	59.8	1.0153
44.8	-0.040	-0.052	-0.723	0.352	44.9	44.0	1.0080
30.0	-0.049	-0.069	-0.722	0.272	30.1	30.1	1.0034
15.0	-0.054	-0.080	-0.721	0.223	15.2	15.1	1.0002
-0.0	-0.056	-0.085	-0.720	0.210	0.2	0.1	0.9972
-15.0	-0.055	-0.081	-0.720	0.234	-14.8	-14.9	0.9943
-30.0	-0.050	-0.070	-0.721	0.294	-29.9	-29.9	0.9909
-44.2	-0.043	-0.055	-0.722	0.378	-44.1	-44.0	0.9868
-59.4	-0.031	-0.037	-0.724	0.489	-59.3	-59.2	0.9790
-74.4	-0.018	-0.019	-0.728	0.614	-74.4	-74.2	0.9605
$E_c/E_g = 5.0$							
74.4	-0.012	-0.013	-0.727	0.610	74.4	73.8	1.0312
59.6	-0.023	-0.027	-0.726	0.513	59.7	58.8	1.0140
44.6	-0.032	-0.040	-0.723	0.431	44.7	44.0	1.0071
29.6	-0.040	-0.051	-0.721	0.370	29.7	29.0	1.0032
14.8	-0.044	-0.059	-0.720	0.332	14.9	14.0	1.0004
0.8	-0.046	-0.062	-0.719	0.321	0.9	0.0	0.9980
-14.2	-0.045	-0.060	-0.719	0.339	-14.1	-14.0	0.9954
-29.4	-0.041	-0.053	-0.720	0.384	-29.3	-29.0	0.9923
-44.4	-0.034	-0.042	-0.722	0.450	-44.3	-44.0	0.9883
-59.6	-0.025	-0.029	-0.725	0.538	-59.6	-59.0	0.9818
-74.6	-0.014	-0.015	-0.726	0.635	-74.6	-74.2	0.9643
$E_c/E_g = 6.0$							
74.6	-0.010	-0.010	-0.729	0.632	74.6	74.6	1.0285
59.7	-0.019	-0.022	-0.728	0.552	59.7	59.6	1.0124
44.8	-0.027	-0.032	-0.726	0.483	44.9	44.7	1.0061
29.8	-0.033	-0.041	-0.724	0.431	29.9	29.7	1.0025
14.8	-0.037	-0.047	-0.723	0.399	14.9	14.7	1.0000
0.9	-0.039	-0.049	-0.723	0.390	1.0	0.7	0.9979
-14.2	-0.038	-0.048	-0.723	0.404	-14.1	-13.3	0.9955
-29.2	-0.034	-0.042	-0.724	0.440	-29.1	-28.3	0.9926
-44.3	-0.029	-0.034	-0.725	0.496	-44.2	-44.3	0.9892
-59.3	-0.021	-0.024	-0.727	0.568	-59.3	-58.4	0.9831
-74.4	-0.012	-0.012	-0.729	0.651	-74.4	-74.4	0.9675

Reproduced with permission of the copyright owner. Further reproduction prohibited without permission.

b. Intermediate Frequency, f = 4.58 MHz, $\Delta\theta_g$ = .177

Table 11

Lens parameters for G5H, f = 4.58 MHz

E_c/E_g = .75

THETA DEG	B/F2	B/F1	D2/B	D1/B	THETA- DEG	THETA+ DEG	DE/V(T)
75.0	-0.036	-0.204	-0.736	-0.634	77.7	75.1	1.1745
60.0	-0.102	0.213	-0.722	-1.538	64.9	60.5	1.0790
45.0	-0.152	0.138	-0.710	-2.475	53.0	45.7	1.0403
29.9	-0.187	0.117	-0.697	-3.205	40.9	30.8	1.0137
14.9	-0.210	0.117	-0.686	-3.516	27.3	15.9	0.9922
-0.1	-0.221	0.127	-0.679	-3.254	11.0	1.0	0.9732
-15.0	-0.222	0.155	-0.676	-2.518	-6.9	-14.0	0.9558
-30.0	-0.212	0.218	-0.678	-1.652	-24.9	-29.0	0.9386
-45.0	-0.191	0.470	-0.683	-0.799	-42.3	-44.1	0.9186
-60.0	-0.158	-0.747	-0.692	-0.087	-59.0	-59.2	0.8848
-75.0	-0.111	-0.132	-0.702	0.527	-75.1	-74.4	0.7960

E_c/E_g = 1.0

75.0	-0.031	-0.074	-0.734	-0.172	76.4	75.1	1.1477
60.0	-0.083	3.807	-0.722	-0.749	62.5	60.3	1.0658
45.0	-0.124	0.285	-0.710	-1.276	48.6	45.5	1.0330
30.0	-0.153	0.203	-0.703	-1.704	34.7	30.6	1.0121
15.0	-0.172	0.190	-0.697	-1.887	20.2	15.7	0.9954
-0.0	-0.181	0.204	-0.692	-1.799	4.9	0.7	0.9806
-15.0	-0.181	0.249	-0.690	-1.473	-11.0	-14.3	0.9666
-30.0	-0.172	0.386	-0.692	-0.995	-27.2	-29.3	0.9519
-45.0	-0.153	1.941	-0.695	-0.470	-43.3	-44.3	0.9326
-60.0	-0.123	-0.242	-0.700	0.017	-59.2	-59.5	0.9037
-75.0	-0.083	-0.099	-0.710	0.523	-75.0	-74.6	0.8254

E_c/E_g = 2.0

74.9	-0.021	-0.024	-0.649	0.400	75.4	75.0	1.0962
60.0	-0.049	-0.065	-0.704	0.250	60.6	60.1	1.0403
44.9	-0.073	-0.101	-0.662	0.275	45.8	45.2	1.0205
29.8	-0.091	-0.139	-0.668	0.168	31.0	30.2	1.0085
14.8	-0.102	-0.173	-0.669	0.039	16.1	15.3	0.9986
-0.2	-0.108	-0.185	-0.671	0.017	1.0	0.3	0.9906
-15.2	-0.106	-0.170	-0.671	0.114	-14.1	-14.7	0.9820
-30.1	-0.099	-0.141	-0.667	0.261	-29.2	-29.7	0.9723
-45.0	-0.085	-0.112	-0.675	0.338	-44.4	-44.7	0.9571
-60.0	-0.066	-0.078	-0.688	0.470	-59.7	-59.8	0.9367
-75.0	-0.041	-0.043	-0.707	0.670	-74.9	-74.9	0.8765

Reproduced with permission of the copyright owner. Further reproduction prohibited without permission.

Table 11 (cont.)

$E_c/E_g = 3.0$

THETA DEG	B/F2	B/F1	D2/B	D1/B	THETA- DEG	THETA+ DEG	DE/V(T)
74.9	-0.016	-0.017	-0.587	0.466	75.2	75.0	1.0758
59.9	-0.036	-0.042	-0.657	0.333	60.3	60.1	1.0298
45.0	-0.053	-0.069	-0.674	0.182	45.4	45.1	1.0105
30.0	-0.066	-0.089	-0.656	0.181	30.5	30.2	1.0000
15.0	-0.075	-0.102	-0.645	0.206	15.5	15.2	0.9923
0.0	-0.079	-0.107	-0.644	0.222	0.5	0.2	0.9853
-15.0	-0.078	-0.105	-0.652	0.229	-14.5	-14.8	0.9783
-30.0	-0.071	-0.093	-0.667	0.249	-29.6	-29.8	0.9704
-45.0	-0.060	-0.073	-0.676	0.345	-44.7	-44.9	0.9637
-60.0	-0.045	-0.049	-0.674	0.512	-59.8	-59.9	0.9470
-75.0	-0.027	-0.027	-0.696	0.644	-74.9	-74.9	0.8997

$E_c/E_g = 4.0$

75.0	-0.012	-0.013	-0.692	0.574	75.1	75.0	1.0701
60.0	-0.026	-0.028	-0.690	0.485	60.2	60.1	1.0281
45.0	-0.038	-0.043	-0.693	0.393	45.2	45.1	1.0126
29.9	-0.047	-0.055	-0.699	0.312	30.3	30.1	1.0043
14.9	-0.053	-0.064	-0.698	0.249	15.3	15.1	0.9975
-0.0	-0.056	-0.067	-0.697	0.235	0.3	0.1	0.9917
-15.0	-0.055	-0.064	-0.696	0.273	-14.7	-14.9	0.9861
-30.0	-0.051	-0.057	-0.696	0.349	-29.8	-29.9	0.9794
-45.0	-0.043	-0.046	-0.695	0.440	-44.8	-44.9	0.9705
-60.0	-0.032	-0.033	-0.699	0.539	-59.9	-59.9	0.9560
-75.0	-0.019	-0.019	-0.705	0.637	-75.0	-75.0	0.9172

$E_c/E_g = 5.0$

75.0	-0.010	-0.011	-0.796	0.654	75.1	75.0	1.0562
60.1	-0.021	-0.024	-0.753	0.566	60.1	60.1	1.0205
45.1	-0.032	-0.036	-0.731	0.532	45.2	45.1	1.0068
30.1	-0.039	-0.046	-0.716	0.518	30.2	30.1	0.9989
15.1	-0.045	-0.052	-0.707	0.510	15.2	15.1	0.9927
0.1	-0.047	-0.054	-0.705	0.509	0.2	0.1	0.9874
-14.9	-0.046	-0.053	-0.709	0.516	-14.8	-14.9	0.9821
-29.9	-0.042	-0.048	-0.717	0.530	-29.8	-29.9	0.9764
-44.9	-0.035	-0.040	-0.727	0.548	-44.8	-44.9	0.9681
-60.0	-0.026	-0.029	-0.733	0.589	-59.9	-59.9	0.9550
-75.0	-0.015	-0.016	-0.730	0.662	-75.0	-75.0	0.9193

$E_c/E_g = 6.0$

75.0	-0.009	-0.009	-0.685	0.608	75.1	75.0	1.0598
60.0	-0.019	-0.021	-0.691	0.556	60.1	60.0	1.0280
45.0	-0.027	-0.031	-0.696	0.506	45.1	45.0	1.0172
30.0	-0.034	-0.040	-0.698	0.463	30.2	30.1	1.0099
15.0	-0.038	-0.045	-0.699	0.437	15.2	15.1	1.0045
-0.0	-0.040	-0.048	-0.699	0.432	0.2	0.1	0.9999
-15.0	-0.039	-0.046	-0.699	0.449	-14.8	-14.9	0.9953
-30.0	-0.036	-0.041	-0.699	0.485	-29.9	-29.9	0.9899
-45.0	-0.030	-0.034	-0.698	0.534	-44.9	-44.9	0.9829
-60.0	-0.022	-0.024	-0.700	0.592	-59.9	-60.0	0.9693
-75.0	-0.013	-0.013	-0.708	0.658	-75.0	-75.0	0.9353

Reproduced with permission of the copyright owner. Further reproduction prohibited without permission.

c. High frequency, f = 22.9 MHz, $\Delta\theta_g$ = .885

Table 12

Lens parameters for G5H, f = 22.9 MHz

E_c/E_g = .75

THETA DEG	B/F2	B/F1	D2/B	D1/B	THETA- DEG	THETA+ DEG	DE/V(T)
74.9	0.167	-2.521	-0.923	-1.401	94.5	71.2	1.0718
59.9	0.064	-0.213	-1.079	-1.396	78.2	58.5	0.8399
44.8	-0.022	0.064	-0.165	-0.778	59.2	45.2	0.7540
30.0	-0.089	0.324	-0.669	-0.538	39.2	31.7	0.7067
15.0	-0.141	1.299	-0.722	-0.088	19.0	17.8	0.6743
-0.0	-0.179	-0.123	-0.738	1.366	-0.3	3.7	0.6483
-15.0	-0.206	-0.124	-0.743	1.673	-18.6	-10.7	0.6226
-30.0	-0.221	-0.124	-0.746	1.860	-36.0	-25.4	0.5916
-45.1	-0.226	-0.122	-0.751	1.952	-52.6	-40.2	0.5454
-60.2	-0.221	-0.121	-0.760	1.990	-68.6	-55.4	0.4598
-75.0	-0.207	-0.118	-0.770	1.980	-84.0	-70.5	0.2077

E_c/E_g = 1.0

74.8	0.096	0.522	-0.918	-0.882	87.7	72.8	1.1904
59.9	0.025	-0.309	-1.310	-1.082	73.4	59.3	0.9410
45.0	-0.036	0.168	-0.444	-0.917	57.1	45.5	0.8441
30.0	-0.087	0.400	-0.647	-0.709	39.5	31.5	0.7890
15.1	-0.126	1.092	-0.694	-0.381	21.3	17.3	0.7495
0.0	-0.155	-3.198	-0.714	-0.020	3.0	2.9	0.7174
-15.0	-0.173	-0.148	-0.725	0.913	-14.9	-11.8	0.6870
-30.0	-0.183	-0.126	-0.733	1.283	-32.3	-26.6	0.6527
-45.0	-0.183	-0.118	-0.739	1.466	-49.0	-41.5	0.6041
-60.0	-0.174	-0.110	-0.749	1.571	-65.2	-56.6	0.5146
-74.9	-0.157	-0.098	-0.759	1.661	-80.9	-71.8	0.2657

E_c/E_g = 2.0

75.0	0.024	0.041	-0.874	0.126	78.8	74.5	1.2939
60.0	-0.009	-0.020	-0.387	-0.265	64.4	60.0	1.0613
45.0	-0.038	-0.109	-0.657	-0.210	49.6	45.5	0.9737
29.9	-0.063	-0.211	-0.688	-0.191	34.3	30.8	0.9221
14.9	-0.082	-0.275	-0.701	-0.119	18.7	16.1	0.8837
-0.0	-0.096	-0.217	-0.707	-0.006	2.8	1.3	0.8509
-15.0	-0.103	-0.187	-0.712	0.169	-13.2	-13.6	0.8188
-30.0	-0.105	-0.153	-0.717	0.367	-29.3	-28.5	0.7833
-45.0	-0.100	-0.103	-0.724	0.685	-45.3	-43.5	0.7353
-60.0	-0.090	-0.075	-0.732	0.952	-61.1	-58.7	0.6542
-75.0	-0.073	-0.060	-0.744	1.074	-76.8	-73.9	0.4308

Reproduced with permission of the copyright owner. Further reproduction prohibited without permission.

Table 12 (cont.)

E_c/E_g = 3.0

THETA DEG	B/F2	B/F1	D2/B	D1/B	THETA- DEG	THETA+ DEG	DE/V(T)
75.0	0.009	0.012	-0.872	0.433	76.8	74.8	1.2848
59.9	-0.012	-0.019	-0.647	0.136	62.2	60.1	1.0812
45.0	-0.031	-0.054	-0.700	0.092	47.4	45.3	1.0048
30.0	-0.048	-0.087	-0.710	0.061	32.4	30.5	0.9585
15.0	-0.060	-0.109	-0.712	0.085	17.2	15.7	0.9250
0.0	-0.069	-0.117	-0.715	0.152	1.8	0.8	0.8961
-15.0	-0.073	-0.112	-0.718	0.255	-13.7	-14.1	0.8685
-30.0	-0.073	-0.098	-0.719	0.392	-29.2	-29.1	0.8369
-45.0	-0.068	-0.081	-0.722	0.535	-44.8	-44.2	0.7942
-60.0	-0.059	-0.056	-0.729	0.772	-60.3	-59.3	0.7218
-75.0	-0.046	-0.041	-0.737	0.907	-75.8	-74.4	0.5223

E_c/E_g = 4.0

75.0	0.004	0.005	-0.894	0.573	76.1	74.9	1.2689
60.0	-0.012	-0.016	-0.678	0.314	61.3	60.1	1.0867
45.0	-0.027	-0.038	-0.706	0.271	46.5	45.2	1.0182
30.0	-0.039	-0.057	-0.712	0.245	31.5	30.4	0.9781
15.0	-0.048	-0.071	-0.714	0.250	16.4	15.5	0.9483
-0.0	-0.054	-0.077	-0.716	0.289	1.2	0.6	0.9226
-15.0	-0.057	-0.077	-0.717	0.357	-14.0	-14.4	0.8972
-30.0	-0.056	-0.070	-0.719	0.448	-29.4	-29.4	0.8685
-45.0	-0.051	-0.059	-0.722	0.556	-44.7	-44.5	0.8296
-60.0	-0.043	-0.046	-0.727	0.669	-60.1	-59.5	0.7635
-75.0	-0.033	-0.031	-0.735	0.812	-75.4	-74.6	0.5833

E_c/E_g = 5.0

75.0	0.001	0.001	-1.011	0.754	75.7	75.0	1.2546
60.0	-0.011	-0.014	-0.695	0.407	60.9	60.1	1.0860
45.0	-0.023	-0.030	-0.708	0.369	46.0	45.2	1.0241
30.0	-0.033	-0.043	-0.712	0.345	31.1	30.3	0.9882
15.0	-0.040	-0.053	-0.714	0.344	16.0	15.4	0.9612
-0.0	-0.044	-0.058	-0.715	0.370	0.9	0.4	0.9378
-15.0	-0.046	-0.059	-0.716	0.419	-14.3	-14.6	0.9148
-30.0	-0.045	-0.054	-0.719	0.488	-29.5	-29.6	0.8879
-45.0	-0.041	-0.046	-0.722	0.572	-44.7	-44.6	0.8530
-60.0	-0.034	-0.036	-0.726	0.664	-60.0	-59.7	0.7924
-75.0	-0.025	-0.024	-0.732	0.784	-75.3	-74.7	0.6266

E_c/E_g = 6.0

75.0	0.000	0.000	-4.421	3.836	75.5	75.0	1.2400
60.0	-0.010	-0.012	-0.707	0.472	60.7	60.1	1.0846
45.0	-0.020	-0.025	-0.715	0.433	45.8	45.2	1.0273
30.0	-0.028	-0.035	-0.717	0.408	30.8	30.2	0.9938
15.0	-0.034	-0.043	-0.718	0.404	15.8	15.3	0.9692
-0.0	-0.038	-0.047	-0.719	0.422	0.7	0.3	0.9477
-15.0	-0.039	-0.047	-0.720	0.460	-14.4	-14.7	0.9263
-30.0	-0.038	-0.044	-0.722	0.516	-29.6	-29.7	0.9016
-45.0	-0.034	-0.038	-0.724	0.586	-44.8	-44.7	0.8688
-60.0	-0.028	-0.030	-0.727	0.664	-60.0	-59.7	0.8124
-75.0	-0.020	-0.020	-0.732	0.754	-75.2	-74.8	0.6596

Reproduced with permission of the copyright owner. Further reproduction prohibited without permission.

CHAPTER V

DISCUSSION OF RESULTS

5.1 Trajectories

In most ion optical systems the width of the lens is small compared to the length of the distance the beam travels or the size of the device. In cyclotrons particularly, an ion crosses the acceleration gap many times, and the gap width is usually smaller than the distance to the following gap. In such cases the most important lens effect is the change in the slope of the trajectories, not the Δz displacement experienced by the particles in the lens. This fact is well illustrated in Fig. 11 which shows computed proton trajectories with energy E_c =.2 MeV, and frequency of 22.9 MHz, at various phase angle θ_c for Geometry 1 and Geometry 5V. The electrode edges are at x = -.9" and x = +.9". For Geometry 5V the posts are located on the "downstream" side of the gap only at x = +.9". For comparison we have also included the trajectory for static potential. Note the z scale of Fig. 11 is enlarged by a factor of 50 compared to the x scale in order to amplify the effects and get a better picture. We can infer from the figure that the thick-lens displacement in the time-varying cases are all relatively small, i.e. for practical purpose we can consider the gaps as thin lenses.

Reproduced with permission of the copyright owner. Further reproduction prohibited without permission.

The trajectories in the case of Geometry 5V shown in Fig. 11 are almost straight from x = .9" which indicates that there is no appreciable electric force z component beyond this point, when posts are present. This shows that the posts terminate the field region almost as effectively as an ideal dense wire mesh. Another interesting feature is the fact that the trajectories of Geometry 1 and Geometry 5V almost coincide in the negative x region for all phase angles. This indicates that the posts do not influence the ion trajectory in the negative x region very much and that this part of the gap acts like a lens without posts. These findings justify our treatment of grid focusing in chapter 2.

We have already stated earlier that the difference between the analytically predicted value of b/f_2 and the exact computer results are no longer negligible for the high frequency case. The difference is particularly pronounced for large phase angle θ_c unlike the situation at the low and intermediate frequencies. This can be understood by examining the detailed behavior of the trajectories for the high frequency case keeping in mind that most of the trajectory slope changes take place in the region where $|\partial^2 V/\partial x^2|$ is a maximum. In the case of Geometry 1 these maxima (according to computer results) are at x = -1.3" and x = +1.3", for Geometry 5V these points are at x = -1.4" and x = +1.15".

During the time an ion, having an energy $E_c/E_g = 1$,

Reproduced with permission of the copyright owner. Further reproduction prohibited without permission.

travels from x = -3" to x = +3" the ion encounters the rf wave shown in Fig. 12. Let us consider the particular trajectory with $\theta_c = 75^\circ$, $E_c/E_g = 1.0$, f = 22.9 MHz shown in Fig. 11. Using the relation $t = t_c + x/v$ we can plot the rf wave as function of distance x to indicate which phase of the rf the ion sees during its travel across the gap region. If the electodes on the left are at positive potential and those at the right at negative potential with respect to ground, then a positive ion experiences a focusing force in the left half of the lens and a defocusing force in the right half of the lens, and vice versa. As Fig.12(a) indicates, the $\theta_c = 75^\circ$ ion experiences a focusing force in the entire negative x region and, in addition, the x coordinate where $\cos(\omega_e t+\theta_c)$ reaches its maximum value is very close to the point where $|\partial^2 V/\partial x^2|$ has its maximum value. But when the ion crosses the gap center line the instantaneous field is already very small, going through zero at about x = .5", and consequently the total defocusing action is much weaker than the focusing effect in the negative x region. Beyond the point x = .5" the electric field changes its sign and the ion experiences an additional focusing force. Thus, the gap acts like a sequence of a strong focusing lens in the region $x < 0$, a weak defocusing lens (for $0 < x < .5"$) and a weak focusing lens in the region $x > .5"$. This sequence of action is clearly seen in the change of the 75° ion

Reproduced with permission of the copyright owner. Further reproduction prohibited without permission.

trajectory in Fig. 11. The overall behavior of the lens depends naturally very much on the transit time involved. At lower frequencies (and of course in the static case) where the transit angle is smaller the ion will not experience the change of sign of the potential, and the right side of the gap acts strictly like a defocusing lens. This is illustrated by the static trajectory in Fig. 11 the slope of which decreases monotonically in the negative x region and then increases again monotonically in the positive x region until it leaves the electric field of the lens.

Now consider the third case of Fig.12(c) where $\theta_c = 0^o$. Here one finds that the ion travels under the influence of a relatively small defocusing force (negative polarity of the electric field) until it reaches -2". From that point to the gap center line it experiences a focusing force, and in the positive x region the force is almost entirely defocusing. Thus, we expect a small slope change for this case which is confirmed by the 0^o trajectory in Fig. 11.

Reversing the arguments presented for $\theta_c = +75^o$, we expect a large defocusing action for the $\theta_c = -75^o$ ion. In this case the ion enters the gap field at a decelerating phase, when the z force is directed away from the median plane. Inspection of Fig.12(d) shows that we have in effect a series of three lenses: a strong defocusing lens at the left, a weak focusing one in the middle, and a strong de-

Reproduced with permission of the copyright owner. Further reproduction prohibited without permission.

focusing lens at the right side of the gap. This behavior is well reflected by the trajectory pattern in Fig. 11.

The possibility that both sides of the gap act like either a focusing lens or a defocusing lens depending on the rf phase angle θ_c is a direct consequence of the large transit time at high frequency. As a rough criterion this effect occurs when $\omega_e b/v_c > .3$, i.e. when the thin-lens approximation of the first-order theory is no longer valid. It occurs at large negative and positive phase angles when the particles experience a change in polarity while traversing the gap field and is the more pronounced the larger the frequency or transit time. At phase angles of 75° and f =22.9 MHz one finds this effect according to Table 6 up to energy $E_c/E_g = 3$.

For comparison we have listed in Table 13 the computed b/f_2 value for several phases θ_c at low (2.29 MHz) and high (22.9 MHz) frequency.

Table 13

Typical b/f_2 values in the low and high frequency case for several values of θ_c and $E_c/E_g = .75$

	75°	45°	0°	-75°
f(MHz)	b/f_2	b/f_2	b/f_2	b/f_2
2.29	.127	.167	.153	.116
22.9	.347	.230	-.035	-.385

Reproduced with permission of the copyright owner. Further reproduction prohibited without permission.

5.2 Focal Length and Convergence

The slope change of an ion trajectory passing through an electric lens is given from Eqs.(2.68), (2.71), and (2.72) as follow:

$$z'_+ - z'_- = -\frac{1}{f_2} z_- - \left(1 - \frac{f_1}{f_2} + \frac{d_1}{f_2}\right) z'_- \qquad (5.1)$$

The most important parameter in this equation is the image-side focal length, f_2, or the inverse of it , $1/f_2$, which is called the convergence. According to the analytical theory presented earlier, as well as the numerical results, the convergence of an electric lens which is considered here depends on the geometry, particularly the ratio of a/b, the kinetic energy of the ions, the rf phase, the frequency and the amplitude of the gap voltage.

Figures 13 to 22 illustrate graphically how the normalized convergence, b/f_2 , depends on these various parameters according to the computer results tabulated in the previous chapter. First, in Fig. 13(a), are shown the b/f_2 curves vs energy for the 5 different geometries at a fixed phase of $\theta_c = 45^o$, and a frequency of 22.9 MHz. One sees a clear a/b dependence (Geometries G1 to G3 differ only in the a/b value) at lower energy. The difference, however, decreases rapidly with energy increase and is almost washed out in the region where $E_c/E_g > 3$. Adding posts at the exit side of

Reproduced with permission of the copyright owner. Further reproduction prohibited without permission.

the gap (Geometry 5V) increases the convergence by almost a factor of 2 at large E_c/E_g values. If posts are used at both sides of the gap (Geometry 4V)', however, the convergence is substantially reduced to less than .02 over the entire energy range. This geometry obviously cannot be employed as an electric lens. In Fig 13(b) we plotted b/f_2 for 3 different frequencies in the case of Geometry 1, again at fixed $\theta_c = 45^o$. We see a clear increase with frequency. The two low frequency curves are very similar and decrease more rapidly with energy than the 22.9 MHz case. The marked difference between the two frequency curves and the 22.9 MHz curve clearly demonstrates the effects of large transit time. For comparison the analytical approximation for the 22.9 MHz case has been added. Fig 14 shows the b/f_2 curves for 3 geometries plotted against θ_c at f =22.9 MHz with the three lowest E_c/E_g values as parameters. The solid lines represent the gap without posts (Geometry 1), which clearly shows the strongest phase dependence. With two posts the convergence is always close to zero and shows very little variation with θ_c . One post only has the effect of reducing the defocusing force at large negative phases and increasing the focusing strength in the phase range at the center. At very large positive phases the convergence is somewhat less than in the no-post situation. Thus the net effect of putting in a post on the exit side of the gap is to increase the useful

Reproduced with permission of the copyright owner. Further reproduction prohibited without permission.

phase interval for focusing; also the phase dependence of the convergence is much less pronounced than without the post. In cyclotrons this behavior is very beneficial as it permits the acceptance of a beam with large phase width. The main advantage of using two posts is in reducing the transit time and increasing the energy gain. Depending on what is more important, one has thus the possibility of a trade-off between vertical focusing and energy gain. Due to the similarity of the focusing action of the two-dimensional geometries 1, 2, and 3 the convergence properties of the last two cases, i.e. G2 and G3, have not been plotted.

To display the general lens behavior of Geometry 1 at different conditions we have plotted the b/f_2 curves in Fig. 15 to 19 as function of the rf phase θ_c with energy as parameter and versus energy with phase as a parameter. These curves show the following general features: (a) The absolute value of b/f_2 decreases rapidly with energy leveling off to a constant value at $E_c/E_g > 3$. (b) the spread $\Delta(b/f_2)$ due to different phases at large energies is the greater the larger the frequency; for the phase interval $-75^\circ \leq \theta_c \leq +75^\circ$ one finds roughly $\Delta(b/f_2) = .02$ at 4.53 MHz and a value of .07 at 22.9 MHz. (c) There is a maximum value of b/f_2 for a given (low) energy which shifts towards larger positive phases as the frequency increases; for 22.9 MHz this peak appears to lie beyond the maximum value of $\theta_c = +75^\circ$ that was computed.

Reproduced with permission of the copyright owner. Further reproduction prohibited without permission.

(d) The phase at which $b/f_2 = 0$ (transition phase) occurs is in the neighborhood of $\theta_c = -60^\circ$ for the low frequency of 2.29 MHz and shifts to about $\theta_c = 0^\circ$ in the high-frequency case.

Both the maximum convergence as well as the transition phase will be discussed in a little more detail in the next section.

The fact that in the 22.9 MHz case the lens is diverging for all negative phases and only weakly focusing between 0° and 15° is a disadvantage in an actual cyclotron such as TRIUMF. Usually the maximum energy gain occurs near $\theta_c = 0^\circ$ and one would like to have as large a phase interval with good vertical focusing properties as possible. Fortunately, the incompatibility of good focusing and high energy gain at high frequency can be corrected somewhat by employing posts in the exit side of the gap. The effects of such posts (Geometry 5V) are well illustrated in figures 20 to 22.

These plots clearly show that the phase width for focusing has been substantially increased. In fact the lens is focusing over the entire phase range for both the 2.29 as well as the 4.58 MHz frequencies. At 22.9 MHz the transition phase occurs between about -20° for low E_c/E_g and -60° for high E_c/E_g values. Focusing near $\theta_c = 0^\circ$ is much better than in the no-post case, but still peaks at large phase angles although the magnitude of the peak is lower than in the case without posts. Also the peaks do occur at phases less than 75° (with

Reproduced with permission of the copyright owner. Further reproduction prohibited without permission.

the exception of $E_c/E_g = .75$). For example θ_m (peak-focusing phase) is about 38^o for $E_c/E_g = 3$ in Geometry 5V whereas the peak is at a phase larger than 75^o in Geometry 1. The shift of θ_m towards smaller phase and the increase of magnitude of b/f_2 is a very important improvement because one can have good focusing action as well as large energy gain with the post geometry at the high frequency of 22.9 MHz.

Reproduced with permission of the copyright owner. Further reproduction prohibited without permission.

5.3 Transition Phase and Non-Focusing Phase

Unlike electrostatic lenses which are always focusing an electric lens with time-varying field may also defocus the ion beam depending on the rf phase. Typically the focusing parameter b/f_2 is negative at large negative phases θ_c and then changes sign at a certain rf phase angle which we call the transition phase, θ_t. According to the first-order theory the transition phase can be found by setting $1/f_2 = 0$ and solving for $\theta_c = \theta_t$ in Eq.(2.73). This yields

$$\theta_t = \sin^{-1}\left[\frac{\pi\omega_e b}{2Fv_c}\frac{E_c}{E_g} \pm \sqrt{\frac{\pi\omega_e bE_c}{2Fv_c E_g}+1}\right] \qquad (5.2)$$

From this equation we determined θ_t for the rf frequencies, 2.29, 4.58, and 22.9 MHz and for seven energy values in the case of Geometry 1. These analytical values are compared with the numerically obtained results in Table 14. We see that the analytical formula predicted the transition phase quite accurately for the low frequencies, but, as expected, fails to give correct values in the 22.9 MHz case. Notice, however, that in this latter case agreement gets better as the energy increases. This, of course, is due to the fact that the transit times get shorter at higher energies so that the assumption $\omega_e b/v_c \ll 1$ made in the theory eventually will be met as v_c increases.

Reproduced with permission of the copyright owner. Further reproduction prohibited without permission.

Table 14

Transition phase (degree) obtained by analytical and numerical methods for Geometry 1 and Geometry 5V

		Geometry 1		Geometry 5V
f(MHz)	E_c/E_g	θ_t(an)	θ_t (num)	θ_t (num)
2.?9	.75	-61	-61	
"	1.0	-59	-58	
"	2.0	-53	-54	
"	3.0	-50	-5?	
"	4.0	-47	-48	
"	5.0	-45	-45	
"	6.0	-43	-43	
4.58	.75	-50	-46	-75
"	1.0	-47	-44	
"	?.0	-41	-40	
"	3.0	-36	-36	
"	4.0	-34	-34	
"	5.0	-31	-3?	
"	6.0	-?9	-30	
??.9	.75	-19	+6	-?3
"	1.0	-16	+2	-31
"	?.0	-1?	-4	-48
"	3.0	-10	-5	-59
"	4.0	-9	-5	-59
"	5.0	-8	-5	-62
"	6.0	-7	-5	-64

Reproduced with permission of the copyright owner. Further reproduction prohibited without permission.

Table 14 also shows very clearly the shift of the transition phase in positive direction, as was discussed earlier. There is at a given frequency also a shift towards less negative phase with increase of energy. At the two low frequencies this shift is in the neighborhood of about 20° as E_c/E_g rises from .75 to 6.At 22.9 MHz, on the other hand, the shift in transition phase is only about 10°.

We have already pointed out the effect of putting in posts. The last column in Table 14 presents the numerical results for Geometry 5V. At the lower frequencies θ_t is beyond -75° (with one exception). At 22.9 MHz the transition phase is shifted from $+6^{\circ}$ in the no-post case (at $E_c/E_g = .75$) to -23° , i.e. the useful phase range for focusing is increased by almost 30°. The very interesting behavior in this case is the fact that, in contrast to the two-dimensional lens geometries, the transition phase shifts towards more negative phases as the energy increases. Thus, at $E_c/E_g = 6$ we find $\theta_t = -64^{\circ}$ rather than -5° without posts, i.e. an increase of the focusing phase interval by 60°. These findings indicate that the analytical theory cannot be applied to the three-dimensional lens. They do, however, clearly demonstrate the great advantage of post focusing, namely the substantial increase of the useful phase range, i.e. a larger beam acceptance, and, in addition a high energy gain due to

Reproduced with permission of the copyright owner. Further reproduction prohibited without permission.

the reduced effective gap width. For cyclotrons both features are of great importance in obtaining larger and better quality beam.

Another important aspect of dynamic focusing is the existence of a peak in the b/f_2 versus θ_c curve, as we pointed out earlier. Again this peak-focusing phase, θ_m can be calculated from Eq.(2.73) of the first-order theory. Differentiating and setting $\frac{d(b/f_2)}{d\theta_c} = 0$ yields

$$\sin \theta_m = \frac{\omega_e b}{2v_c} \frac{\pi}{F} \frac{E_c}{E_g} \tag{5.3}$$

From this equation we determined θ_m for the rf frequencies 2.29, 4.58, 22.9 MHz and for the lowest three energy values in the case of Geometry 1. These analytical values are compared with the numerically obtained results in Table 15. When the right side of Eq.(5.3) is greater than 1, there exists no real value of θ_m . This is true for the 22.9 MHz case where no maximum within $-75^\circ \leq \theta_c \leq +75^\circ$ exists both in the analytical approximation as well as in the numerical results. Table 15 shows again a good agreement between the analytical prediction and numerical results for the two low frequencies. The peak-focusing phase shifts towards large positive angle in Geometry 1 for all frequencies. But it shifts towards small angle in Geometry 5V. For instance, it shifts from 7° to 14° as E_c/E_g increases from .75 to 3 for

Reproduced with permission of the copyright owner. Further reproduction prohibited without permission.

f = 2.29 MHz in the case of Geometry 1. On the other hand, the peak-focusing phase shifts from 8° to 2° as E_c/E_g increases from .75 to 3 for f = 2.29 MHz in the case of G5V. In the case of f = 4.58 MHz, the peak-focusing phase is 2° for Geometry 5V and is 32° for Geometry 1 at $E_c/E_g = 3$. This demonstrates the very important role the posts can play in cyclotron beam dynamics.

Table 15

Peak-focusing phases(in degree) obtained by analytic and numerical methods for Geometry 5V and Geometry 1

		Geometry 1		Geometry 5V
f(MHz)	E_c/E_g	θ_m (an)	θ_m(num)	θ_m(num)
2.29	.75	7	7	8
"	1.0	9	8	7
"	2.0	12.7	13	5
"	3.0	15.7	14	2
4.58	.75	15.7	20	17
"	1.0	18.3	22	14
"	2.0	26.4	25	9
"	3.0	33.0	32	2
22.9	.75	none	none	none
"	1.0	"	"	65
"	2.0	"	"	50
"	3.0	"	"	38

Reproduced with permission of the copyright owner. Further reproduction prohibited without permission.

5.4 Principal Planes and Width of the Electric Lenses

The width of an electrostatic lens, defined by the distance between its two principal planes, originates from the finite extent of the electric field between the electodes. Therefore, the width depends on the geometric parameters of the lenses. In addition there should be a dependence on the energy of the particle and, in the dynamic case, also on the rf frequency and phase of the particle. This dependence is illustrated in Fig. 23 to 25. In the first of these figures we plotted the normalized width $\Delta d/b = |d_1 + d_2|/b$ of Geometry 1 as a function of rf phase at various energies for f = 2.29 MHz. We see that at this low frequency the width does not vary much with θ_c except at and near the transition phase θ_t. Also notice that there is little variation with energy above $E_c/E_g = 1$. Clearly, for $\theta_c > \theta_t$, $E_c/E_g > 1$ the width $\Delta d/b$ is so close to zero that one can consider the gap as a thin lens. The dependence of the width on the geometry, i.e. the ratio a/b, can be seen in Fig. 24 where $\Delta d/b$ was plotted versus energy for constant phase $\theta_c = 45^\circ$. From this figure one obtains the conclusions: $\Delta d/b$ increases with the a/b ratio and frequency and it decreases rapidly with energy. At 2.29 MHz and above $E_c/E_g = 2$ one can consider all three two-dimensional geometries as thin lenses for all practical purposes. At 4.58 MHz the thin-lens idealization holds above

Reproduced with permission of the copyright owner. Further reproduction prohibited without permission.

about $E_c/E_g = 4$. As expected, the high frequency case is markedly different from the other curves reflecting again the complication due to large transit times. The three-dimensional Geometry 5V (curve on the bottom) behaves as an ideally thin lens for all energies and frequencies considered.

The actual location of principal plane II with respect to the gap center (x=0) is shown for various cases in Fig.25. The distance d_2 of principal plane II from the center line in all two-dimensional geometries is seen to increase with energy, the increase being roughly proportional to E_c/E_g. In view of what has been said about $\Delta d/b$ we can therefore approximate the action of the gap by a thin lens located at distance d_2 at the left of the gap center line (x=0).

Reproduced with permission of the copyright owner. Further reproduction prohibited without permission.

5.5 Energy Gain

We were concerned so far only with the focusing properties of the electric field of the gap. But in cyclotrons, for instance, the energy gain, not the focusing effect , is the most important aspect of the gaps. An ion with charge q can obtain a maximum energy gain of $2qV_o$ under static conditions in crossing an acceleration gap having peak-to-peak applied voltage of $2V_o$. If the applied voltage is sinusoidally varying in time the energy gain will be $2qV_o\cos\theta_c$ for an ideal short gap and it decreases with the increase of the gap length as well as with the rf frequency. From Tables 4 through 9 we can see that, in general, the energy gain decreases as the rf frequency increases. In the case of Geometry 1, the energy gain can be approximated by $E_g\cos\theta_c$ for all energies and phases for both f = 2.29 and 4.58 MHz. At high frequency the energy gain deviates significantly from $E_g\cos\theta_c$ and the deviation depends strongly on E_c . This qualitative behavior of the energy gain is also true for Geometry 5V. Fig. 26 shows the energy gain as function of the phase angle θ_c for the lowest (E_c/E_g =.75) and hightest (E_c/E_g= 6) energies at f =22.9 MHz in Geometry 1 and Geometry 5V. Other energy gain curves at different energy E_c are in between these two extreme curves and have similar functional forms. For comparison we have also included a genuine cosine curve in Fig. 26. This figure shows that for f = 22.9 MHz the energy gain in Geometry 1 is about 55 %

Reproduced with permission of the copyright owner. Further reproduction prohibited without permission.

of the energy gain in an ideal thin lens at $E_c/E_g = .75$ and is about 93 % at $E_c/E_g = 6$. The peak of the energy gain curve is at 0° in both cases. But in Geometry 5V the energy gain curve looks like $.65\ E_g\cos(\theta_c - 10^\circ)$ for $E_c/E_g = .75$ and f = 22.9 MHz. In other words, the maximum energy gain phase shifts in positive direction by 10°. And at $E_c/E_g = 6$ the energy gain curve is $.935\ E_g\cos(\theta_c - 4^\circ)$. Consequently the energy gain of Geometry 5V is always larger than that of Geometry 1 for the positive phase angles. It is also worthwhile to mention the fact that at large phases the energy gain in Geometry 5 is larger than $E_g \cos\theta_c$. The gap with posts at both sides not shown in Fig.26 will give even larger energy gain than the G5V case or the other field geometries considered here.

The pronounced difference between Geometry 1 and Geometry 5V can be seen in Table 16 which shows the b/f_2 values at the peak-energy gain phases, the transition phases, the peak-focusing phase, θ_m, and the peak-energy gain phase θ_o for f = 22.9 MHz and the lowest three energy values of E_c.

From Table 16 we can see that Geometry 5V has a great advantage over Geometry 1 in every aspect.

Reproduced with permission of the copyright owner. Further reproduction prohibited without permission.

Table 16

Comparison of Geometry 1 and Geometry 5V

E_c/E_g	Geometry 1				Geometry 5V			
	$b/f_2(\theta_o)$	θ_t	θ_m	θ_o	$b/f_2(\theta_o)$	θ_t	θ_m	θ_o
.75	-.035	$+6^\circ$	*	0°	+.115	-23°	*	10°
1.0	-.010	$+2^\circ$	*	0°	+.100	-31°	$+65^\circ$	5°
2.0	+.007	-4°	*	0°	+.075	-48°	$+50^\circ$	4°
3.0	+.005	-5°	*	0°	+.060	-54°	$+38^\circ$	4°

* indicares that there is no peak-focusing phase in the phase interval, $-75^\circ \leq \theta_c \leq +75^\circ$

Reproduced with permission of the copyright owner. Further reproduction prohibited without permission.

5.6 Horizontal Motion in the Three-Dimensional Lens

As has been mentioned earlier, posts at the exit side of a gap have the effects of "redistribution" of the force components in the vertical and horizontal planes. This "redistribution" effect resulted in the improved vertical focusing of Geometry 5V. The effects of the posts of Geometry 5 on the horizontal lens properties are shown in Fig. 27 and 28 for f = 2.29 nad 22.9 MHz, respectively. In the case of low frequency, the horizontal convergence b/f_2 is, crudely speaking, the "mirror image" of the convergence in the vertical plane. The b/f_2 curves of Fig.27 are smoother than the corresponding curves of the vertical motion of Fig.20. In the high-frequency case shown in Fig.28 we can see a markedly different behavior of b/f_2 compared to the low frequency. At the high frequency b/f_2 is positive in the horizontal as well as vertical motion for low energy ($E_c/E_g < 1$) and large phase ($\theta_c > 50^\circ$). It is negative in the horizontal plane for all energies at phase $\theta_c < 45^\circ$.

It is interesting to compare Geometry 5 with the two-dimensional Geometry 1 results. The normalized convergence b/f_2 was larger in Geometry 1 than in Geometry 5V for $E_c/E_g = .75$ and $\theta_c > 50^\circ$. Also, in the defocusing phase range, for $E_c/E_g = .75$ and $\theta_c < -23^\circ$, the magnitude of b/f_2 in Geometry 1 is larger than in Geometry 5V. The same is true fo for $E_c/E_g = 1.0$ and some other phase angles in the case of

Reproduced with permission of the copyright owner. Further reproduction prohibited without permission.

f = 22.9 MHz. These facts indicate that the large vertical focusing or defocusing force in Geometry 1 at those phase angles and energies mentioned above is divided or redistributed into smaller focusing (or defocusing) forces in the vertical and horizontal directions.

The relative amount of defocusing (or focusing at large phase angles for f = 22.9 MHz) in the horizontal plane depends strongly on the width of the posts. It decreases with increasing slit width and drops to zero in the two-dimensional limit where $W \rightarrow \infty$.

Reproduced with permission of the copyright owner. Further reproduction prohibited without permission.

CHAPTER VI

APPLICATION TO CYCLOTRONS

As has been mentioned earlier, in the immediate neighborhood of an ion source of a cyclotron we have to treat the particle motion by numerical methods. When the ion beam has gained a sufficient amount of energy, for instance several hundred electron volts, one can simulate the acceleration process by computing the ion motion in the magnetic field and simply adding appropriate energy, $2qV_0 \cos \theta_c$, to the ion every time it crosses the acceleration gap. All other effects of the electric field inside the gaps can be neglected. In between these two extreme situations one can apply our results to obtain the vertical motion, energy gain, phase shift, etc. in the first few orbits.

For simplicity we will consider a 180° straight dee machine. We assume the magnetic field effects on the vertical motion are negligible compared to the electric field effects inside the dee gaps, and the electric field effects are zero inside the dee between gap crossings. With this assumption we can separate the electric and magnetic field effects completely. The vertical displacement and slope of the ion orbit after traveling through the acceleration gap are, in the linear region mentioned earlier, related with the initial displacement and slope by the matrix of Eq.(2.68). The displacement and slope at next gap entrance are determined by a magnetic transition matrix which is given by[30]:

Reproduced with permission of the copyright owner. Further reproduction prohibited without permission.

$$\begin{pmatrix} z_2 \\ z_2' \end{pmatrix} = \begin{pmatrix} \cos \nu_{zm} \frac{l}{r} & \frac{r}{\nu_{zm}} \sin \nu_{zm} \frac{l}{r} \\ -\frac{\nu_{zm}}{r} \sin \nu_{zm} \frac{l}{r} & \cos \nu_{zm} \frac{l}{r} \end{pmatrix} \begin{pmatrix} z_1 \\ z_1' \end{pmatrix} \tag{6.1}$$

where ν_{zm} is the magnetic axial (vertical) betatron oscillation frequency, r is the orbit radius and l is the path length from one gap center line to the following gap center line. In our case of a 180° dee system we have $l = \pi r$ for a perfect circular orbit. After completion of one half circle the displacement and slope are thus given in terms of the initial conditions (z_o, z_o') by

$$\begin{pmatrix} z_2 \\ z_2' \end{pmatrix} = \begin{pmatrix} \cos \nu_{zm}\pi & \frac{r}{\nu_{zm}} \sin \nu_{zm}\pi \\ -\frac{\nu_{zm}}{r} \sin \nu_{zm}\pi & \cos \nu_{zm}\pi \end{pmatrix} \begin{pmatrix} a_{11} & a_{12} \\ a_{21} & a_{22} \end{pmatrix} \begin{pmatrix} z_o \\ z_o' \end{pmatrix} \tag{6.2}$$

The combined 2x2 matrix M has then the diagonal elements

$$M_{11} = a_{11} \cos \nu_{zm}\pi + a_{21} \frac{r}{\nu_{zm}} \sin \nu_{zm}\pi \tag{6.3}$$

$$M_{22} = -a_{12} \frac{\nu_{zm}}{r} \sin \nu_{zm}\pi + a_{22} \cos \nu_{zm}\pi \tag{6.4}$$

In completing a closed orbit the particle undergoes exactly the same operation as expressed in Eq.(6.2) one more time. Generally the matrix involved in the second half turn is

Reproduced with permission of the copyright owner. Further reproduction prohibited without permission.

not identical to the first half-turn matrix. But assuming a quasi-equilibrium orbit (energy gain per revolution is much smaller than particle's energy) we can assume that the matrices for both half turns are identical. Then, following the method described by Livingood[30], we can find the combined electric and magnetic axial betatron oscillation frequency ν_z by the following equation.

$$\cos \pi \nu_z = \tfrac{1}{2} (M_{11} + M_{22}) \tag{6.5}$$

Eq.(6.5) tells us that, in order for the particle to have an axially stable orbit, the half of the trace of matrix M should be bounded between +1 and -1.

If ν_{zm} is a very small number, e.g. $\nu_{zm} < .1$, as is the case in the central region of many cyclotrons, we can replace the magnetic transition matrix by a free-space drift matrix. In such a case Eq. (6.2) becomes;

$$\begin{pmatrix} z \\ z' \end{pmatrix} = \begin{pmatrix} 1 & \pi r \\ 0 & 1 \end{pmatrix} \begin{pmatrix} a_{11} & a_{12} \\ a_{21} & a_{22} \end{pmatrix} \begin{pmatrix} z \\ z' \end{pmatrix}_{in} \tag{6.6}$$

The axial oscillation in this case originates from the electric force alone, and we denote it by ν_{ze}. ν_{ze} can be calculated from the following equation:

$$\cos \pi \nu_{ze} = \tfrac{1}{2} (a_{11} + a_{21} \pi r + a_{22})$$

$$= \tfrac{1}{2} \left(1 - \frac{d_2}{f_2} + \frac{f_1}{f_2} - \frac{d_1}{f_2} - \frac{\pi r}{f_2} \right)$$

Reproduced with permission of the copyright owner. Further reproduction prohibited without permission.

Take the following example; a/b = .6 (Geometry 1 or 5), $E_c/E_g = 3$, V_g = 200 kV, r = 14.7" (the average magnetic field is 3 G), f = 22.9 MHz. Using Eq.(6.7) and the numerical data of Tables 6 and 9 we found ν_{ze} and the energy gain per gap crossing, ΔE (MeV), as listed in Table 17.

Table 17

Electric axial betatron oscillation frequency for geometry 1 and 5V $E_c/E_g = 3$, f = 22.9 MHz $\theta_c = 75^\circ, 45^\circ, 0^\circ, -15^\circ$

	Geometry 1		Geometry 5V	
θ_c(deg)	ν_{ze}	ΔE	ν_{ze}	ΔE
75	.54	.0449	.47	.0664
45	.46	.1225	.56	.1419
0	.19	.1725	.52	.1776
-15	imaginary	.0673	.42	.1650

From Table 17 we can see that we have sufficient electric focusing for $\theta^\circ > -15^\circ$ in Geometry 1 and for the entire phase range in Geometry 5.

Reproduced with permission of the copyright owner. Further reproduction prohibited without permission.

CHAPTER VII

CONCLUSION

Electric focusing properties of cyclotron-type elctric lenses with time-varying electric fields were studied. Lens geometries related closely to the TRIUMF cyclotron were chosen, i.e. for the two-dimensional cases a/b = .6, 1.0, 1.6, and c/b = 3.0, and for the three-dimensional cases a/b = 1/1.5, c/b = 2.6/1.5, with the horizontal width of the posts, W/b=1/3. The effects of these electric lenses on a proton moving across the gap at an applied peak-to-peak voltage E_g = 200 kV were determined. The gap height was taken as 2b = 3 inches. Numerical computations were made for rf frequencies of 2.29, 4.58, 22.9 MHz, seven energy values (from E_c/E_g = .75 to E_c/E_g= 6) at each frequency, and rf phase angles from -75° to $+75^\circ$ in 15° steps. Altogether 1617 different cases were numerically investigated.

From these investigations we found the following electric focusing properties:

1. The first-order theory is applicable for the two-dimensional geometries) if the transit time is considerably shorter than the rf period, i.e. $\omega_e b/v_c < .3$ or $\Delta\theta_g (E_c/E_g)^{1/2} < .3$. From the latter criterion we conclude that the first-order theory holds for f less than 4.58 MHz ($\Delta\theta_g$ = .177) over all energy ranges considered here to an error in b/f_2 of better than 15%. But for f = 22.9 MHz ($\Delta\theta_g$ = .885) the first-order

Reproduced with permission of the copyright owner. Further reproduction prohibited without permission.

theory cannot be applied for energies with E_c/E_g less than 5.

2. Within 30 % of the lens height (i.e. $z < .3b$) the convergence b/f_2 is independent of the initial displacement z_o of a particle off the median plane to better than about 2 %. Thus, in this "linear" region we can replace the effects of the electric field on the particle motion by an electric lens defined by four cardinal points and the correspoding four distances f_1, f_2, d_1, and d_2.

3. In accordance with first-order theory the two-dimensional gap geometries are defocusing at large negative phase and focusing at phases above the so called transition phase θ_t. There is a phase angle θ_m which yields a maximum value of b/f_2 for a given energy E_c and frequency f which is called peak-focusing phase θ_m ($\theta_m > \theta_t$). Both the peak-focusing phase θ_m as well as the transition phase θ_t shift in positive direction, i.e. towards larger phase angles, as the energy of the particle increases. Thus, the focusing phase range is narrowed by increasing the particle's energy.

4. At high frequency of f =22.9 MHz ($\Delta\theta_g$= .885) the two-dimensional geometries may be considered as a series of three lenses with focusing-defocusing-focusing or defocusing-focusing-defocusing action depending on the rf phase. The transition phase shifts to near 0^o and almost the entire negative phase interval ($\theta_c < 0^o$) gives defocusing. In marked contrast to the low-frequency cases the transition phase

Reproduced with permission of the copyright owner. Further reproduction prohibited without permission.

shifts towards more negative phases as the energy increases. The peak-focusing phase appears to be beyond the upper phase limit ($\theta_c = 75^\circ$) of the phase range that was studied. Above θ_t the normalized convergence b/f_2 is increasing monotonically without reaching a true maximum.

6. In the three-dimensional case with posts (Geometry 5V) vertical electric focusing is quite different as expected. If $\Delta\theta_g < .177$ b/f_2 is positive for all energy values and phase angles. Thus we have focusing action over the entire phase region. The peak-focusing phase occurs closer to 0° and the b/f_2 curves are smoother, i.e. their variation with phase angle θ_c is much less pronounced than in the two-dimensional case. For the high frequency case there is defocusing at large negative phase; at -23° for $E_c/E_g = .75$ and at -64° for $E_c/E_g = 6$. Thus, the transition phase shifts towards more negative phase angles with increasing energy. There exists a peak-focusing phase in this case within the interval $-75^\circ \leq \theta_c \leq +75^\circ$. Unlike the no-posts case where the energy gain is maximum for $\theta_c = 0^\circ$, the peak-energy gain phase shifts towards larger positive phase with decrease of energy. This peak-energy gain phase shift is as much as 10° in he lowest energy and 4° in the highest energy.

7. Another advantage of Geometry 5 where posts are placed on the downstream side of the gap is the fact that peak-focusing phase and peak-energy gain phase are closer together than in the gap without posts. Thus, Geometry 5V

Reproduced with permission of the copyright owner. Further reproduction prohibited without permission.

provides larger and more uniform vertical focusing in the useful phase interval with larger energy gain than gap Geometry 1.

8. The gap with posts at both sides (Geometry 4) gives small b/f_2 values, namely less than .02 for all cases, but it gives the largest energy gain of all lenses. This type of geometry is therefore not very useful as a lens. But it has a clear advantage if high energy gain is desired and focusing is not so important.

9. Geometry 5 gives defocusing action in the horizontal plane which, in a sense, is complementary to the focusing in the vertical direction. At low frequencies, it always defocuses horizontally at phases which are focusing vertically. At high frequency it was found, however, that at large positive phases there may be focusing in both directions.

10. The computed results for the lens properties were applied to proton motion in the center of a 180° two-dee cyclotron, such as TRIUMF, with operating conditions of V_o = 100 kV, B (average magnetic field) = 3kG, r = 14.7", f = 22.9 MHz. It was found that the corresponding electric axial betatron oscillation frequency is sufficient ($\nu_{ze} > .2$) for $\theta_c > -15^{\circ}$ in Geometry 1 and for the entire phase range in Geometry 5V.

11. The numerical results presented in this paper can be applied to different geometries, operating conditions, and particles if the pertinent scaling laws described in chapter 2 are used.

Reproduced with permission of the copyright owner. Further reproduction prohibited without permission.

APPENDIX A

Derivation of Two-Dimensional Paraxial Ray Equation in Cartesian Coordinates

The nonrelativistic equations of motion of a charged particle in x and z directions in cartesian coordinates with static electric field can be written as follow:

$$m\ddot{x} = q\, E_x(x,z) \tag{A.1}$$

$$m\ddot{z} = qE_z(x,z) \tag{A.2}$$

We will consider, as in all the previous cases, only the motion very close to the median plane. Then from Eq.(2.3)

$$\frac{\partial V}{\partial x} = \frac{\partial V(x,0)}{\partial x} \tag{A.3}$$

and from Eq.(2.5)

$$\frac{\partial V}{\partial z} = -\left(\frac{\partial^2 V}{\partial x^2}\right)_{Z=0} Z = -\left(\frac{d^2 V}{dx^2}\right)_{Z=0} Z \tag{A.4}$$

Multipling both sides of Eq.(A.1) by x, we have

$$\frac{1}{2}\frac{d}{dt}(\dot{x}^2) = \frac{q}{m}\frac{d(V(x))}{dt}$$

We can integrate above equation with initial conditions

$x = x_o$, $\dot{x} = \dot{x}_o$, at t= o as follow.

$$\dot{x}^2 - \dot{x}_o^2 = \frac{2q}{m}\left[\, V(x) - V(x_o)\right]$$

where $V(x_o)$ is the voltage equivalent of the particle's initial kinetic energy, Then, $\dot{x}_o^2 = \frac{2q}{m} V(x_o)$ and

Reproduced with permission of the copyright owner. Further reproduction prohibited without permission.

$$\dot{x} = \sqrt{2q/m \cdot V(x)}$$

The condition of Eq.(2.11) is also true in this case, i.e. $v_z \ll v_x = v$. With this condition we can write

$$\ddot{z} = \frac{d}{dx}\left[\frac{dz}{dx}\sqrt{\frac{2q}{m}V(x)}\right]\frac{dx}{dt} = \frac{2q}{m}V(x)\frac{d^2z}{dx^2} + \frac{2q}{m}\frac{dV(x)}{dx}\frac{dz}{dx} \qquad (A.5)$$

Substituting Eqs.(A.5) and (A.4) into Eq.(A.2) we get;

$$\frac{d^2z}{dx^2} + \frac{V'}{V}\frac{dz}{dx} + \frac{V''}{2V}z = 0 \qquad (A.6)$$

which is the two-dimensional paraxial ray equation in cartesian coordinates.

Reproduced with permission of the copyright owner. Further reproduction prohibited without permission.

APPENDIX B

Derivation of the Relations Between the Transition Marix Elements and Cardinal Point Parameters

The outgoing trajectory $z_f(x)$ of Fig.4 is related to the incoming trajectory by the transition matrix A defined in Eq.(2.62) as follow:

$$\begin{pmatrix} z_+ \\ z_+' \end{pmatrix} = \begin{pmatrix} a_{11} & a_{12} \\ a_{21} & a_{22} \end{pmatrix} \begin{pmatrix} z_- \\ 0 \end{pmatrix} = \begin{pmatrix} a_{11} z_- \\ a_{21} z_- \end{pmatrix} . \tag{B.1}$$

From Fig.4 we can express z_+ in terms of f_2 and d_2 as follows:

$$\frac{z_-}{f_2} = \frac{z_+}{f_2 - d_2} ,$$

which gives

$$z_+ = z_-\left(1 - \frac{d_2}{f_2} \right) . \tag{B.2}$$

The slope of the outgoing trajectory of $z_f(x)$ is

$$z_+' = -\frac{z_-}{f_2} \tag{B.3}$$

Equating z_+ and z_+' of Eqs.(B.1), (B.2), and (B.3) we get

$$a_{11} = 1 - \frac{d_2}{f_2} \tag{B.4}$$

$$a_{21} = -\frac{1}{f_2} \tag{B.5}$$

which are identical to Eqs.(2.69) and (2.71).

Reproduced with permission of the copyright owner. Further reproduction prohibited without permission.

Using similar arguments on the trajectory $z_b(x)$ we have:

$$\begin{pmatrix} a_{11} & a_{12} \\ a_{21} & a_{22} \end{pmatrix} \begin{pmatrix} z_- & (1 - \frac{d_1}{f_1}) \\ & \frac{z_-}{f_1} \end{pmatrix} = \begin{pmatrix} z_- \\ 0 \end{pmatrix}$$

which can also be written as

$$\begin{pmatrix} a_{11} & a_{12} \\ a_{21} & a_{22} \end{pmatrix} \begin{pmatrix} 1 - \frac{d_1}{f_1} \\ \frac{1}{f_1} \end{pmatrix} = \begin{pmatrix} 1 \\ 0 \end{pmatrix}$$

Multiply the inverse matrix A^{-1} from left,

$$\begin{pmatrix} 1 - \frac{d_1}{f_1} \\ \frac{1}{f_1} \end{pmatrix} = \begin{pmatrix} a_{11} & a_{12} \\ a_{21} & a_{22} \end{pmatrix}^{-1} \begin{pmatrix} 1 \\ 0 \end{pmatrix} = \frac{\begin{pmatrix} a_{22} & a_{12} \\ a_{21} & a_{22} \end{pmatrix} \begin{pmatrix} 1 \\ 0 \end{pmatrix}}{a_{11}a_{22} - a_{12}a_{21}}$$

$$= \frac{1}{a_{11}a_{22} - a_{12}a_{21}} \begin{pmatrix} a_{22} \\ -a_{21} \end{pmatrix}$$

If the electric field x and z components are uncoupled, we can apply Liouville's theorm to the (z, p_z) space transformation

$$\begin{pmatrix} z \\ p_z \end{pmatrix}_+ = \begin{pmatrix} M_{11} & M_{12} \\ M_{21} & M_{22} \end{pmatrix} \begin{pmatrix} z \\ p_z \end{pmatrix}_- \qquad (B.7)$$

The determinant of the transition matrix should be unity. Therefore, we have:

$$M_{11} M_{22} - M_{12} M_{21} = 1$$

Now,

$$p_{z\pm} = p_{x\pm} \frac{dz}{dx} \equiv p_{x\pm} z' \qquad (B.8)$$

Reproduced with permission of the copyright owner. Further reproduction prohibited without permission.

Substituting Eq.(B.8) into (B.7) we can write:

$$\begin{pmatrix} Z_+ \\ Z'_+ \end{pmatrix} = \begin{pmatrix} M_{11} & M_{12}p_{x-} \\ \dfrac{M_{21}}{p_{x+}} & \dfrac{M_{22}p_{x-}}{p_{x+}} \end{pmatrix} \begin{pmatrix} Z_- \\ Z'_- \end{pmatrix} \qquad (M.9)$$

This transition matrix should be identical to $\begin{pmatrix} a_{11} & a_{12} \\ a_{21} & a_{22} \end{pmatrix}$.

Thus,

$$\begin{pmatrix} M_{11} & M_{12}p_{x-} \\ \dfrac{M_{21}}{p_{x+}} & \dfrac{M_{22}p_{x-}}{p_{x+}} \end{pmatrix} = \begin{pmatrix} a_{11} & a_{12} \\ a_{21} & a_{22} \end{pmatrix}$$

Therefore, the determinant of Eq.(B.6) is related to the determinant of matrix M as follow:

$$a_{11}a_{22} - a_{12}a_{21} = \frac{p_{x-}}{p_{x+}}(M_{11}M_{22} - M_{12}M_{21}) = \frac{p_{x-}}{p_{x+}} \qquad (B.10)$$

f_2 and f_1 are related to the energies of the incoming and outgoing particle by the formula

$$\frac{f_1}{f_2} = \sqrt{\frac{E_{in}}{E_{out}}} = \frac{p_-}{p_+} = \frac{p_{x-}}{p_{x+}} \qquad (B.11)$$

Combining Eqs.(B.10) and (B.11)

$$a_{11}a_{22} - a_{12}a_{21} = \frac{f_1}{f_2} \qquad (B.12)$$

With Eqs. (B.12) and (B.6) we can find,

$$a_{22} = \frac{f_1}{f_2}\left(1 - \frac{d_1}{f_1}\right) \qquad (B.13)$$

Reproduced with permission of the copyright owner. Further reproduction prohibited without permission.

and a_{12} can be found from Eq.(B.10) as follows:

$$a_{12} = \frac{1}{a_{21}}(a_{11}a_{22} - \frac{p_{x-}}{p_{x+}})$$

$$= f_1(\frac{d_1}{f_1} + \frac{d_2}{f_2} \frac{d_1 d_2}{f_1 f_2}) \qquad (B.14)$$

Reproduced with permission of the copyright owner. Further reproduction prohibited without permission.

REFERENCES

1. H. Busch, Ann. Phys., Lpz., 81, 974 (1926)
2. C. J. Davison and C. J. Calbick, Phys. Rev. 42, 580 (1932)
3. E. Bruche and H. Johanson, Naturwissenschaften, 20, 49 (1932)
4. M. E. Rose, Phys. Rev. 53, 392 (1938)
5. W. R. Wilson, Phys. Rev. 53, 408 (1938)
6. B. L. Cohen, Rev. Sci. Instr., 24, 589 (1953)
7. M. Reiser, "First-Order Theory of Electrical Focusing in Cyclotron-type Two-Dimensional Lenses with Static and Time-varying Potential", the University of Maryland Tech. Report No.70-125
8. W. I. B. Smith, Nucl. Inst. & Method 9, 49 (1960)
9. M. Reiser, Nucl. Inst. & Method 13, 55 (1961)
10. P. A. Sturrok, "Static and Dynamic Electron Optics", p. 148 Cambridge University Press (1955)
11. E. M. McMillan, Phys. Rev. 80, 493 (1950)
12. D. W. Fry and W. Walkinshaw, Progr. Phys. 12, 102 (1949)
13. J. P. Blewett, Phys. Rev. 88, 1197 (1952)
14. H. G. Blosser and F. Irwin, Bull. Amer. Phys. Soc., Series II, Vol. 3, 180 (1958)
15. S. Bertram, Proc. Inst. Radio Engrs., 28, 418 (1940)
16. R. Murray and L. Ratner, J. Appl. Phys. 24, 67 (1953)
17. M. Reiser and J. Mullendor, Nucl. Instr. & Method 59, 93 (1968)
18. T. Zinneman, "Three-Dimensional Electrolytic Tank Measurements and Vertical Motion in Central Region of Cyclotron", the University of Maryland Tech. Report No.986 (1969)
19. D. Nelson, H. Kim, and M. Reiser, IEEE Trans. NS-16, 776 (1969)

Reproduced with permission of the copyright owner. Further reproduction prohibited without permission.

20. M. Reiser and J. Kopf, Rev. Sci. Instr., 36, 1022 (1965)

21. C. Han, "Computer Results for the Focal Properties of Two- and Three-Dimensional Electric Lenses with Time-Varying Fields", Technical Report No. 70-126 (1970)

22. J. R. Pierce, "Theory and Design of Electron Beams" D. Van Nostrand Co., Inc. p 44 (1961)

23. A. B. Karen, Symposium on Electron, Ion, and Laser Beam Technology, San Francisco Press, Inc., p. 393 (1969).

24. L. Smith, Handbuch der Physik, XLIV 341 (1959)

25. D. A. Lind, NAS-NRC 656, 76 (1959)

26. H. A. Willax and A. A. Garren, Nucl. Instr. & Method. 18, 19, 347 (1962)

27. P. Kramer, H. L. Hagedoorn, and N. F. Verster, CERN 63-19, 214 (1963)

28. H. G. Blosser, M. M. Gordon, and M. Reiser, CERN 63-19, 193 (1963)

29. M. Reiser et al., IEEE Trans. NS-16, 449 (1969)

30. J. J. Livingood, "Principles of Cyclic Particle Accelerators" D. Van Nostrand Co., Inc. p. 44-52 (1961)

Reproduced with permission of the copyright owner. Further reproduction prohibited without permission.

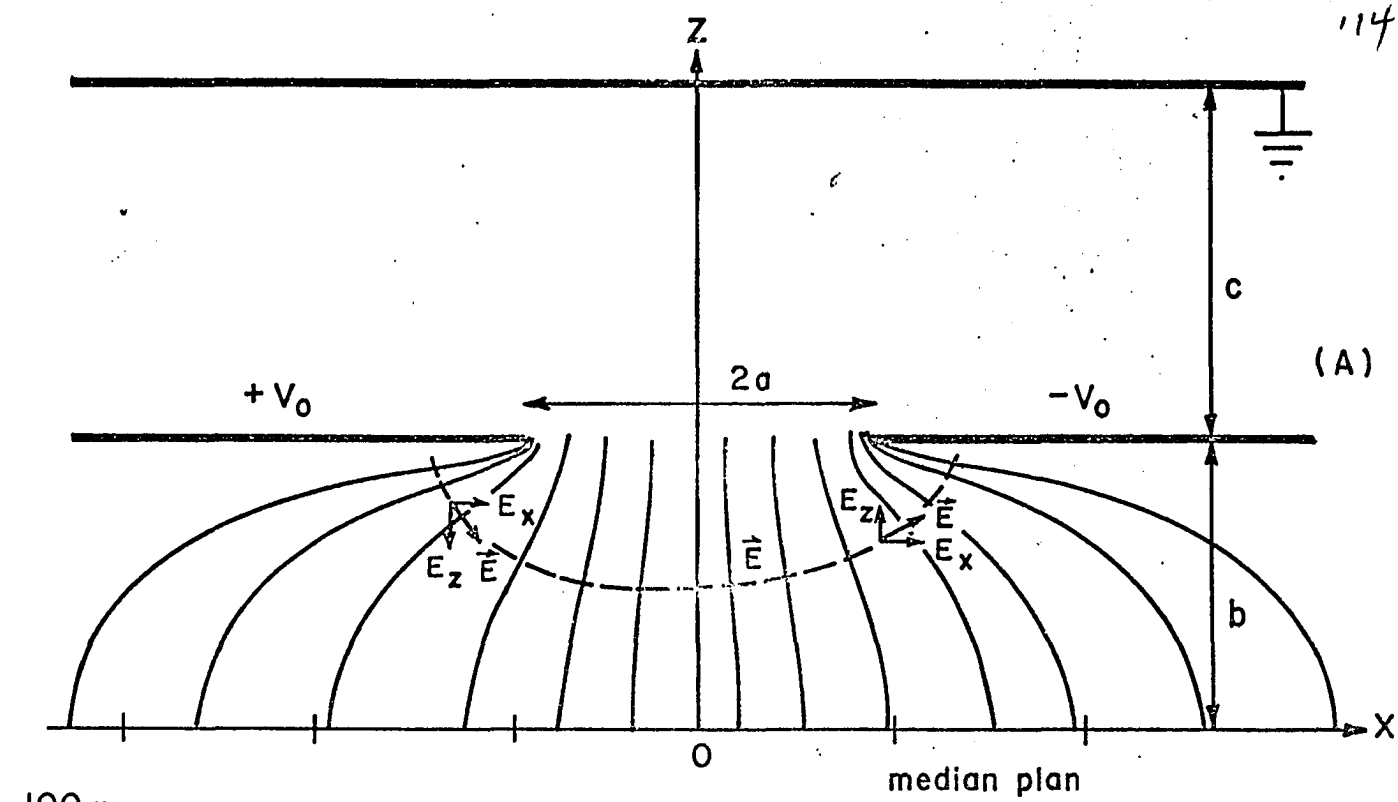

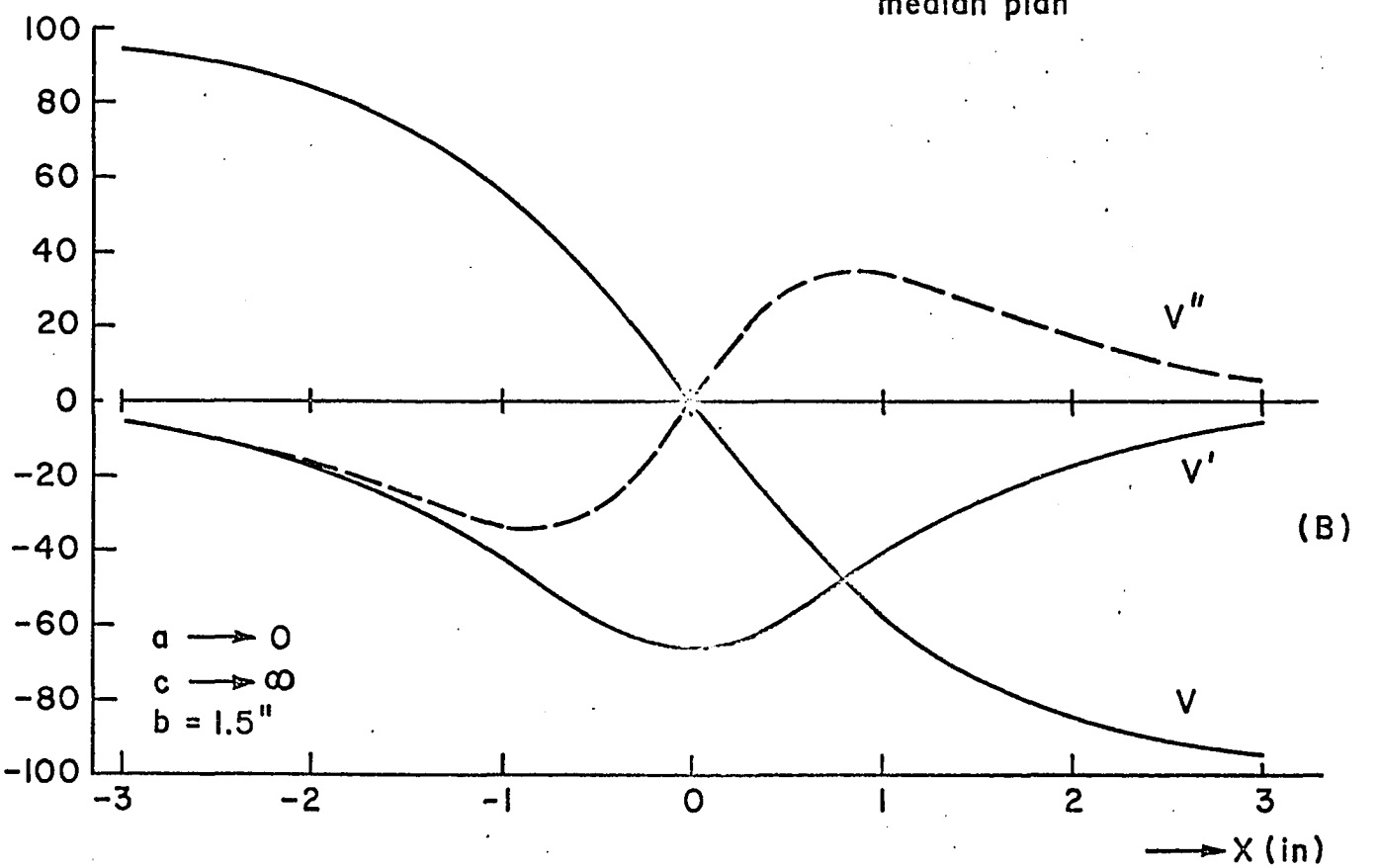

Fig 1 (A) A typical cyclotron-type electric lens Geometry
(B) Potential function V(x), $\partial V/\partial x$, $\partial^2 V/\partial x^2$ on the median plane for $a \to 0$, $c \to \infty$, b=1.5"

Reproduced with permission of the copyright owner. Further reproduction prohibited without permission.

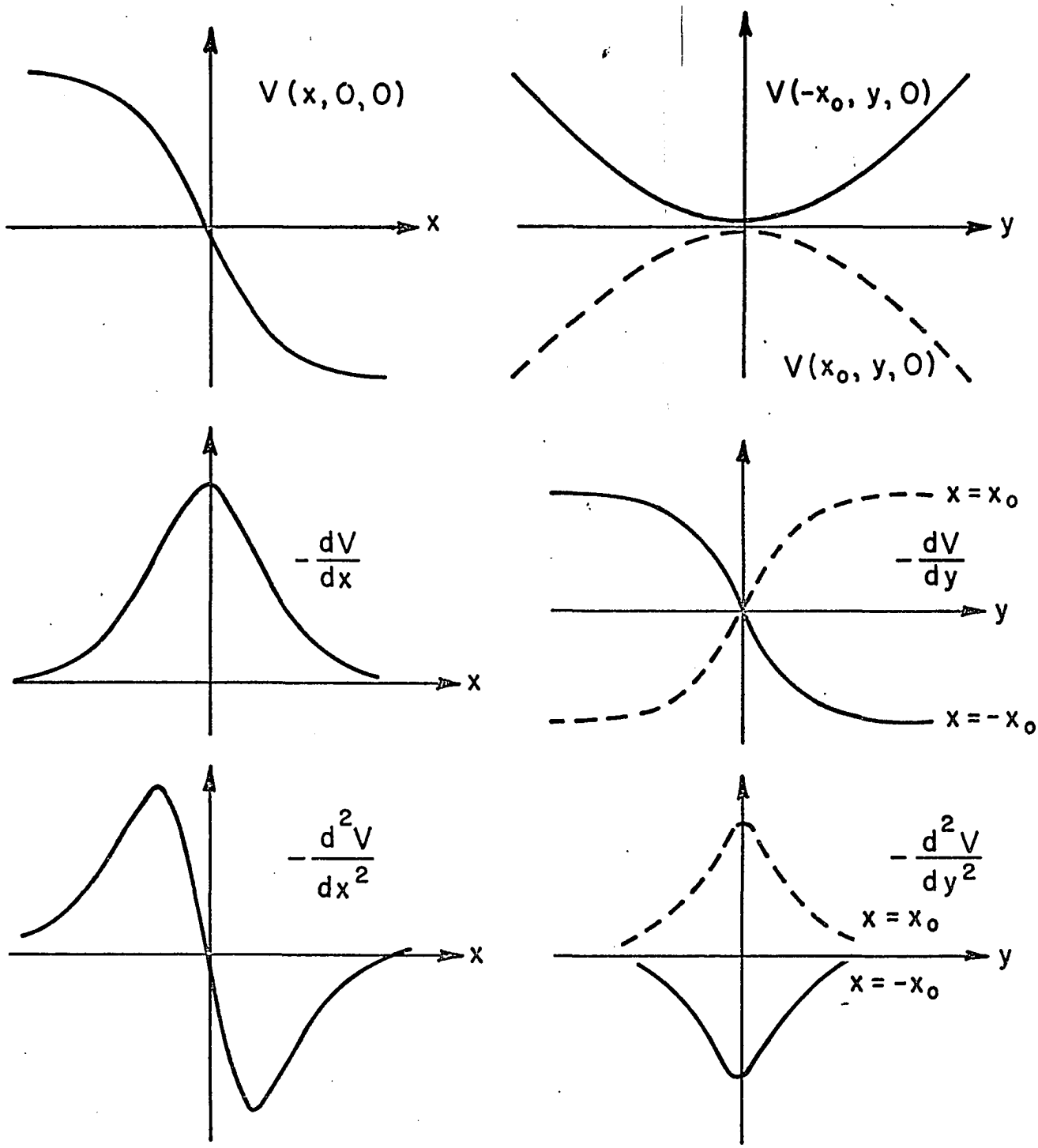

Fig 2 Qualitative representation of V(x,0,0) and the first and second derivatives in arbitrary units

Reproduced with permission of the copyright owner. Further reproduction prohibited without permission.

Reproduced with permission of the copyright owner. Further reproduction prohibited without permission.

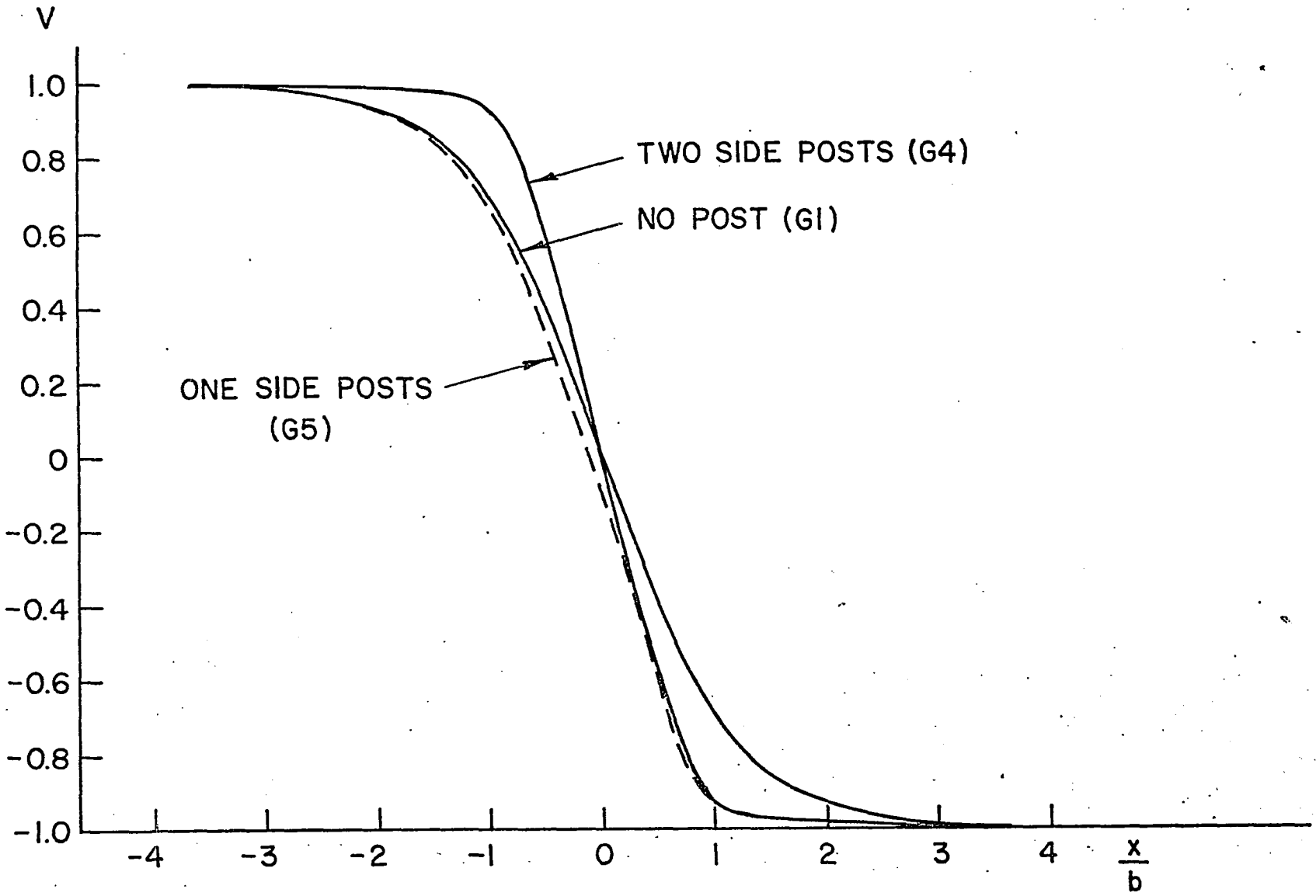

Fig. 3 Potential distribution along z axis for no posts (Geometry 1), posts on one side (Geometry 5), and posts on two sides (Geometry 4)

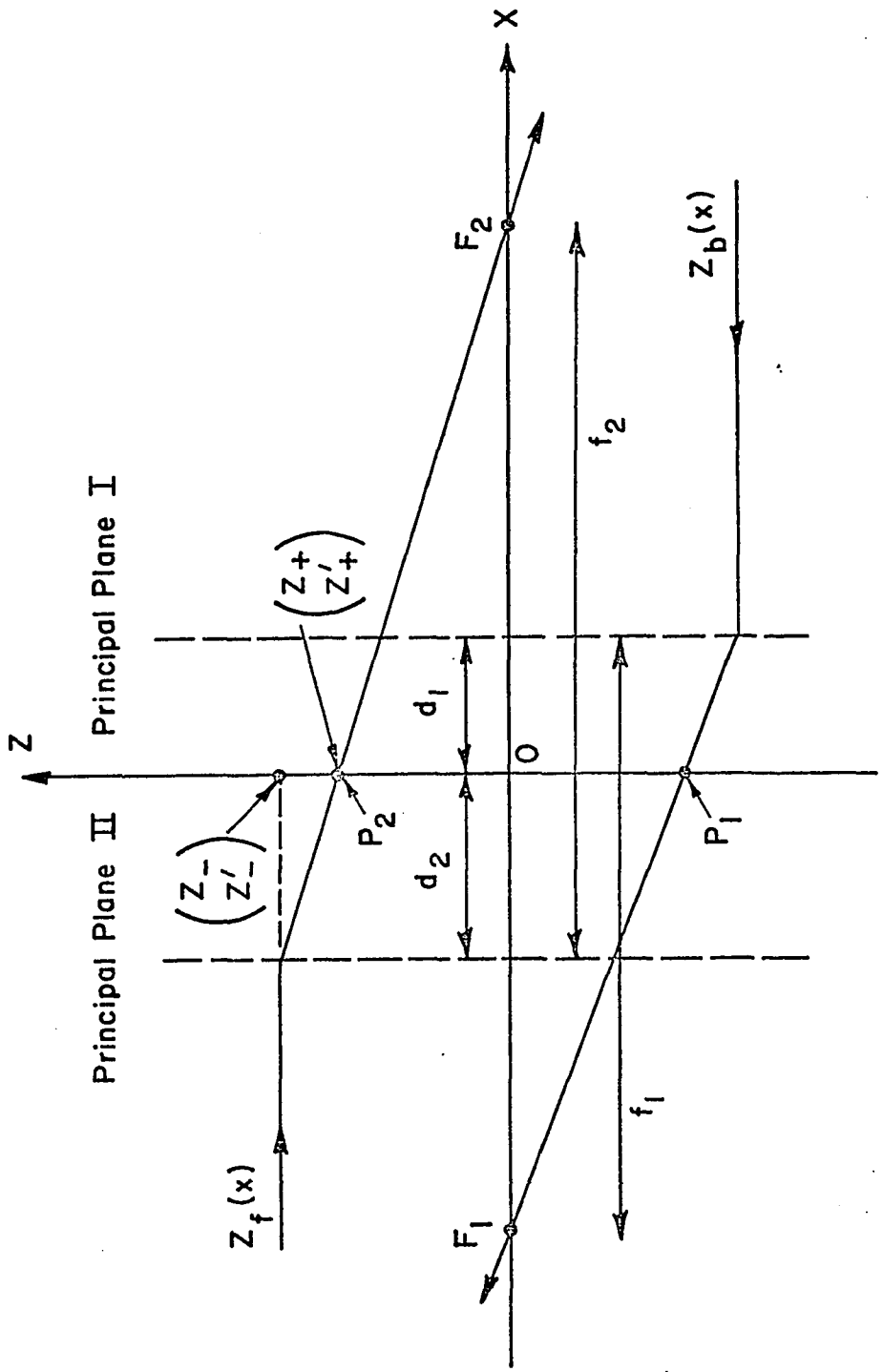

Fig. 4 FOCAL POINTS AND PRINCIPAL PLANES OF A THICK LENS.

Reproduced with permission of the copyright owner. Further reproduction prohibited without permission.

Reproduced with permission of the copyright owner. Further reproduction prohibited without permission.

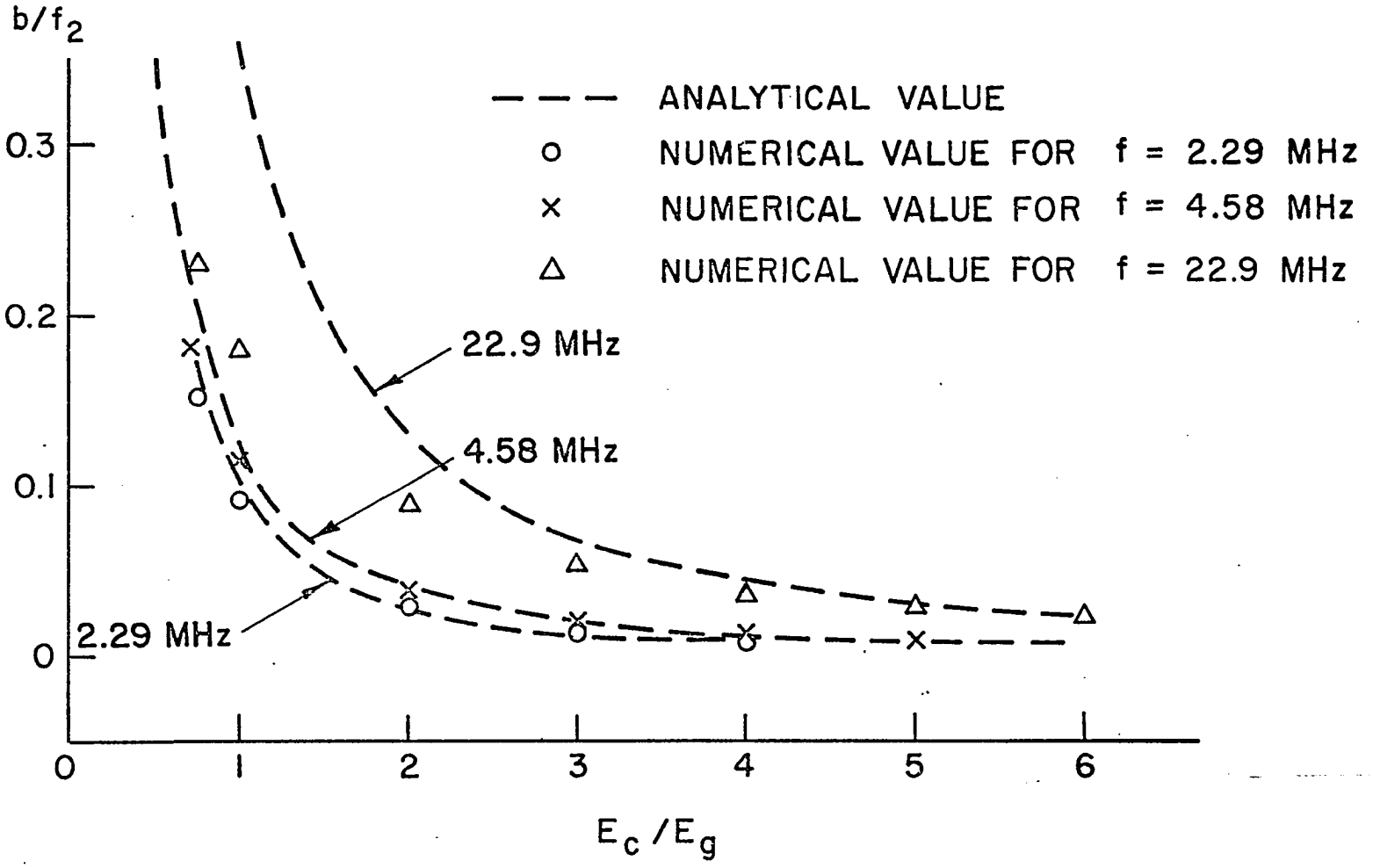

Fig. 5 Normalized convergence, b/f_2 in Geometry 1 for phase angle θ_c =45°, frequency f=22.9 MHz

Reproduced with permission of the copyright owner. Further reproduction prohibited without permission.

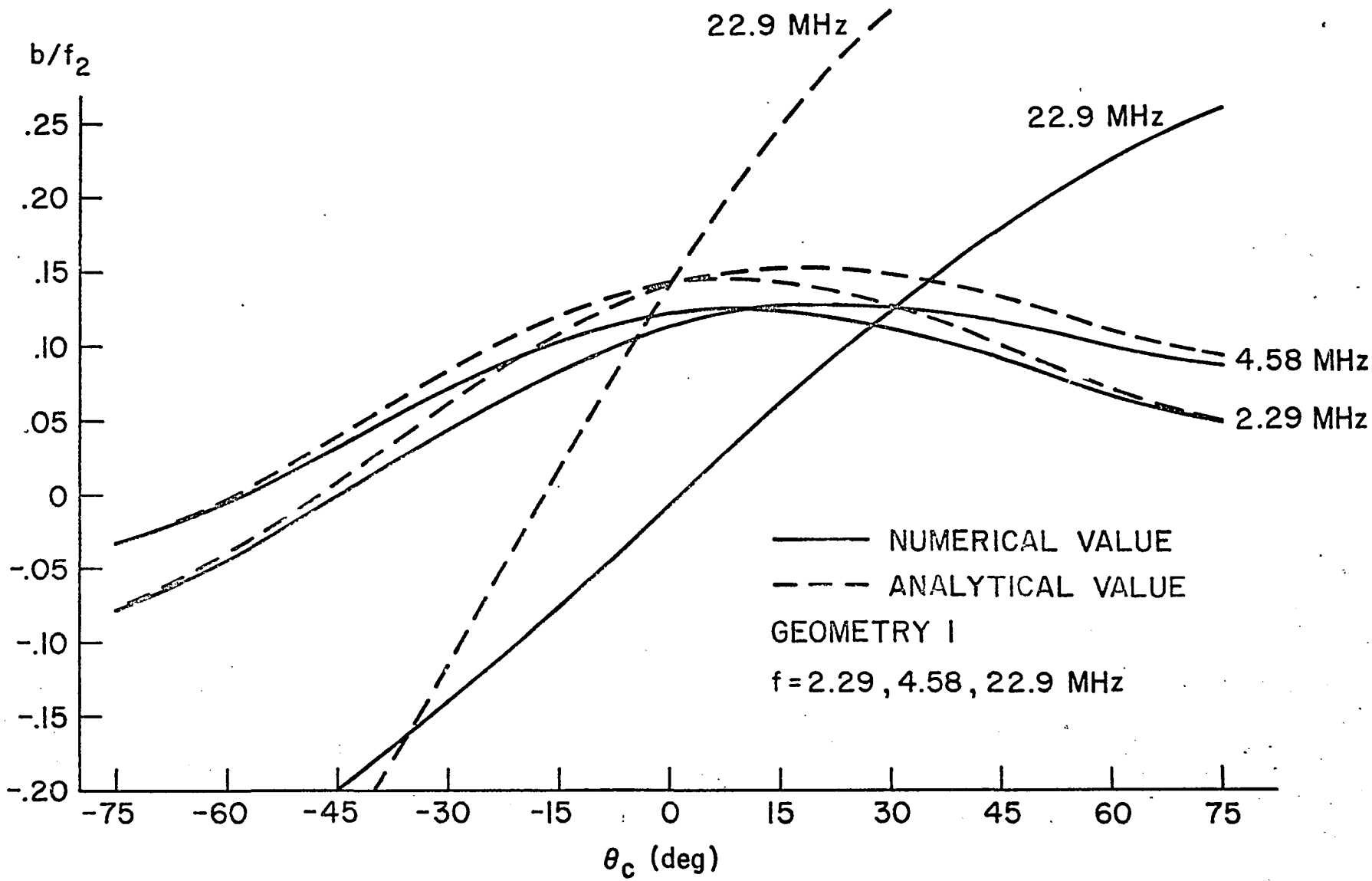

Fig. 6 Comparison of normalized convergence f=2.29, 4.58, 22.9 MHz in Geometry 1 for energy ratio $E_c/E_g = 1.0$

Reproduced with permission of the copyright owner. Further reproduction prohibited without permission.

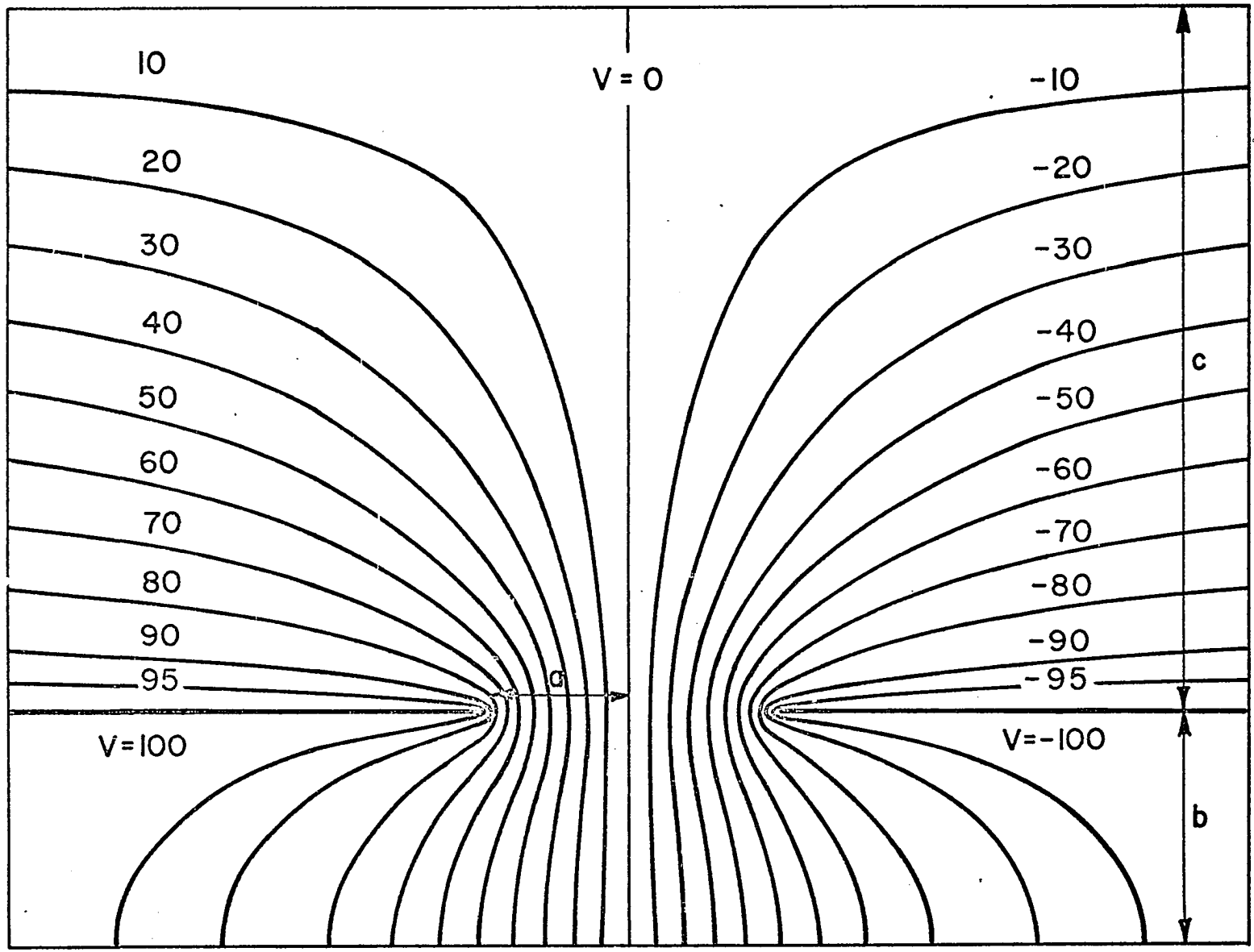

Fig.7 LENS GEOMETRY I AND POTENTIAL DISTRIBUTION
(a/b = .6, c/b = 3)

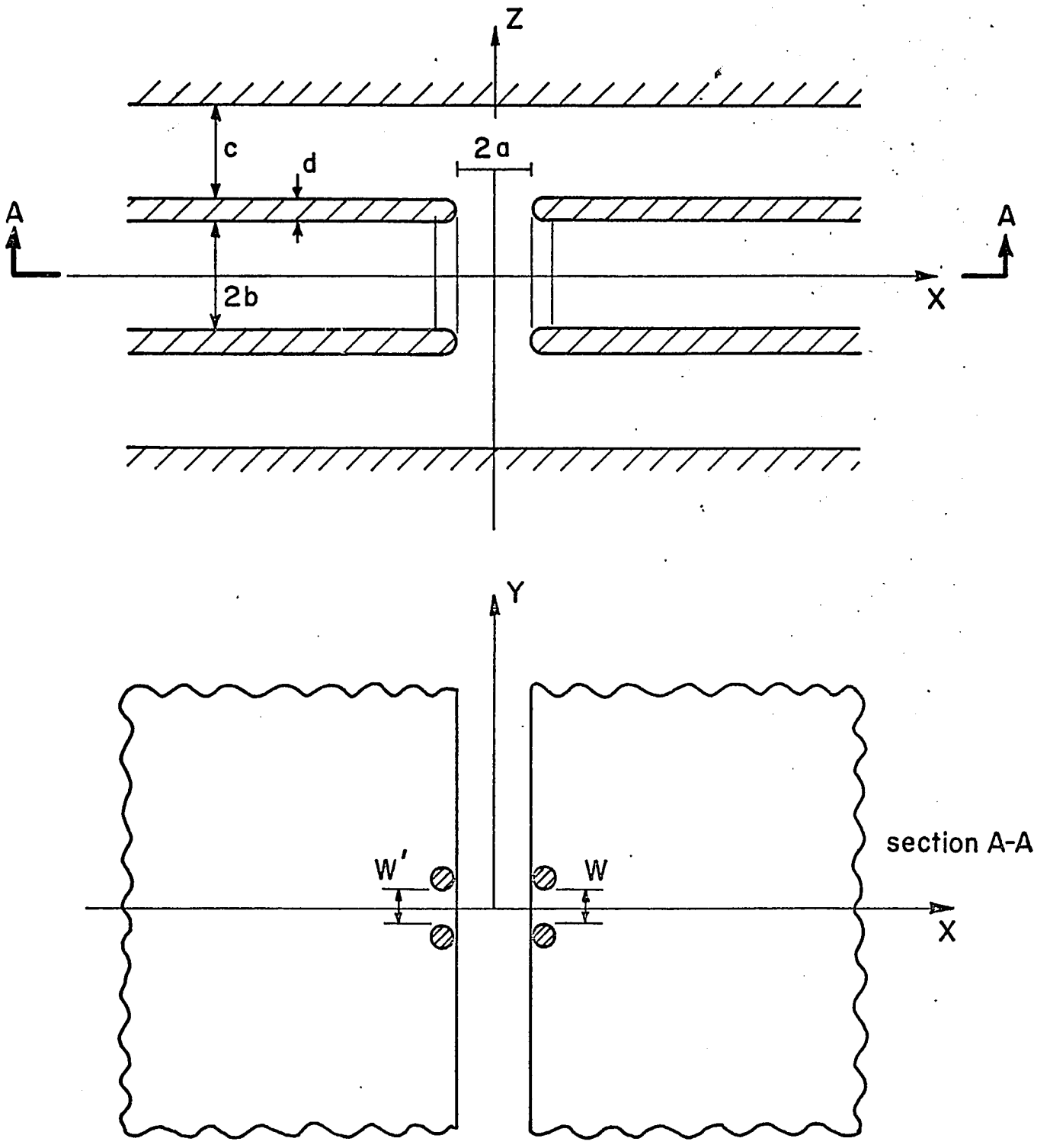

Fig. 8 LENS GEOMETRIES 4 AND 5.

Reproduced with permission of the copyright owner. Further reproduction prohibited without permission.

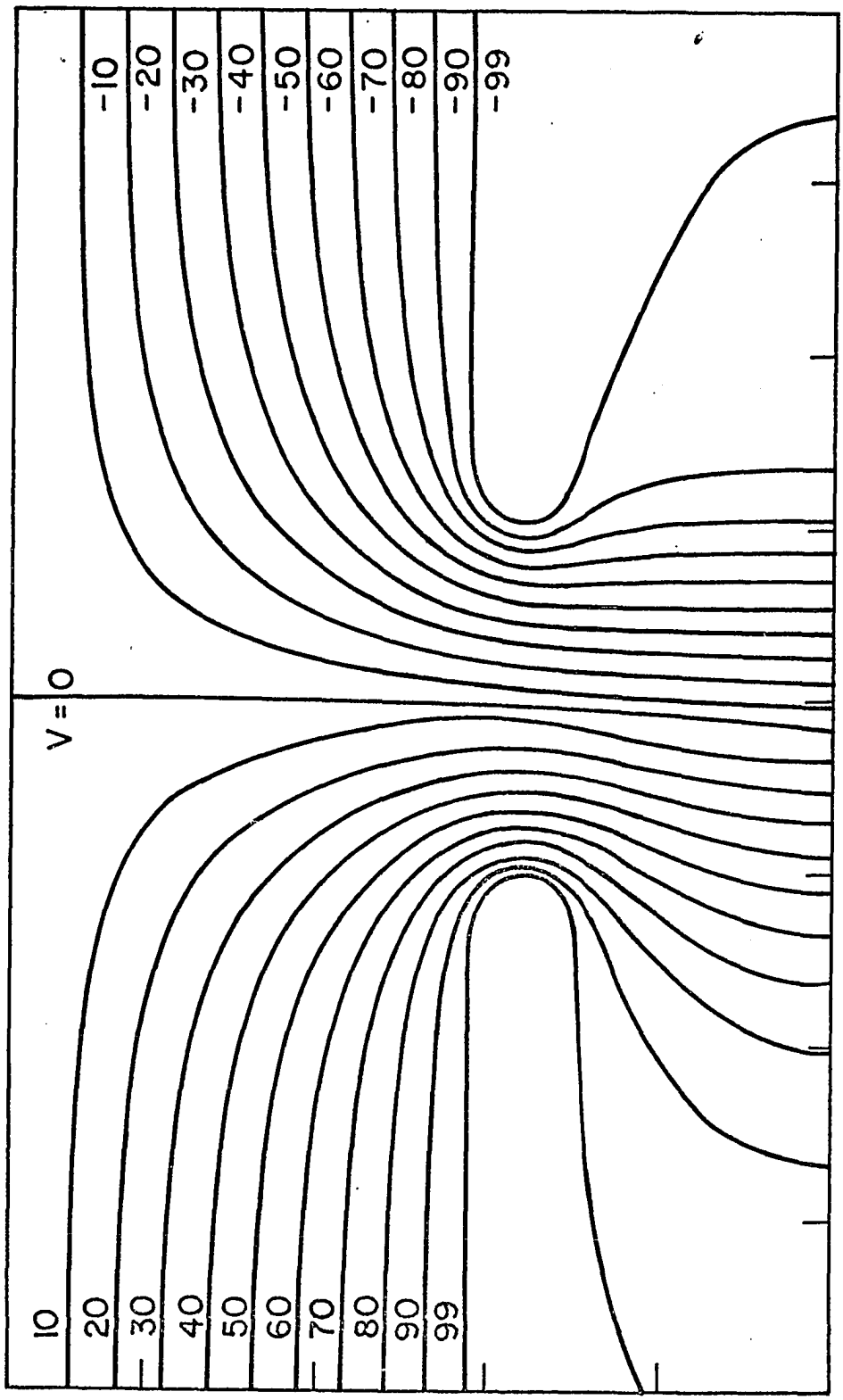

Fig. 9 Potential distribution in x-z plane of the lens, Geometry 5

Reproduced with permission of the copyright owner. Further reproduction prohibited without permission.

Reproduced with permission of the copyright owner. Further reproduction prohibited without permission.

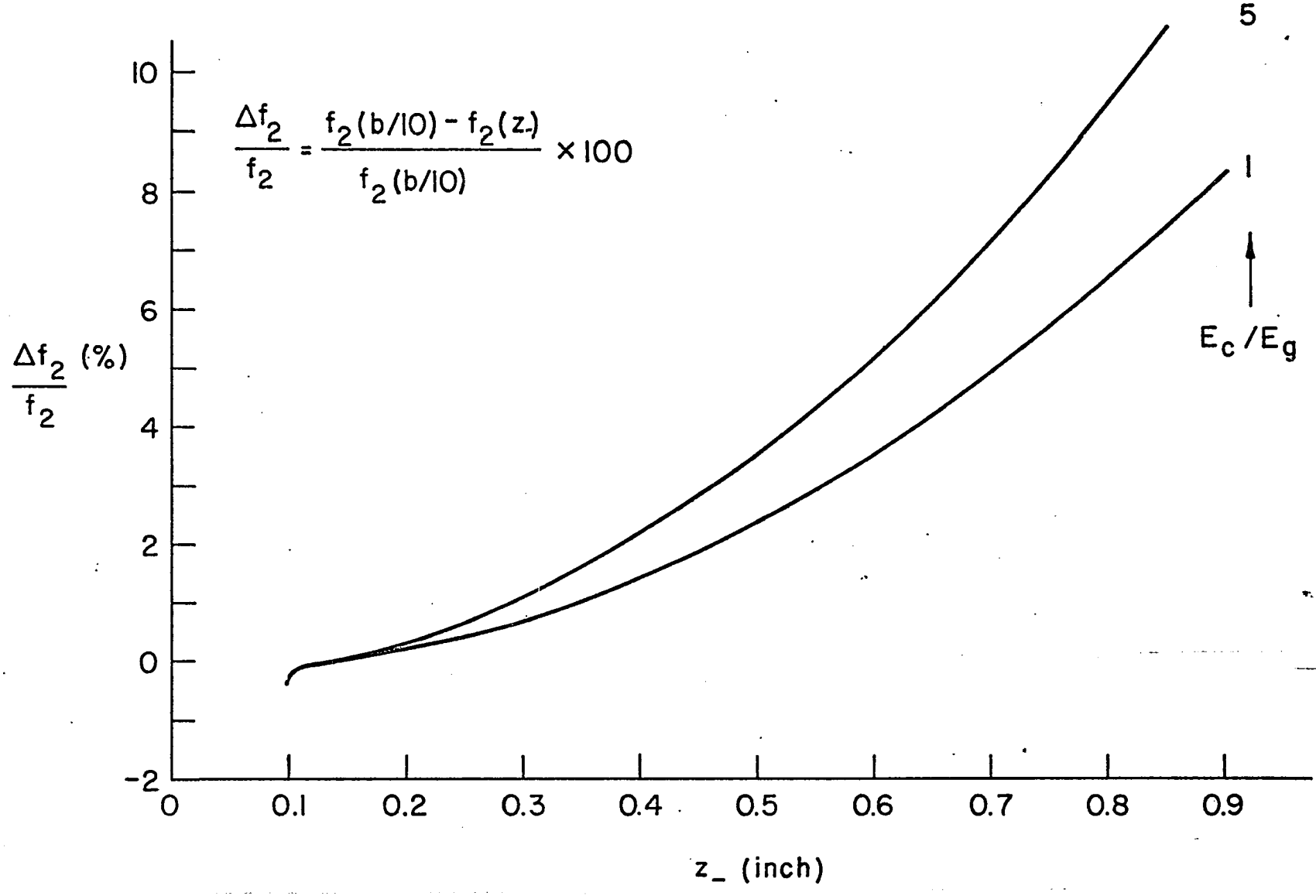

Fig 10 Difference in computed focal length, f_2 , due to different initial z displacement (Geometry 1, Static conditions) for two energies

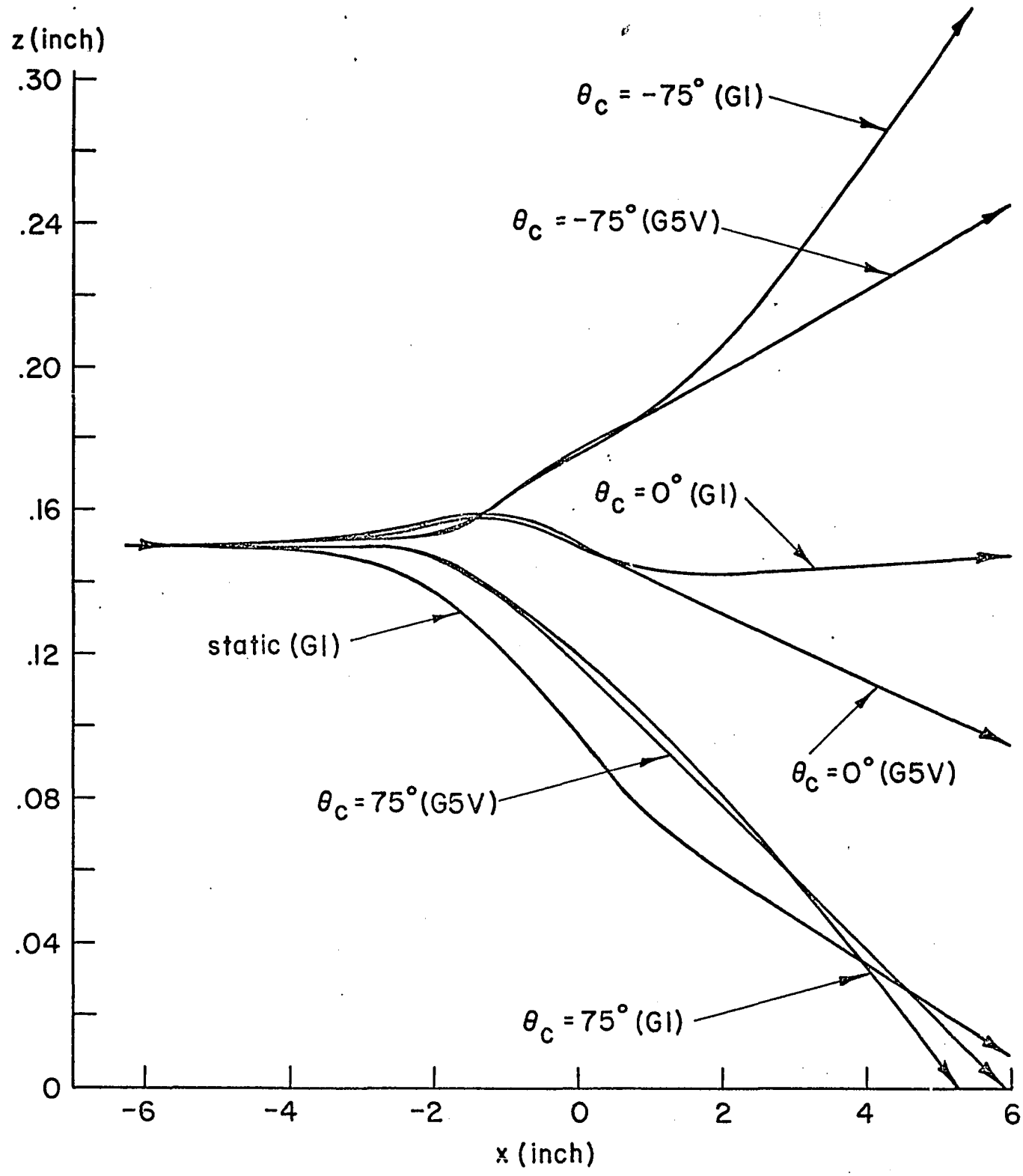

Fig. 11 Ion Trajectories for different phases θ_c in Geometry 1 and Geometry 5V for f=22.9 MHz E_c= .2 MeV

Reproduced with permission of the copyright owner. Further reproduction prohibited without permission.

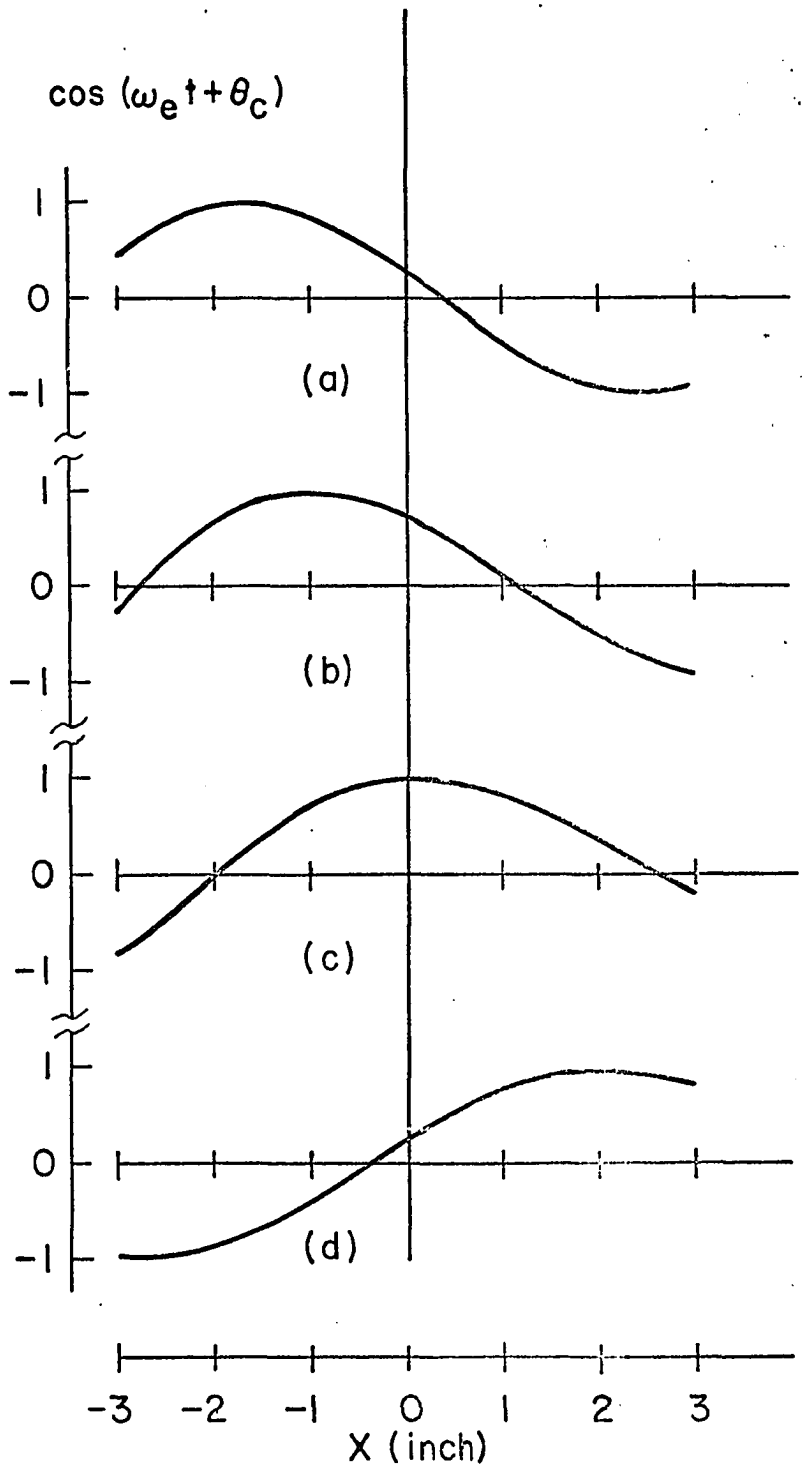

Fig. 12 Time-variation factor of electric field seen by a particle on its path through the gap along x axis for different phase angles 0_c , f=22.9 MHz, E_c/E_g= 1.0
(a) $\theta_c=75^\circ$, (b) $\theta_c=45^\circ$, (c) $\theta_c=0^\circ$, (d) $\theta_c= -75^\circ$

Reproduced with permission of the copyright owner. Further reproduction prohibited without permission.

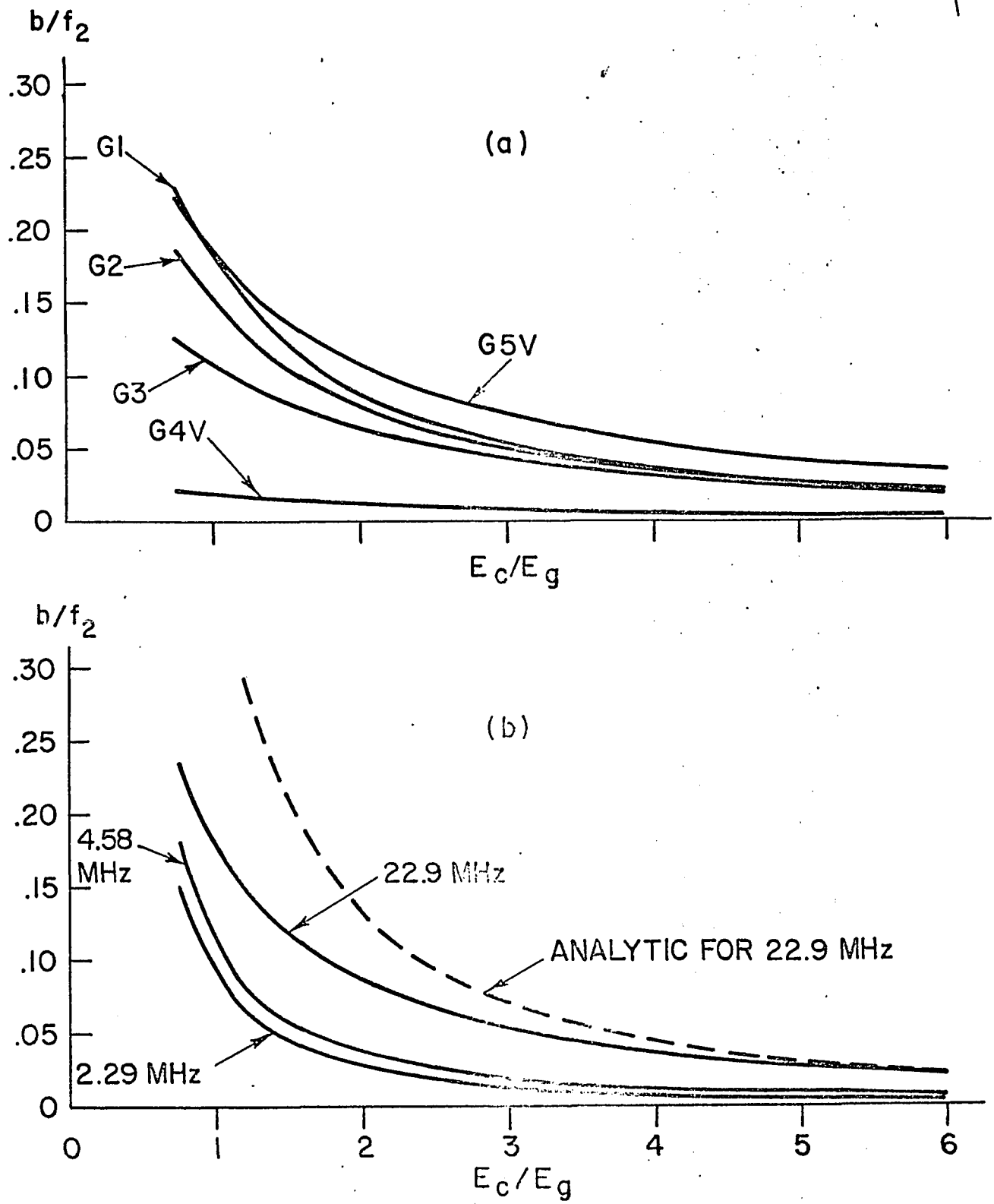

Fig. 13 Comparison of normalized convergence, b/f_2 at $\theta_c=45^\circ$
(a) for different lens geometries, f=22.9 MHz
(b) for different rf frequencies, Geometry 1

Reproduced with permission of the copyright owner. Further reproduction prohibited without permission.

Reproduced with permission of the copyright owner. Further reproduction prohibited without permission.

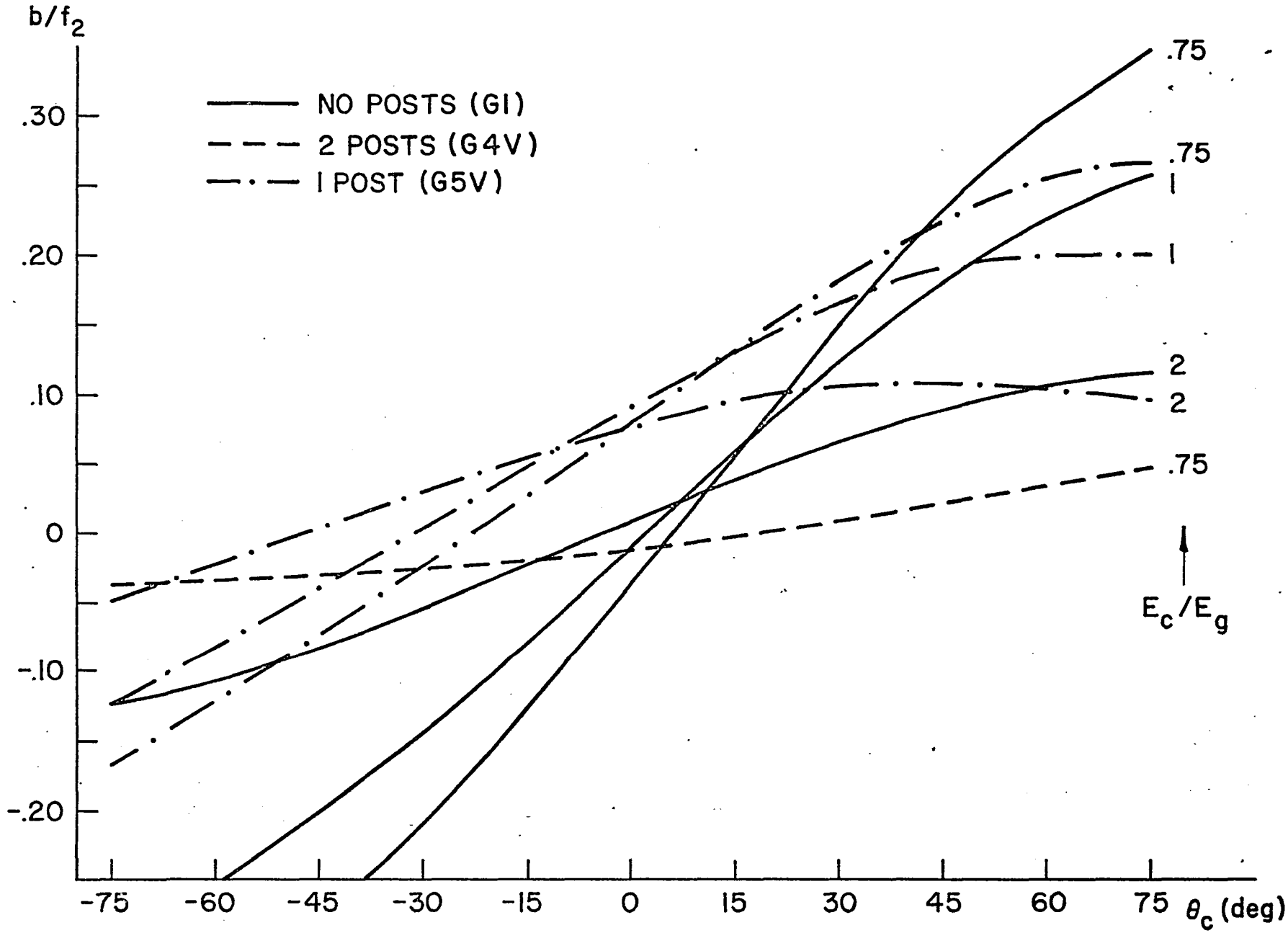

Fig. 14 Normalized convergence, b/f_2 of Geometry 1 for f=??.9 MHz at E_c/E_g= .75, 1.0, ?.0

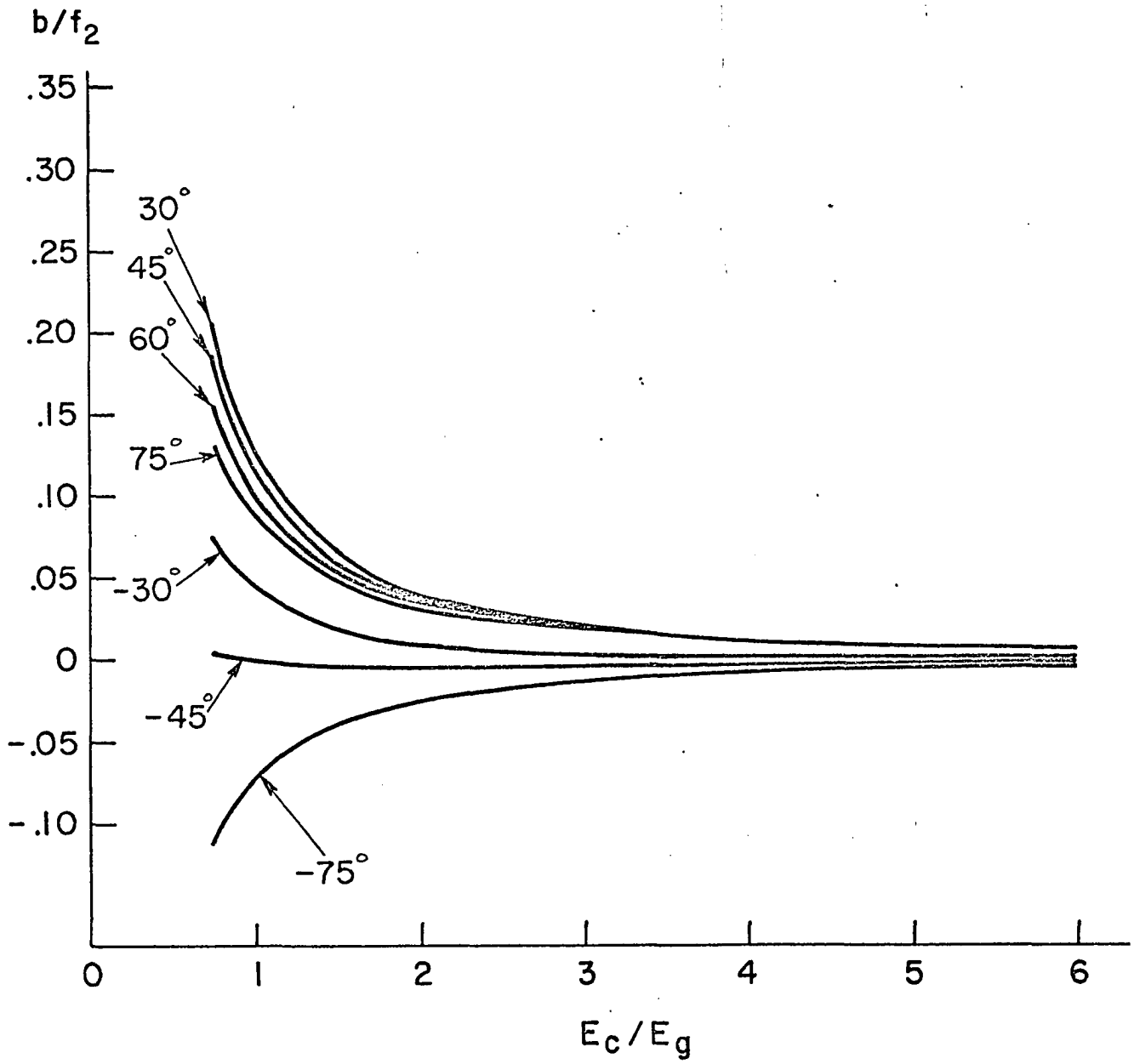

Fig. 15 Normalized convergence, b/f_2 in Geometry 1, f=4.58 MHz

Reproduced with permission of the copyright owner. Further reproduction prohibited without permission.

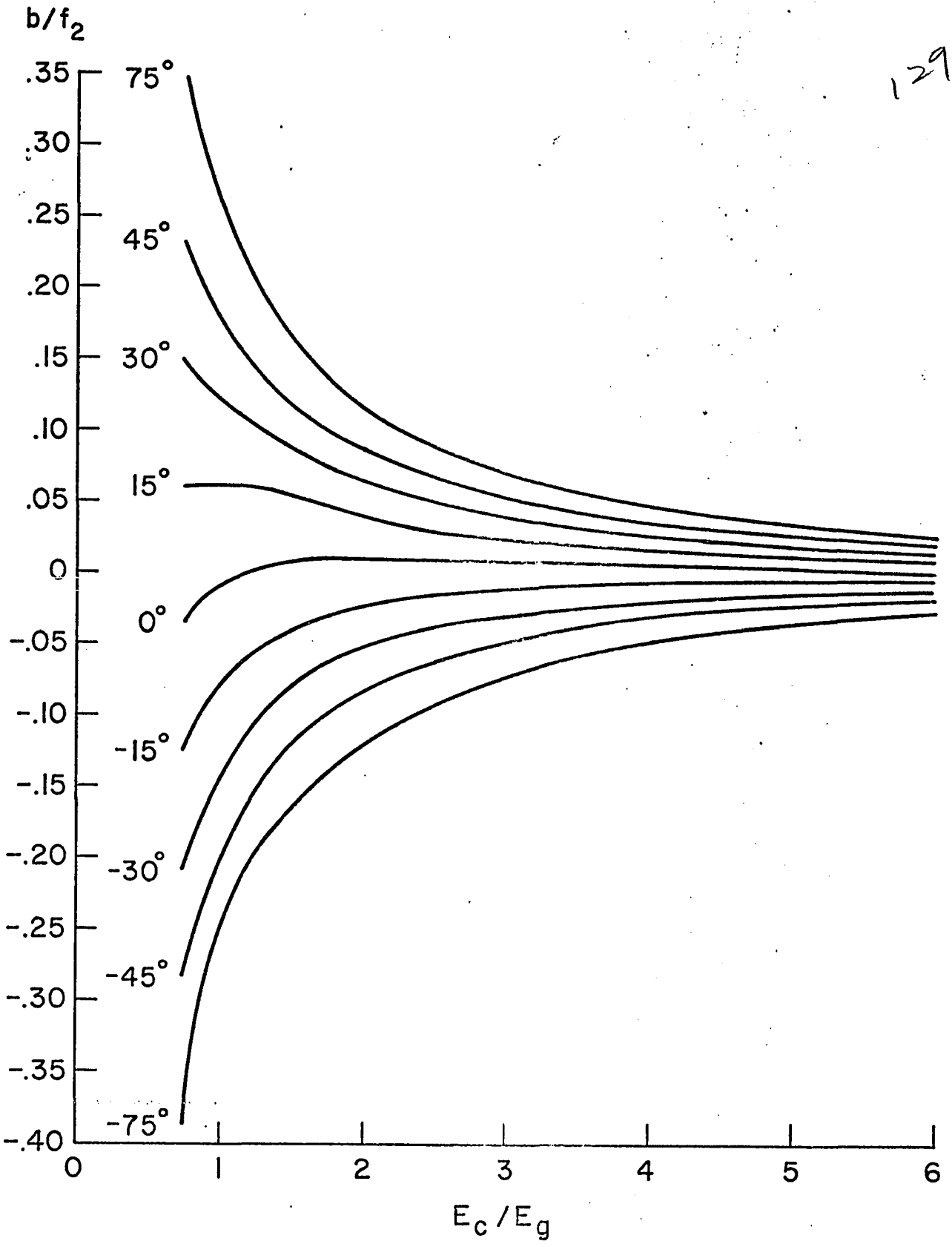

Fig. 16 Normalized convergence, b/f_2, in Geometry 1, f=22.9 MHz

Reproduced with permission of the copyright owner. Further reproduction prohibited without permission.

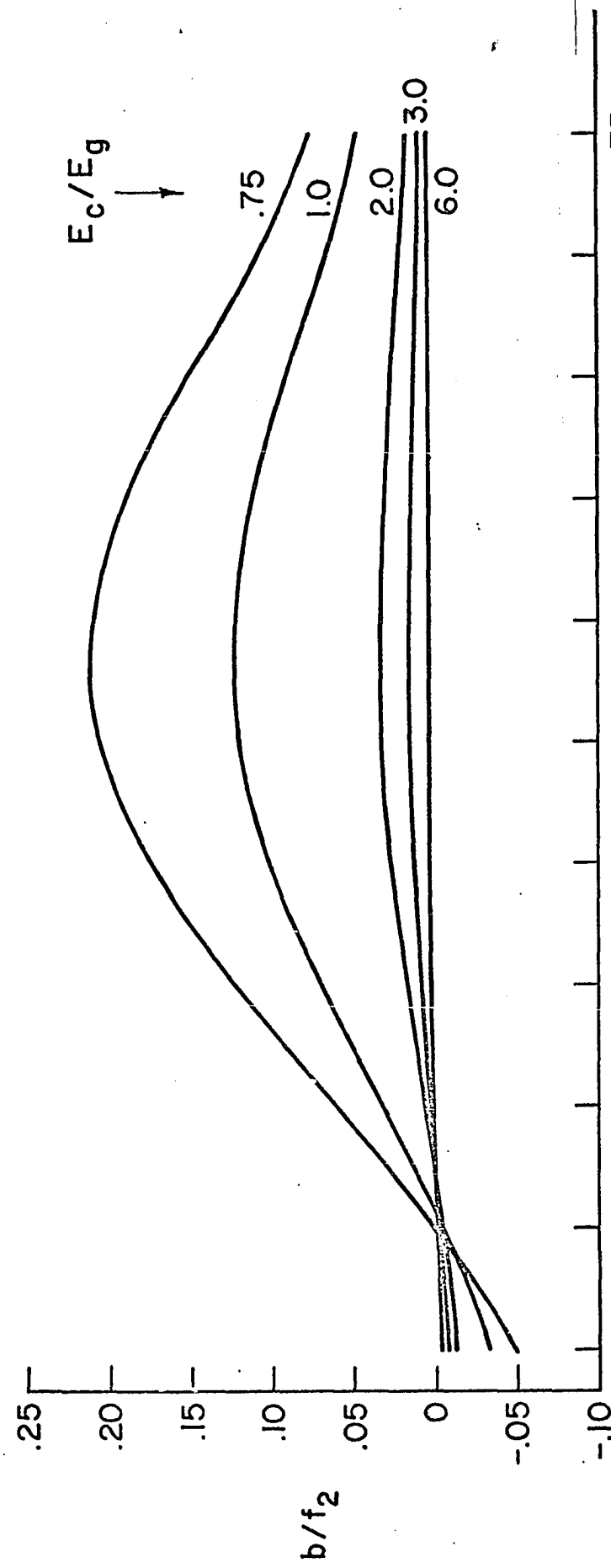

Fig. 17 Normalized convergence, b/f_2, in Geometry 1, f=2.29 MHz

Reproduced with permission of the copyright owner. Further reproduction prohibited without permission.

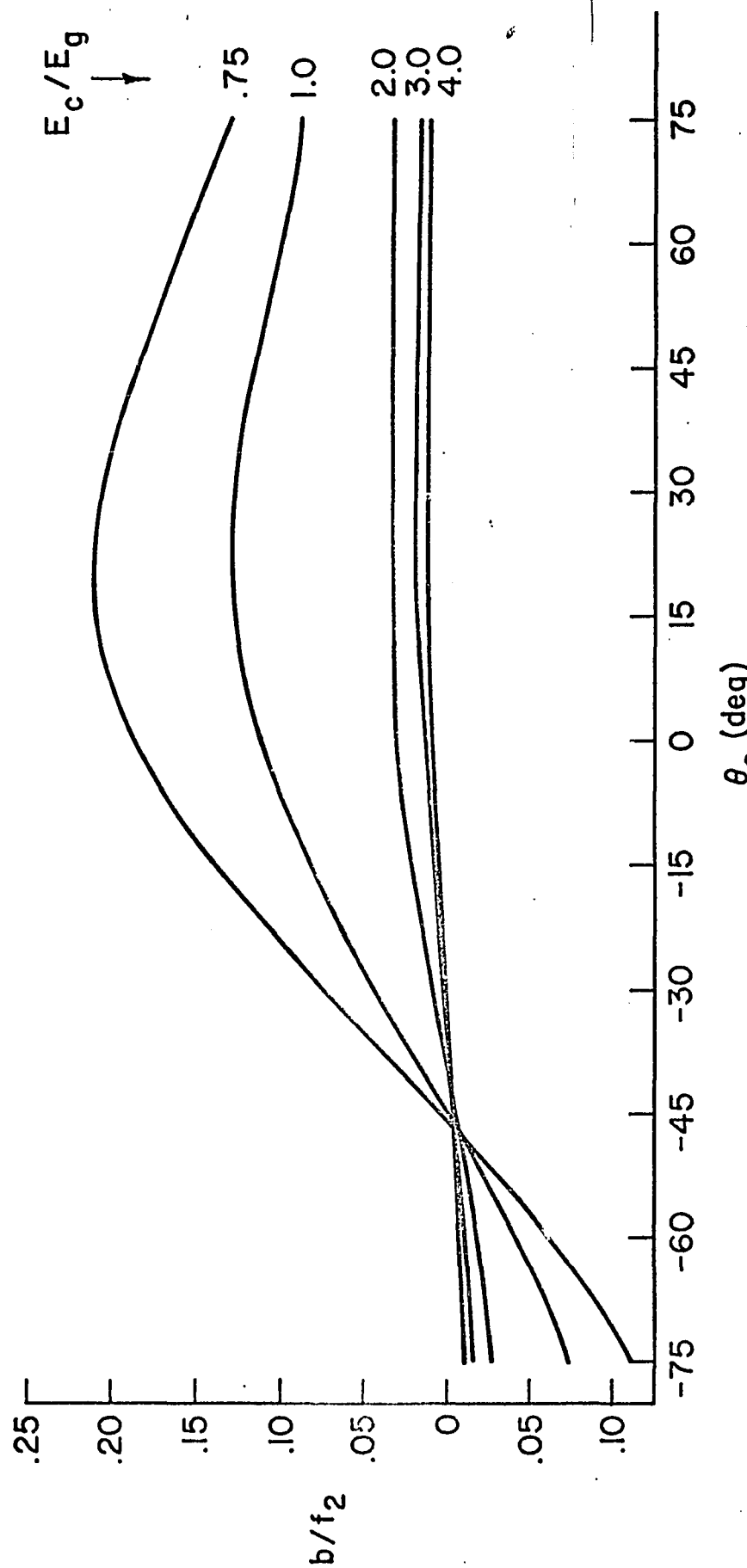

Fig. 18 Normalized convergence, b/f_2, in Geometry 1, f=4.58 MHz

Reproduced with permission of the copyright owner. Further reproduction prohibited without permission.

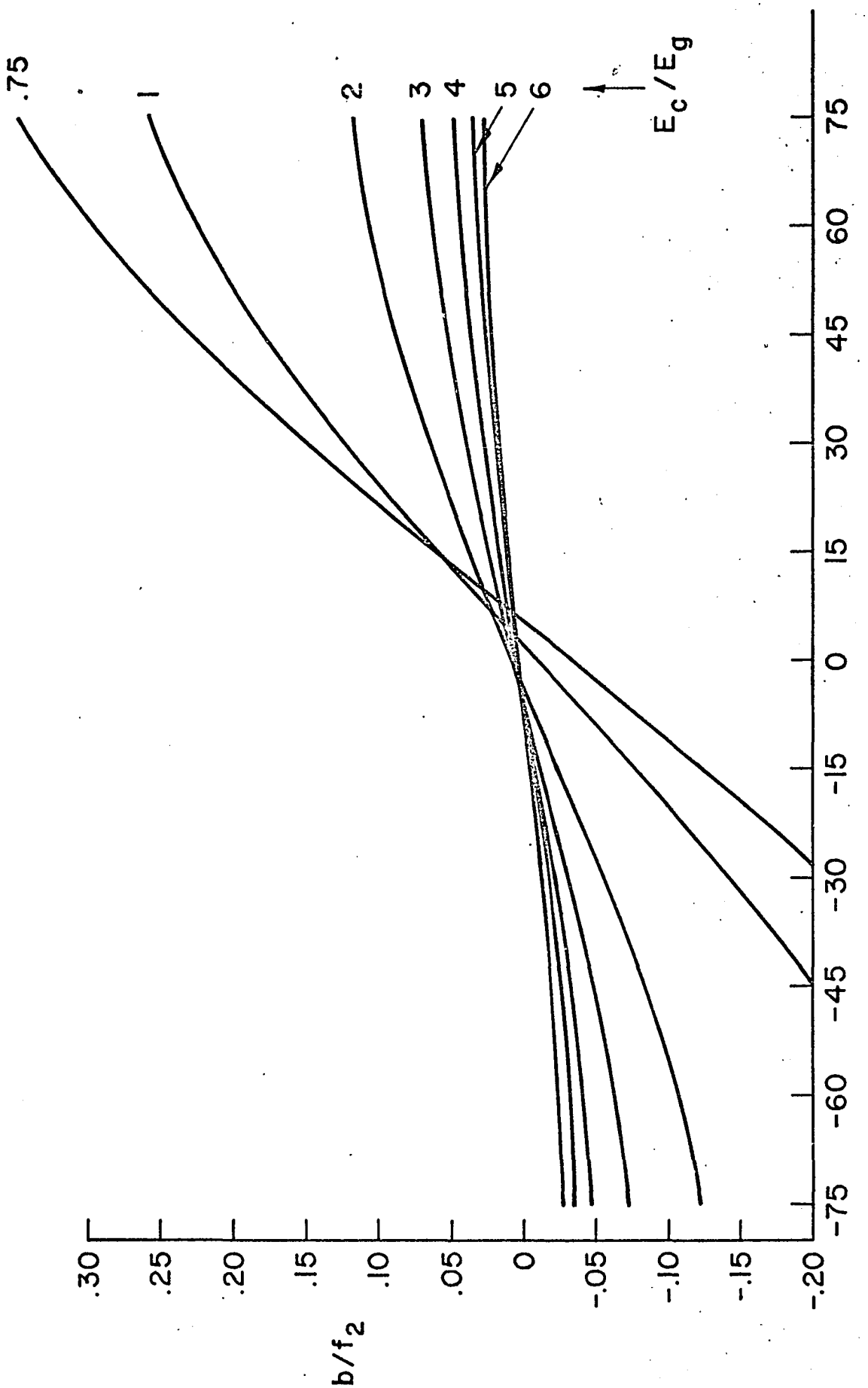

Fig. 19 Normalized convergence, b/f_2, in Geometry 1, f=22.9 MHz

Reproduced with permission of the copyright owner. Further reproduction prohibited without permission.

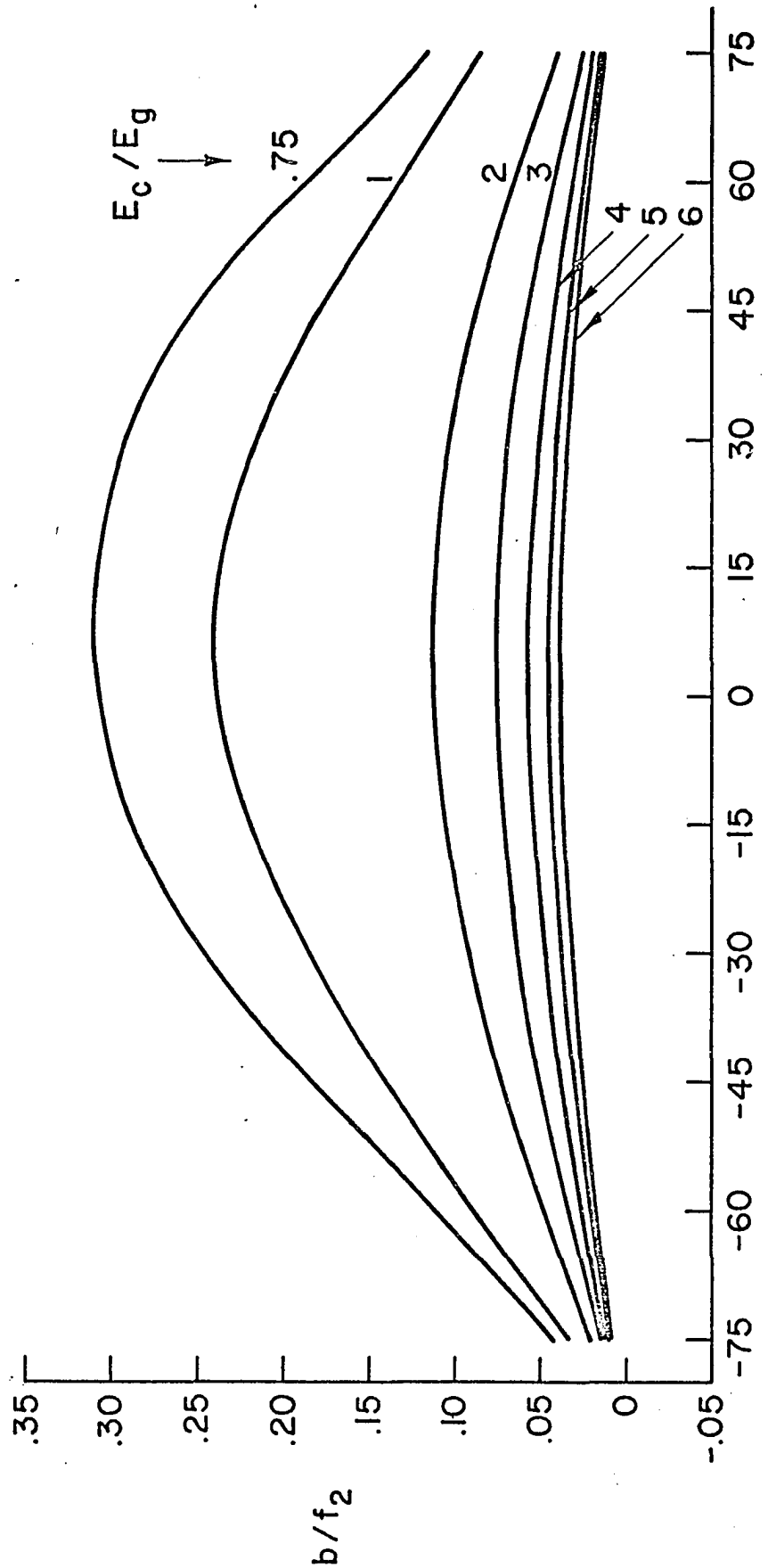

Fig. 20 Normalized convergence, b/f_2, in Geometry 5V, f=2.29 MHz

Reproduced with permission of the copyright owner. Further reproduction prohibited without permission.

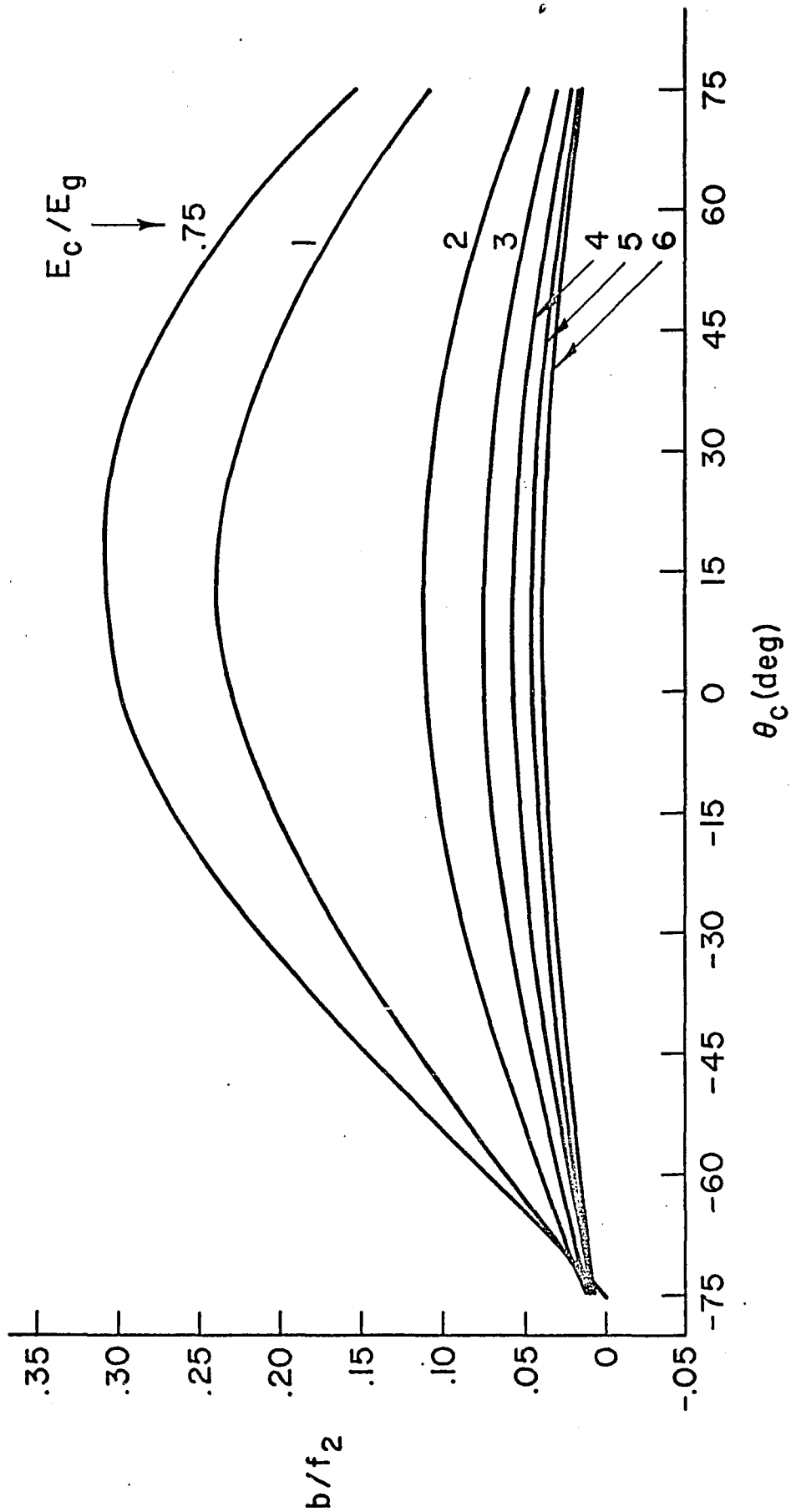

Fig. 21 Normalized convergence, b/f_2, in Geometry 5V, f=4.58 MHz

Reproduced with permission of the copyright owner. Further reproduction prohibited without permission.

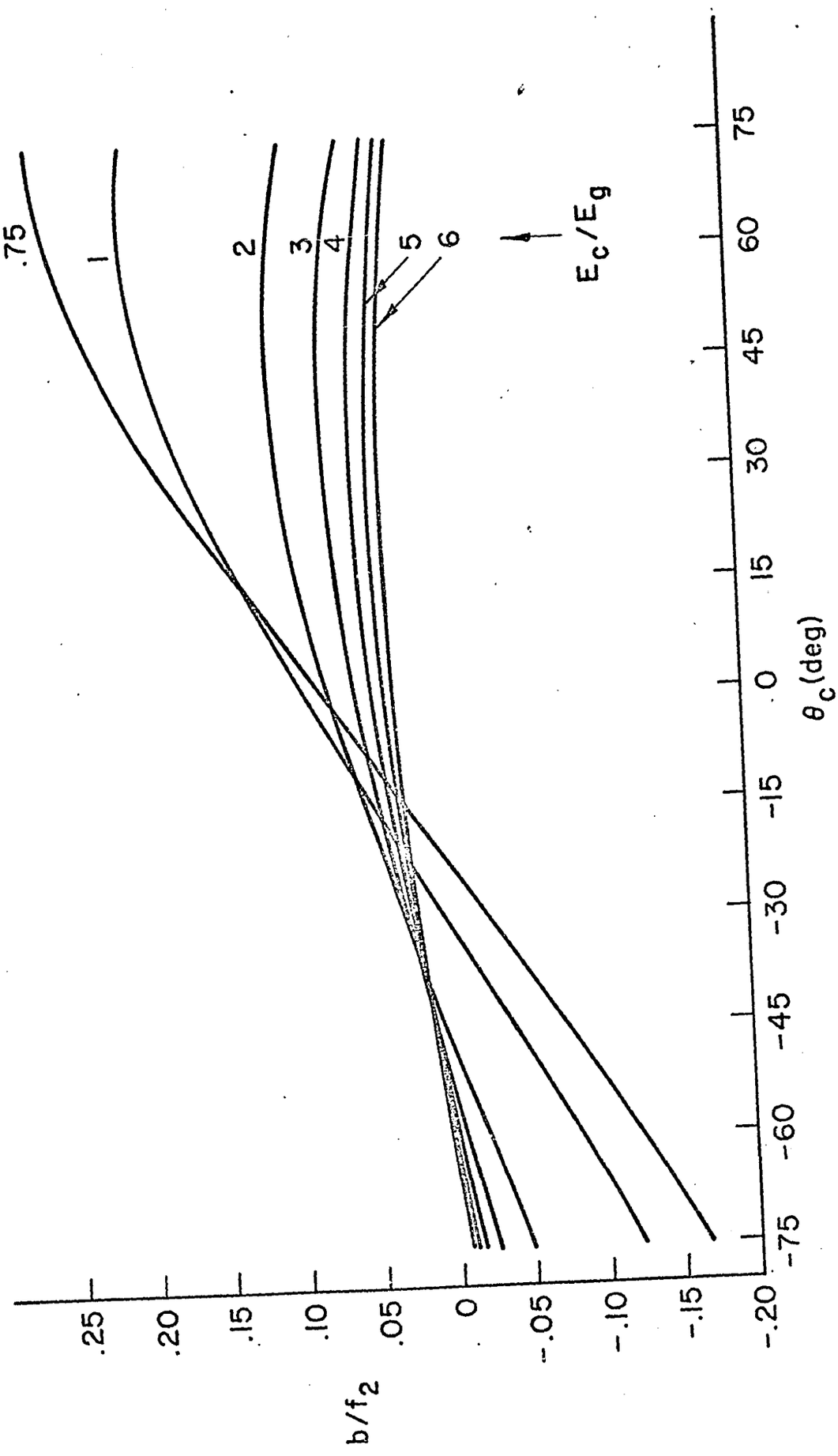

Fig. 22 Normalized convergence, b/f_2, in Geometry 5V, f=22.9 MHz

Reproduced with permission of the copyright owner. Further reproduction prohibited without permission.

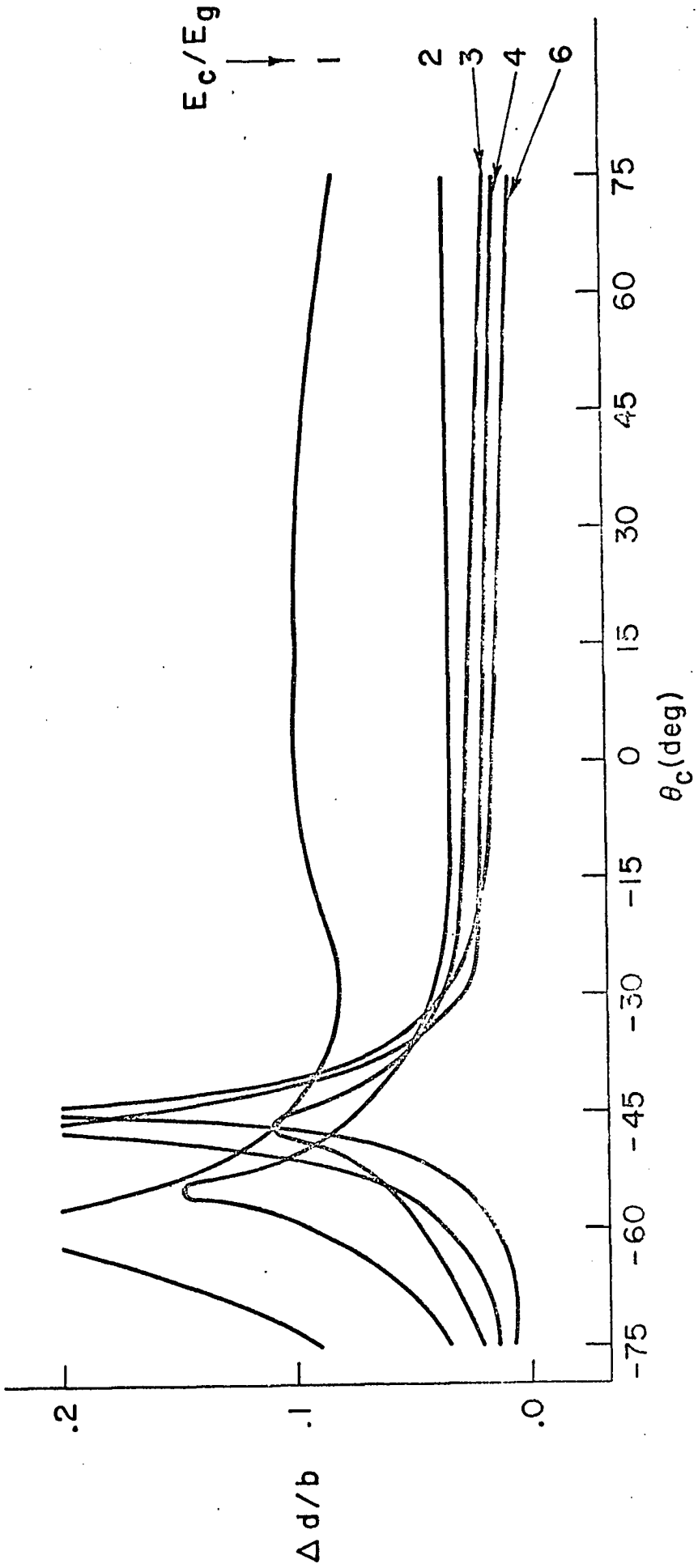

Fig. 23 Normalized thickness of the lens
Lens, Geometry 1, f=2.29 MHz

Reproduced with permission of the copyright owner. Further reproduction prohibited without permission.

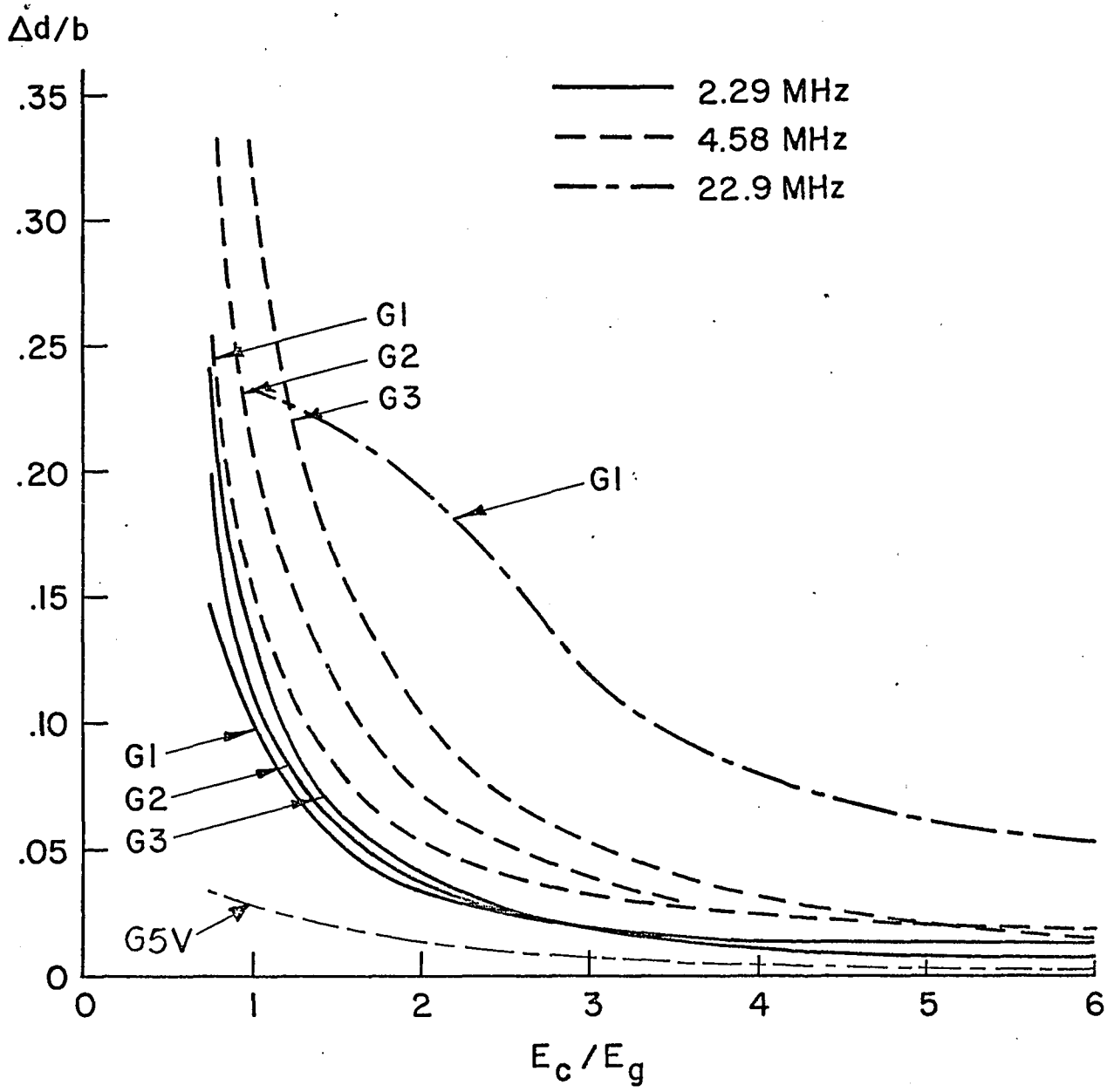

Fig. 24 The normalized thickness of the lenses at rf phase $\theta_c=45°$ for different rf frequencies and geometries

Reproduced with permission of the copyright owner. Further reproduction prohibited without permission.

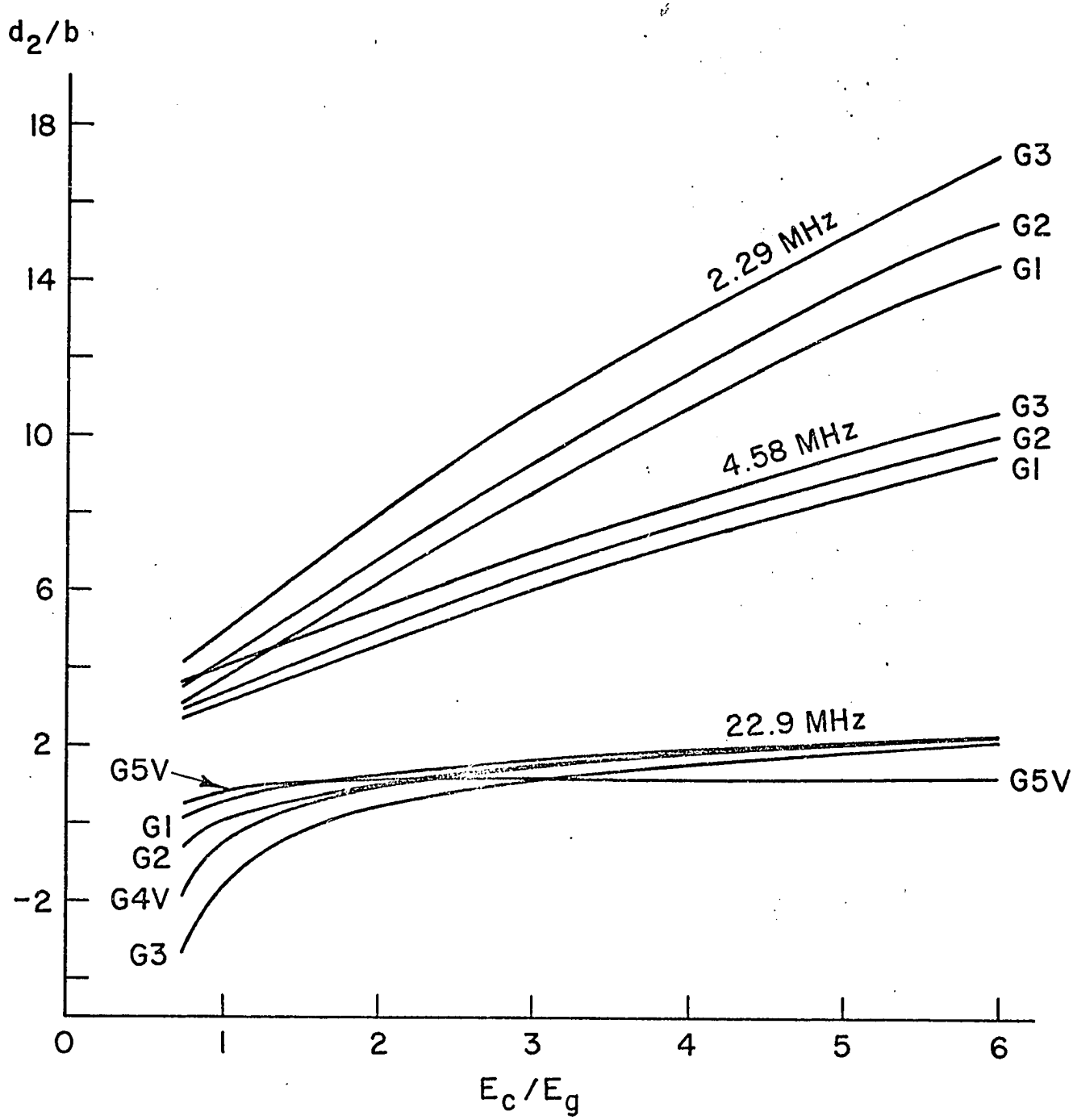

Fig. 25 Location of object-side principal plane d_2/b, at rf phase $\theta_c = 45°$ for different geometries and frequencies

Reproduced with permission of the copyright owner. Further reproduction prohibited without permission.

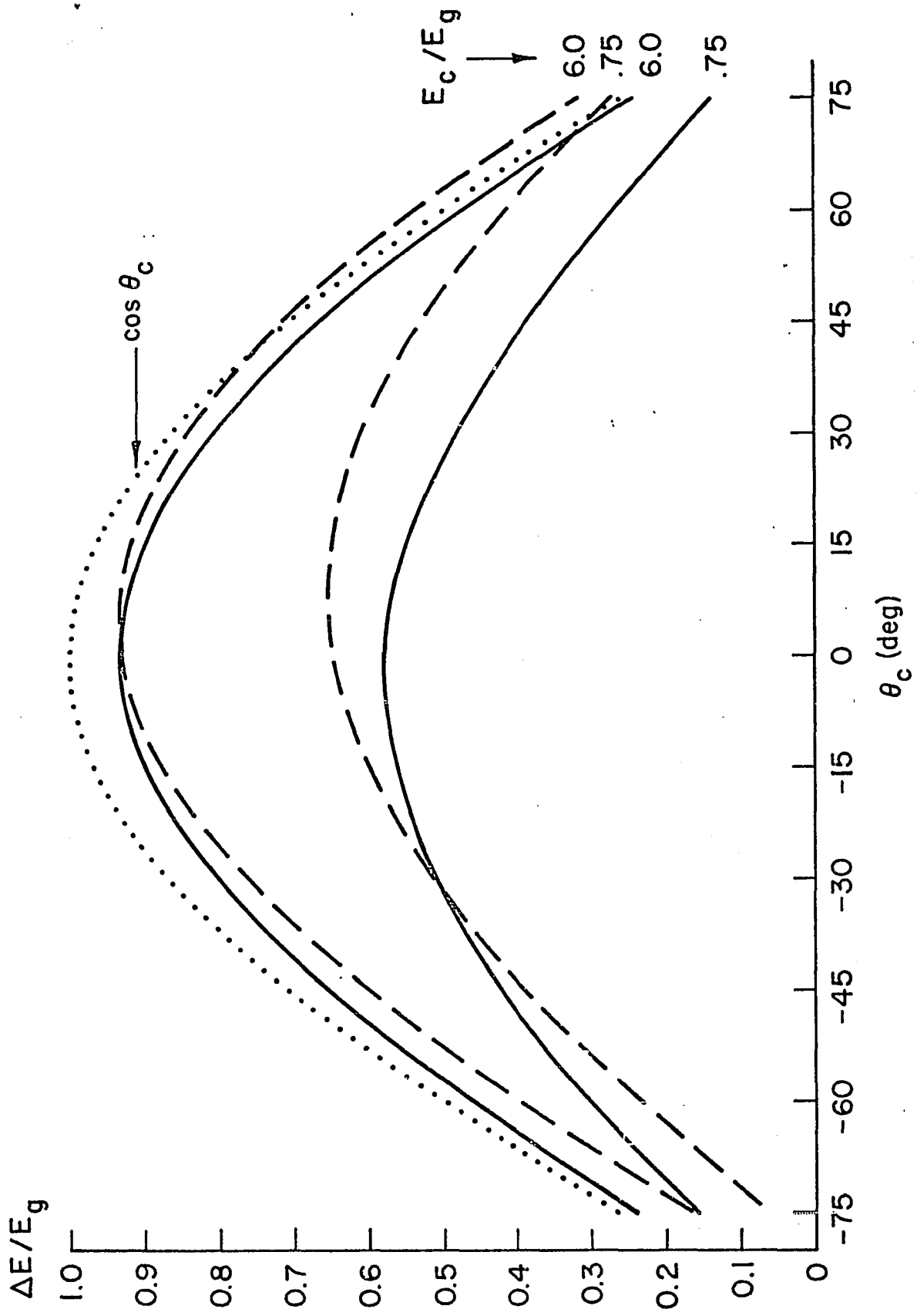

Fig 26 Relative energy gain $\Delta E/E_g$ for f=22.9 MHz at E_c/E_g=.75 and 6.0. Solid curve: Geometry 1 Dashed curve: Geometry 5V. Dotted curve: cos θ_c

Reproduced with permission of the copyright owner. Further reproduction prohibited without permission.

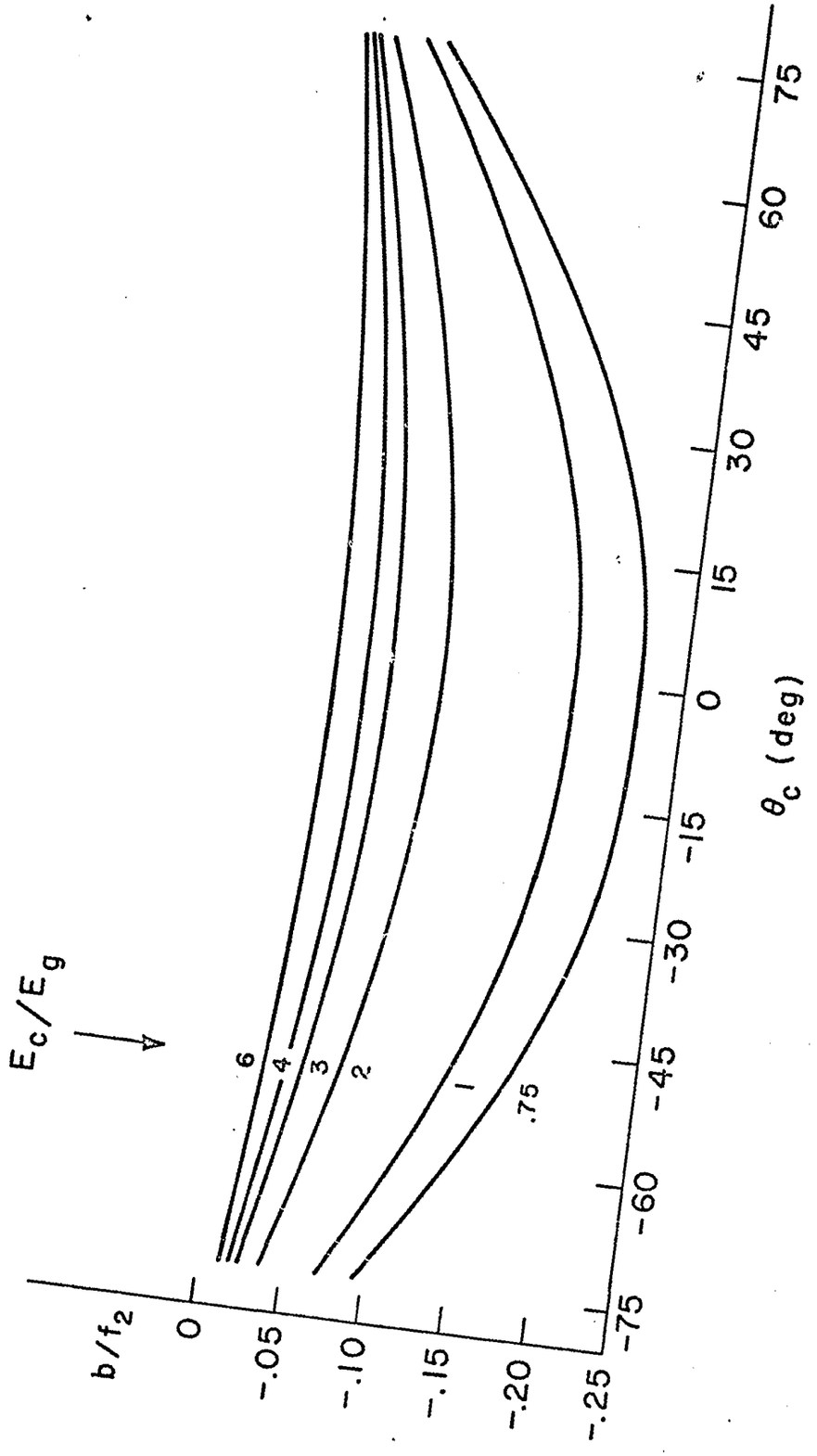

Fig. 27 Normalized convergence, b/f_2, in Geometry 5H, f=2.29 MHz.

Reproduced with permission of the copyright owner. Further reproduction prohibited without permission.

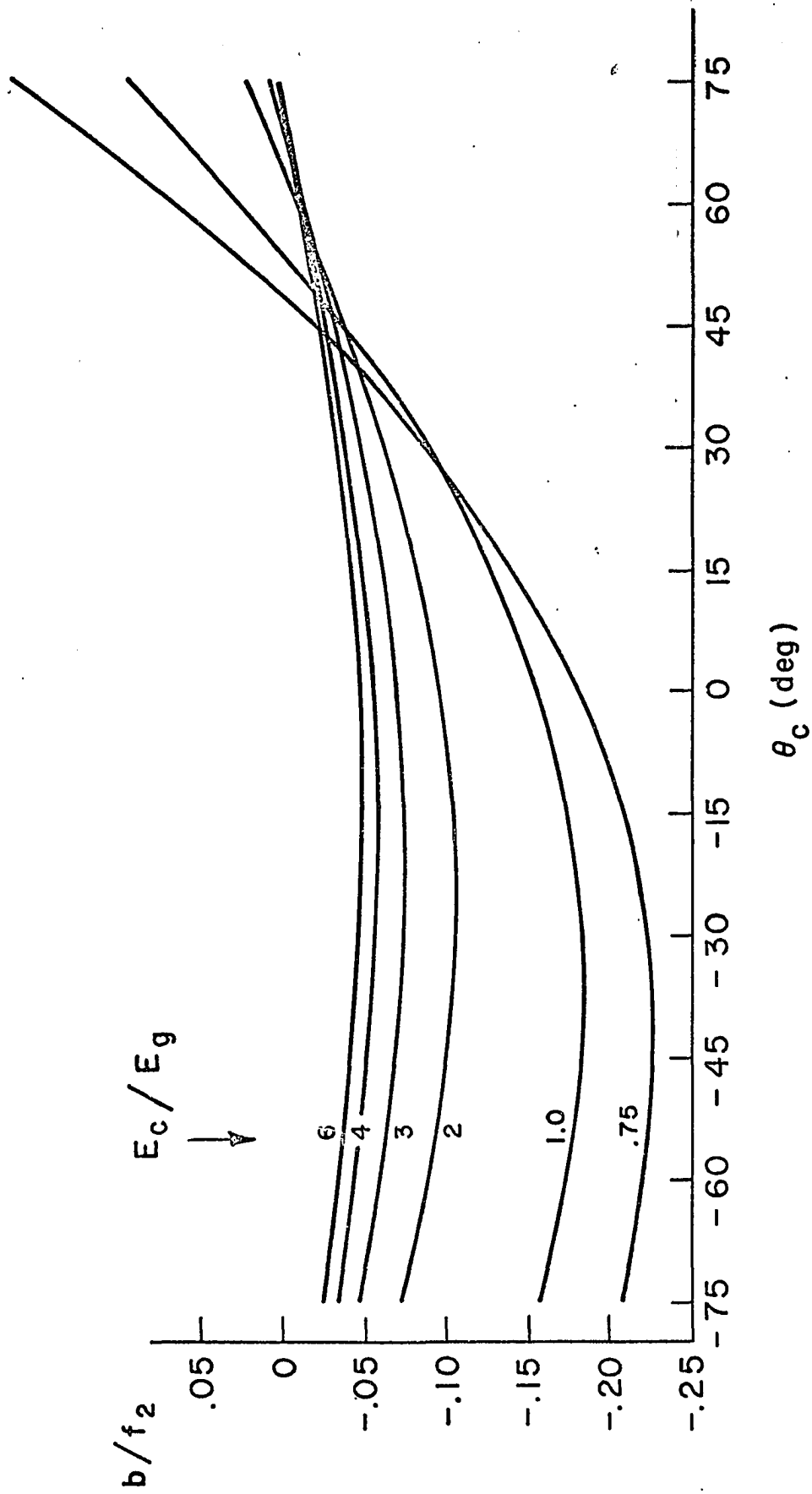

Fig. 28 Normalized convergence, b/f_2, in Geometry 5H, f=22.9 MHz

Reproduced with permission of the copyright owner. Further reproduction prohibited without permission.

VITAE

Name: Chang Sun Han

Permanent Address: 538 Sinchon-Dong Taegu, Korea

Degree and date to be confered: Ph.D., 1971

Date of birth: May 20, 1935

Place of birth: Pyongyang, Korea

Secondary Education: Pyong Yang High School

Collegiate Institution attened	Dates	Degree	Date of Degree
Kyong Puk University	1952-1956	B.S.	April, 1956
Korea University	1957-1958		
University of Maryland	1960-1965	M.S.	June, 1966
University of Maryland	1966-1970	Ph.D.	January, 1971

Publications:

"Spectroscopic Studies with the B^{10} (He^3, $p\alpha\alpha\alpha$) reaction" Rev. Mod. Phys., 34, 444 (1965) with H.D. Holmgren, M. Waggoner, J.E. Etter and C. Moazed

"Computer Results for the Focal Properties of Two- and Three-Dimensional Electric Lenses with Time-Varying Fields" the University of Maryland Tech. Report No.70-126

Positions Held:

Research Engineer, The Cyclotron Corp. Berkeley, California, 1970

Research Assistant, the University of Maryland, College Park, Maryland, 1966-1970

Faculty Assistant, the University of Maryland, College Park, Maryland, 1966

Research Assistant, the University of Maryland, College Park, Maryland, 1963-1965

Research Assistant, National Academy of Science, Washington D.C. 1961-1963

Reproduced with permission of the copyright owner. Further reproduction prohibited without permission.